ANTIOXIDANTS & REDOX SIGNALING
Volume 13, Number 3, 2010

DOI: 10.1089/ars.2009.2931

COMPREHENSIVE INVITED REVIEW

# Redox Biocatalysis and Metabolism: Molecular Mechanisms and Metabolic Network Analysis

Lars M. Blank, Birgitta E. Ebert, Katja Buehler, and Bruno Bühler

**Abstract**

Whole-cell biocatalysis utilizes native or recombinant enzymes produced by cellular metabolism to perform synthetically interesting reactions. Besides hydrolases, oxidoreductases represent the most applied enzyme class in industry. Oxidoreductases are attributed a high future potential, especially for applications in the chemical and pharmaceutical industries, as they enable highly interesting chemistry (*e.g.*, the selective oxyfunctionalization of unactivated C–H bonds). Redox reactions are characterized by electron transfer steps that often depend on redox cofactors as additional substrates. Their regeneration typically is accomplished via the metabolism of whole-cell catalysts. Traditionally, studies towards productive redox biocatalysis focused on the biocatalytic enzyme, its activity, selectivity, and specificity, and several successful examples of such processes are running commercially. However, redox cofactor regeneration by host metabolism was hardly considered for the optimization of biocatalytic rate, yield, and/or titer. This article reviews molecular mechanisms of oxidoreductases with synthetic potential and the host redox metabolism that fuels biocatalytic reactions with redox equivalents. The tools discussed in this review for investigating redox metabolism provide the basis for studies aiming at a deeper understanding of the interplay between synthetically active enzymes and metabolic networks. The ultimate goal of rational whole-cell biocatalyst engineering and use for fine chemical production is discussed. *Antioxid. Redox Signal.* 13, 349–394.



Reviewing Editors: *Donald Buerk, Enrique Cadenas, Daniël C. de Geus, Pablo Domínguez de María, Juan J. Poderoso, and Jean–Claude Voegel*

Laboratory of Chemical Biotechnology, Faculty of Biochemical and Chemical Engineering, TU Dortmund, Dortmund, Germany.

## I. Introduction

Redox biocatalysis is nature's solution for the catalysis of demanding reactions necessitating the specific transfer of reduction equivalents in aqueous reaction media, under ambient conditions, and mostly in a polymer solution, where reaction rates might be determined not only by kinetic properties of the catalysts involved, but also by mass transfer. Catalyst efficiency is defined by nature's objectives of growth, reproduction, and optimal function of individual reactions in metabolic networks in cells, tissues, organs, or organisms. In contrast to these highly evolved and optimized reaction systems, technical solutions are rather crude. Isolated enzymes or whole cells can be used for redox biocatalysis. Whereas the first approach often requires an additional cofactor regeneration system, in whole cells, cofactor regeneration is achieved via the intrinsic carbon and energy metabolism or heterologous enzymes such as recombinant formate or glucose dehydrogenases. The awareness of the high level of interdependency between redox biocatalysis and intracellular metabolism has led to metabolic engineering concepts to optimize cell metabolism for redox biocatalysis. In the future, synthetic biology will provide new strategies to engineer artificial redox metabolism networks sustaining highly efficient redox cofactor regeneration for biocatalysis.

This review will focus on the use of whole-cell systems for redox biocatalysis and will discuss the interplay between biocatalytic reaction and host metabolism. This will be done on the basis of the most important mechanisms of oxidoreductase-catalysis and the up-to-date knowledge on microbial redox metabolism and its analysis.

## II. Molecular Mechanisms of Synthetically Relevant Biocatalytic Redox Reactions

From a synthetic perspective, oxidoreductases and hydrolases are the most applied enzyme classes in industry (311). Thereby, oxidoreductases are attributed a high future potential, especially for applications in the chemical and the pharmaceutical industries, as they feature, beside the inherent selectivity of enzymes, highly interesting chemistry such as the selective introduction of oxygen from $O_2$ into chemically inert C–H bonds. Furthermore, oxidoreductases often catalyze the formation of a chiral product from a prochiral substrate at close to 100% yield. Other reactions with a high synthetic potential include, on the oxidative side, the oxyfunctionalization of C=C and C–N bonds, Baeyer–Villiger oxidations, and the oxidation of alcohols, aldehydes, acids, and aromatic compounds and, on the reductive side, the reduction of ketones, aldehydes, C=C bonds, and C=N bonds as well as reductive animations (73, 93, 201).

Figure 1 shows a simplified tree of oxidoreductase classes. This tree will lead through the present section highlighting the molecular aspects of the most important catalytic mechanisms involved in redox-biocatalysis. On the first level in the tree, four enzyme classes are differentiated. Dehydrogenases (or reductases) are generally considered to catalyze reversible reactions and thus can be used for both oxidative as well as reductive biocatalysis, whereas oxygenases, oxidases, and peroxidases catalyze oxidation reactions, which are considered to be irreversible due to their high standard enthalpy change of reaction. The latter is attributed to the highly exothermic reduction of $O_2$ or hydrogen peroxide, which function

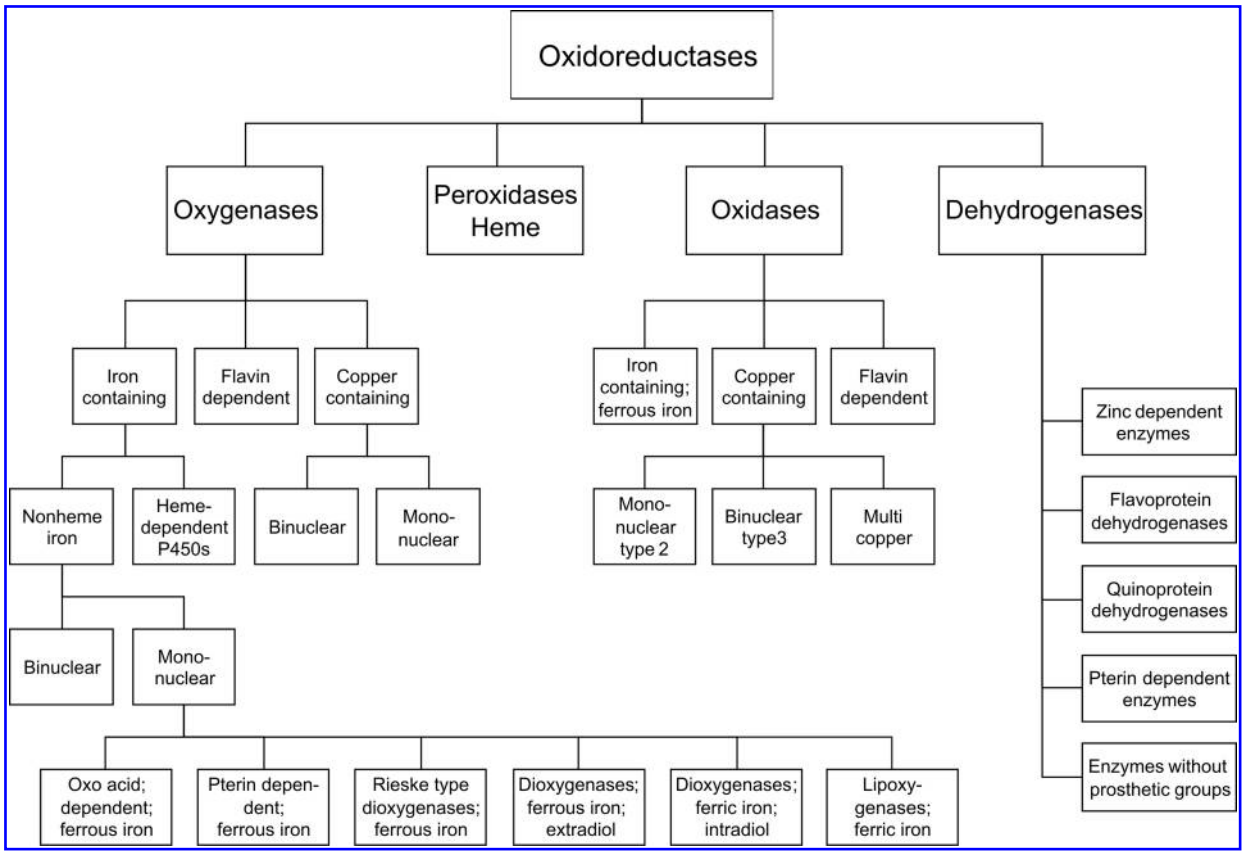


**FIG. 1. Classification of oxidoreductases.**

as electron acceptors in the case of oxygenases and oxidases or peroxidases, respectively. In contrast to oxidases, oxygenases incorporate one or both oxygen atoms of $O_2$ into their substrate.

Typically, oxidoreductases depend on a redox cofactor such as NAD(P)H or $NAD(P)^+$, which functions as an electron donating or accepting co-substrate, and thus are coupled to redox metabolism in whole cells, the most common form in which oxidoreductases are applied for biocatalysis (63, 192, 287, 360, 361). Exceptions include peroxidases, which couple the reduction of hydrogen peroxide to water with the two-electron oxidation of the substrate, oxidases, which couple the reduction of $O_2$ to hydrogen peroxide or water with the two- or four-electron oxidation of the substrate, and those dioxygenases, which couple the reduction and incorporation of $O_2$ with the four-electron oxidation of an activated carbon scaffold (see below).

All reactions dealing with $O_2$ or hydrogen peroxide reduction involve reactive oxygen species such as oxygen radicals or hydrogen peroxide itself, which cause extensive damage to biomolecules including enzymes. These reactive oxygen species and damage caused by them can be handled by the metabolism of living or, even better, growing cells, an advantage which can be exploited for productive redox biocatalysis (63, 191). In the following four subsections, catalytic mechanisms and metabolic implications of the four main oxidoreductase classes (Fig. 1) are reviewed with a focus on enzymes, which are important for redox-biocatalysis.

### *A. Oxygenases*

Oxygenases catalyze the specific introduction of one or two oxygen atoms from $O_2$ into the substrate under mild conditions. Such highly specific oxyfunctionalization reactions, especially the activation of C-H bonds, are synthetically very interesting and often inaccessible by chemical means (42).

Oxygenases can be found in almost all kinds of living cells, ranging from bacterial to mammalian, and several different catalytic centers and mechanisms are known in this extraordinarily versatile enzyme class (see below). Monooxygenases and dioxygenases introduce one and two oxygen atoms from $O_2$ into the substrate, respectively. In doing so, the former produce one molecule of water as a co-product. These enzymes have important physiological roles in detoxification, for example, in mammalian liver cells, in the biosynthesis of secondary metabolites, hormones, signaling molecules, and many other compounds, and in microbial hydrocarbon degradation. Due to the high flexibility needed for detoxification and especially degradation of hydrocarbons and xenobiotics, oxygenases functionalize a huge variety of substrates (Table 1). This includes the hydroxylation of alkyl-, allyl-, or benzyl carbons, vinyl group epoxidations, aromatic (di)oxygenations, Baeyer–Villiger oxidations, and heteroatom oxygenations. Several excellent reviews with comprehensive coverage of the literature on oxygenase catalyzed reactions have appeared in journals and text books (28, 49, 64, 112, 193, 220, 248, 320, 323, 328). The high abundance and versatility of oxygenases, their ability to specifically introduce oxygen from $O_2$,

Table 1. Classification of Oxyfunctionalization Reactions According to Substrate Type

| *Type of Substrate* | *Typical Enzyme Examples* | *Catalytic Center* | *Natural Electron Donor/Acceptor* | *References* |
|---|---|---|---|---|
| Alkyl-C; non-activated | Methane monooxygenase | Nonheme di-iron | NADH | 217, 271 |
| | Alkane monooxygenase | Nonheme di-iron | NADH | 302 |
| | P450 BM3 | Heme | NADPH | 224 |
| | P450cam | Heme | NADH | 286 |
| | Proline hydroxylases | Nonheme ferrous iron | 2-oxoglutarate | 76 |
| Benzyl-C, allyl-C; non-activated | Xylene monooxygenase | Nonheme di-iron | NADH | 15, 314 |
| | Ethylbenzene dehydrogenase | Molybdenum cofactor | unknown | 157, 175 |
| | Chloroperoxidase | Heme | not required | 125 |
| Vinyl-C, aryl-C; non-activated | Styrene monooxygenase | FAD | NADH | 241 |
| | Toluene dioxygenase | Nonheme ferrous iron | NADH | 49 |
| | Toluene 4-monooxygenases | Nonheme di-iron | NADH | 222 |
| | Chloroperoxidase | Heme | not required | 125 |
| Activated carbons | Cyclohexanone monooxygenase | FAD | NADPH | 309 |
| | Hydroxybiphenyl monooxygenase | FAD | NADH | 313 |
| | *p*-cresol methylhydroxylase | Flavocytochrome | Cytochrome oxidase, azurin | 85 |
| | Nicotinate dehydrogenases | Molybdenum cofactors | unknown | 10, 226 |
| | Vanillyl-alcohol oxidase | FAD | $O_2$ | 214 |
| | Catechol 1,2-dioxygenase | Nonheme ferric iron | not required | 97 |

and the absence of enzyme-destabilizing peroxides as reactants have lead to considerable advances in process implementation and to first examples of industrial processes (63, 161, 287, 311). Most published biocatalytic processes for preparative oxyfunctionalizations include oxygenase-catalysis. Various catalytic centers have evolved for the activation of $O_2$ (Table 1). The main classes of oxygenases are iron-, copper-, or flavin-dependent.

Copper-containing oxygenases such as the mononuclear dopamine $\beta$-monooxygenase and the binuclear copper-based methane monooxygenase (particulate MMO) are able to catalyze *inter alia* the hydroxylation of unactivated alkyl carbons (89, 140, 174, 272, 303), but are, except for tyrosinases (130), rarely used for biocatalytic purposes and thus not discussed in this review. Tyrosinases feature both oxygenase and oxidase activity and will be discussed below in the oxidase section. Iron-containing oxygenases are the most abundant and best-studied enzymes catalyzing carbon oxyfunctionalizations and can be divided in two categories: heme monooxygenases and nonheme iron oxygenases (Fig. 1). The latter group catalyzes diverse reactions including the oxyfunctionalization of all types of carbon listed in column one of Table 1, which classifies oxyfunctionalization reactions according to substrate type. The understanding of biological significance and chemical properties of nonheme iron oxygenases has increased dramatically in recent years (41, 57, 58, 182, 276). This enzyme category again can be divided into two groups, mononuclear nonheme iron enzymes and binuclear nonheme iron enzymes (Fig. 1).

1. Binuclear nonheme iron enzymes. Among the known reactions catalyzed by $O_2$-dependent binuclear nonheme iron enzymes, usually containing a bridged di-iron center in the active site, are monooxygenations of all carbon types listed in Table 1, fatty acid desaturations, and ribonucleotide reduction (304, 346). With respect to carbon oxyfunctionalization, soluble methane monooxygenase (MMO), alkane monooxygenase (AMO), xylene monooxygenase (XMO), toluene-2-monooxygenase (T2MO), and toluene-4-monooxygenase (T4MO) are prominent examples (see Table 1).

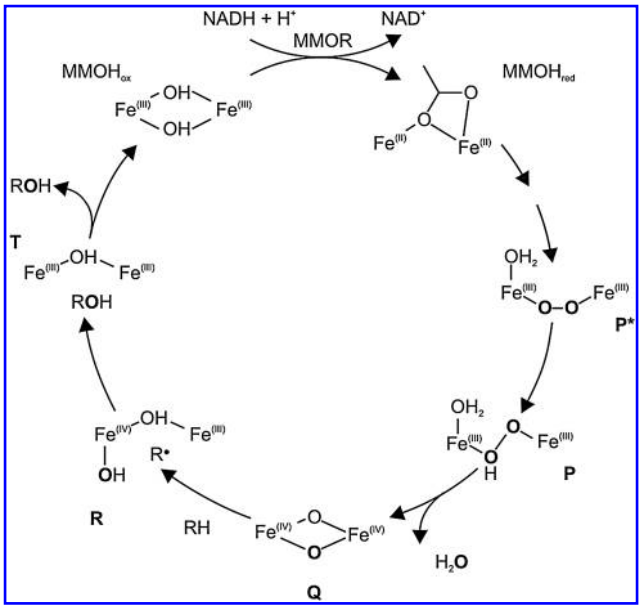


**FIG. 2. The catalytic cycle of soluble MMO.** Oxygen atoms derived from molecular oxygen are shown in **bold**. Compounds P*, P, Q, R, and T are intermediates of the catalytic cycle following the nomenclature given in literature. MMOH, hydroxylase component of MMO; MMOR, reductase component of MMO. Figure adapted from Wallar *et al.* (346) and Brazeau *et al.* (51).

Soluble MMOs are the best-studied nonheme di-iron monooxygenases, catalyze the NADH-dependent insertion of one oxygen atom from $O_2$ into the exceptionally stable C-H bond of methane to form methanol, and typically have a broad substrate spectrum (100, 217, 271). Carboxylate-bridged nonheme di-iron enzymes such as MMO, T2MO, and T4MO consist of three or four protein components, depending on the involvement of a ferredoxin in electron transfer (346). The regular components include a hydroxylase containing a carboxylate-bridged di-iron cluster in the active site, a reductase channeling electrons from NADH to ferredoxin or directly to the hydroxylase, and a small effector protein modulating the conformation of the hydroxylase with several roles in catalysis, including control of substrate access as well as enhancement of the electron transfer and $O_2$ activation (20, 52, 294, 347). Typically, four glutamate and two histidine residues coordinate the di-iron center. The remainder of the coordination sites is occupied by solvent-derived ligands. The catalytic cycle of MMO (Fig. 2) involves the reaction of $O_2$ with the reduced diferrous form to give a differric peroxy or hydroperoxy species (compounds P* and P, respectively) (195, 299), which spontaneously converts to compound Q containing a bis $\mu$-oxo $Fe(IV)_2$ cluster, the so-called "diamond core" (18, 179, 299). Compound Q, but also compound P, have been proposed to be the oxygenating species, depending on the type of reaction to be catalyzed (193, 326).

AMO and XMO show similar reaction mechanisms (15, 16) but differ from water-soluble proteins of the di-iron-carboxylate type in that their oxygenase component is membrane bound and the di-iron cluster is complexed by histidines only (147). Members of this group of binuclear nonheme iron enzymes contain a characteristic 8-histidine motif and consist of a variable number of subunits. AMO, for example, consists of an integral membrane hydroxylase and two soluble proteins, rubredoxin and rubredoxin reductase (256), whereas XMO is a two-component enzyme, consisting of an integral membrane hydroxylase and a soluble NADH:acceptor reductase (314). Both enzymes show a large substrate spectrum. AMO, naturally catalyzing the NADH dependent $\omega$-hydroxylation of medium chain length alkanes (C5–C12), accepts a wide range of linear, branched, and cyclic alkanes as well as alkyl benzenes (327, 329). Furthermore, epoxidation of terminal alkenes, sulfoxidations, demethylations, and aldehyde formation have been reported (114, 167, 168, 215). XMO accepts *m*- and *p*-ethyl-, methoxy-, nitro-, and chlorosubstituted toluenes, *m*-bromosubstituted toluene, and styrene, which is transformed into (*S*)-styrene oxide with an enantiomeric excess of 95% (364). Furthermore, *Escherichia coli* recombinants containing XMO were found to catalyze the multistep oxidation of xylenes to corresponding alcohols, aldehydes, and acids via individual monooxygenation reactions (59, 60). As emphasized by the described examples, most binuclear nonheme iron enzymes depend on NADH as an electron source, whereas NADPH-dependence is rather uncommon. Thus, in living cells and in biocatalytic applications, these oxygenases are typically coupled to catabolic NADH regeneration.

2. Mononuclear nonheme iron enzymes. Mononuclear nonheme iron enzymes contain either a high-spin ferrous site which is involved in $O_2$ activation or a high-spin ferric site which activates substrates (2, 58, 80, 304). The ferric site is coordinated by a variable histidine-rich ligand environment and known to catalyze intradiol aromatic ring cleavage and lipoxygenations. In contrast, the ferrous site is invariably coordinated by two histidines and one aspartate or glutamate, a recurring motif referred to as the 2-His-1-carboxylate facial triad (Fig. 3). The remaining three ligand sites, which, in the resting enzyme, can be vacant or occupied by solvent water, $OH^-$, or a weak protein ligand, are readily available for the binding of substrate, cofactor, and/or $O_2$ during catalysis. Thus, this ferrous site is very versatile, catalyzing a wide variety of reactions including extradiol aromatic ring cleavage, aromatic (di)hydroxylations, desaturations, halogenations, epoxidations, and aliphatic C-H bond hydroxylations (178, 261). Most oxygenases featuring the 2-His-1-carboxylate facial triad can be classified into four main groups: 2-oxo acid dependent enzymes, pterin-dependent hydroxylases, Rieske oxygenases, and extradiol cleaving catechol dioxygenases (Fig. 1) (57, 183).

2-Oxo acid-dependent iron enzymes catalyze all the mentioned reaction types except for intramolecular dioxygenations (132, 259, 261). Enzymes of this versatile family are thought to initiate catalysis by oxidative decarboxylation of the 2-oxo acid co-substrate (*e.g.*, 2-oxoglutarate), which mediates the formation of a highly oxidizing Fe(IV)=O intermediate (Fig. 3). In most cases, this intermediate activates C-H bonds in substrates by abstraction of the H-atom, followed by oxygen rebound leading to substrate hydroxylation. However, different reactivities such as oxidative ligand transfer involved in halogenations have also been reported (186). With respect to hydroxylations, 2-oxoglutarate-dependent hydroxylases can be classified as intermolecular dioxygenases and directly depend on the central carbon metabolism providing 2-oxoglutarate. Thus, efficient catalysis of these enzymes in whole cells directly depends on the flux through the central carbon metabolism, which in turn is affected by the oxygenase-related shortcut in the TCA-cycle (*i.e.*, from 2-oxoglutarate to succinate). Mononuclear nonheme iron enzymes depending on 2-oxoglutarate catalyze C-H bond oxygenations primarily in large and highly functionalized molecules, and thus are important for medicine and agriculture. Some 2-oxoglutarate dependent dioxygenases (*e.g.*, proline 4-hydroxylase) are used for synthetic purposes (298).

Beside 2-oxo acid-dependent oxygenases, pterin-dependent hydroxylases [*e.g.*, amino acid hydroxylases (9, 111, 249)], also catalyze aromatic monohydroxylations, whereas aromatic dihydroxylations are catalyzed by Rieske oxygenases (48, 49, 107, 345). Both pterin-dependent hydroxylases and Rieske oxygenases also have been reported to catalyze benzylic hydroxylations and epoxidations. In pterin-dependent hydroxylases, the pterin cofactor was proposed to fulfill a dual role, the delivery of two electrons and the activation of $O_2$ together with ferrous iron resulting in the formation of hydroxylated pterin and a Fe(IV)=O hydroxylating intermediate (Fig. 3) (105, 250). Regeneration of tetrahydrobiopterin involves dehydration and NAD(P)H-dependent reduction of the hydroxylated pterin cofactor.

Rieske dioxygenases form a diverse group of two- or three-component enzymes with a reductase component that obtains electrons from NAD(P)H, often a ferredoxin component that shuttles the electrons, and an oxygenase component where $O_2$ activation and substrate *cis*-dihydroxylation occur (190). The mononuclear iron receives the electrons needed for catalysis

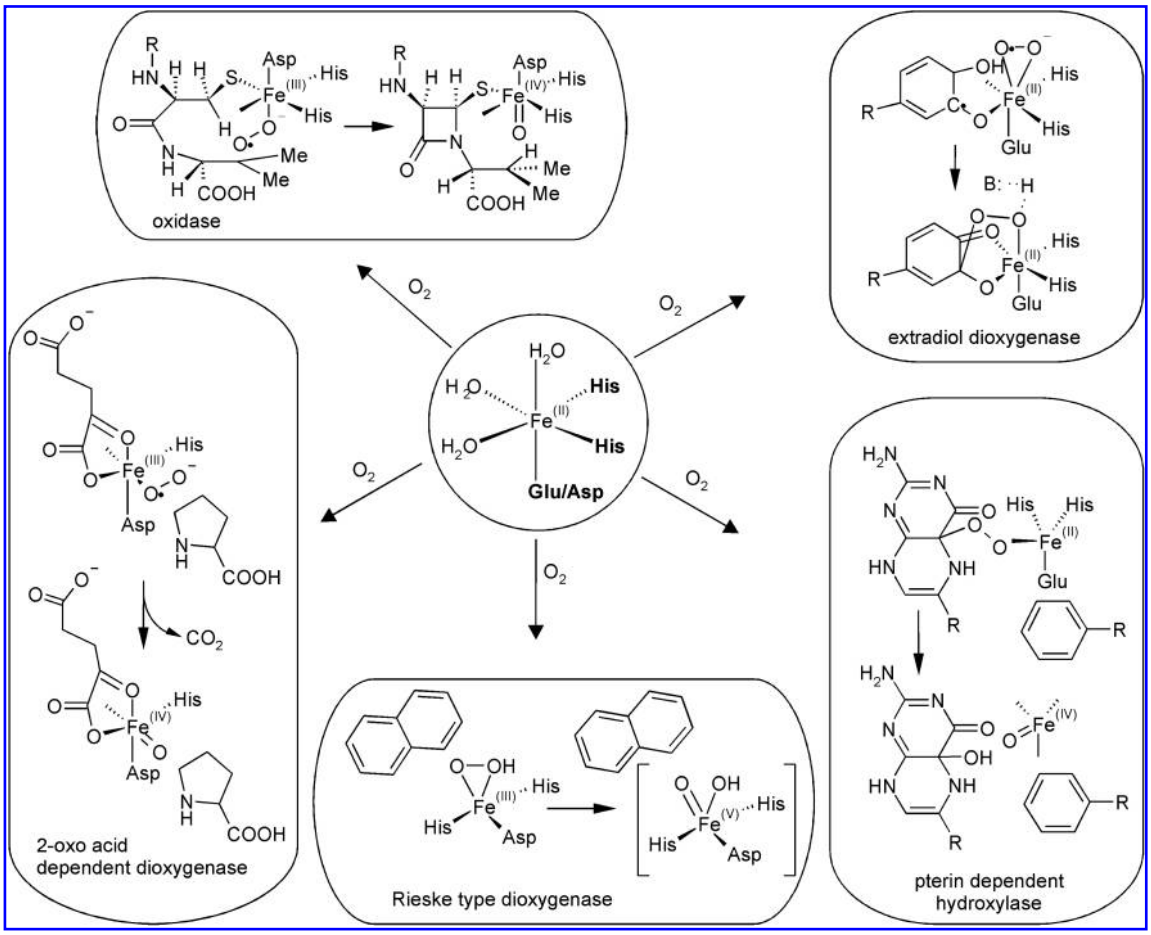


**FIG. 3. Various modes of oxygen activation by members of the 2-His/Glu facial triad family.** The triad is shown in **bold**. In a first reaction, a substrate or cofactor is bound and concomitantly solvent water is released to open an oxygen binding site at the iron. The three ligand sites shown to be occupied by $H_2O$ in the central structure can be vacant, occupied by $OH^-$, or occupied by a weak protein ligand in different enzymes from the family. Figure adapted from Kovaleva *et al.* (183).

from the Rieske cluster of the neighboring oxygenase subunit. Side-on binding of $O_2$ leads to the formation of an iron–(hydro)peroxide complex (Fig. 3) (57). From this point on, different mechanisms for the actual oxygen insertion steps have been proposed. A key difference is the fate of the iron(III)–(hydro)peroxide intermediate, which can either act as the reactive species itself and directly attack a substrate or, alternatively, first undergo O–O bond cleavage to yield HO-Fe(V)=O as the hydroxylating species. Beside the mentioned reactions, Rieske dioxygenases also catalyze oxidative ring closure, desaturation, sulfoxidation, amine oxidation, and O- and N-dealkylation (80, 262, 266).

For catalysis in whole cells (*e.g.*, in biocatalytic applications), both pterin-dependent hydroxylases and Rieske oxygenases depend on the efficient regeneration of reduction equivalents in the form of NAD(P)H via the intracellular redox metabolism or heterologous enzymes (typically dehydrogenases) converting a cosubstrate.

Dioxygenases catalyzing ring cleavage in dihydroxybenzenes do not require an additional electron delivering substrate, since all four electrons for $O_2$ reduction are derived from the substrate (80, 324). Thus, concerning the delivery of reduction equivalents, these enzymes operate independently from intracellular redox metabolism. As the mononuclear enzymes described above, extradiol-cleaving dioxygenases also contain Fe(II) [or Mn(II)] coordinated with the 2-His-1-carboxylate facial triad (343). An ordered mechanism has been proposed with asymmetric catechol binding to the Fe(II) centre as a monoanion followed by $O_2$ binding in an adjacent metal binding site and the transfer of one electron from the substrate via the iron to $O_2$ resulting in the formation of a Fe(II)-superoxo-species involving a semiquinone radical (Fig. 3). Recombination of the resulting radicals leads to the formation of a proximal alkylperoxo intermediate, which undergoes alkenyl migration and heterolytic O-O cleavage to yield a lactone species and a metal-bound hydroxide. The latter hydrolyzes the lactone and the ring-opened product is formed (181, 183, 184).

In contrast to the very recent characterization of the extradiol cleavage mechanism, the catalytic mechanism of intradiol cleaving chatechol dioxygenases containing an [Fe(III)-$(His)_2(Tyr)_2$] active site is established since a longer time. The substrate binds asymmetrically as a dianion replacing one tyrosine residue and a hydroxyl ligand at the ferric iron center (101, 240, 324). This introduces semiquinonate radical character to bound substrate and makes it susceptible to $O_2$ attack generating a transient alkylperoxoiron(III) intermediate. O–O bond cleavage and acyl migration then result in the formation

of muconic anhydride and an Fe(III)-OH species acting as the nucleophile to convert the anhydride into muconic acid. As a difference to intradiol cleavage, acid-base catalysis by means of outer sphere amino acids and binding of the alkylperoxo intermediate in a tridentate rather than a bidentate fashion were proposed to favor alkenyl over acyl migration during extradiol cleavage (58). Overall, extradiol dioxygenases appear to be more versatile than their intradiol counterparts, as the former cleave a wider variety of substrates (324).

Lipoxygenases, catalyzing the hydroperoxidation of polyunsaturated fatty acids via $O_2$ incorporation, also involve Fe(III) with a histidine-rich ligand environment. Fe(III) has been proposed to activate the substrate by hydrogen abstraction yielding Fe(II) and a carbon centered radical intermediate (120). This is followed by $O_2$ addition to the activated radical species, producing a peroxy radical intermediate, which can reoxidize Fe(II) to Fe(III) forming the hydroperoxy product (2). Remarkably, the resting as-isolated Fe(II) containing enzyme is activated by the fatty acid hydroperoxide product (274). Lipoxygenases are primarily involved in the synthesis of secondary metabolites and the metabolism of endo- and xenobiotics (188) and do not require an additional electron source. Thus, as the ring cleaving dioxygenases, these enzymes do not directly depend on the intracellular redox metabolism.

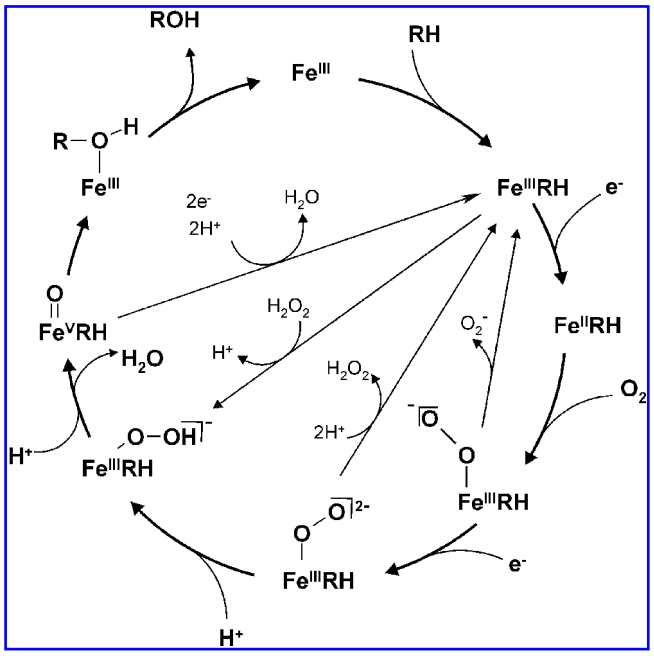


**FIG. 4. Generalized CYP450 reaction cycle showing the three possible uncoupling reactions and the peroxide shunt pathway.** Figure adapted from Julsing *et al.* (161).

3. Heme-dependent monooxygenases. Heme monooxygenases harbor a protoporphyrin IX tetrapyrrole system containing one catalytic iron nucleus; the resulting prosthetic group is designated a heme group. Such heme monooxygenases usually belong to the class of cytochrome P450s and catalyze, except for dioxygenations, a range of reactions as broad as found for nonheme iron oxygenases. Mammalian cytochrome P450 monooxygenases have been thoroughly studied in the context of drug metabolism and hormone biosynthesis (127, 128, 371), whereas microbial P450 monooxygenases typically are investigated with respect to the degradation and biotransformation of xenobiotics and hydrocarbons (321, 328). Thus, although P450s have so far hardly been used for biotechnological processes, these enzymes are highly interesting candidates for biocatalytic applications (28, 161, 322). The majority of the cytochrome P450 systems reported to date are multicomponent enzymes with additional proteins for the transport of reducing equivalents from NAD(P)H to the terminal cytochrome P450 component. Typical electron transfer chains of class I P450 systems (bacterial or from mammalian adrenal mitochondria, soluble, NADH as typical electron donor) consist of a NADH:ferredoxin oxidoreductase and a ferredoxin, whereas class II P450 systems (mammalian hepatic drug-metabolizing isoforms, membrane bound, NADPH as typical electron donor) include a flavin containing P450 reductase (306). An exception is cytochrome P450 BM-3 of *Bacillus megaterium* that consists of a single soluble polypeptide with a P450 domain and an electron transport domain of the microsomal type (class II) (224). Nitric acid synthases (NOS) constitute a special class of heme-dependent monooxygenases being active as a Zinc-stabilized homodimer. Each monomer consists of a heme-containing oxygnease domain and an FAD- and FMN-containing class II-type reductase domain connected by a short domain, which must bind calmodulin to enable electron transfer (123, 239). NOS catalyzes the two-step oxygenation of L-arginine to L-citrulline and nitric oxide, an important cell signaling molecule. Thus, NOS does not have synthetic potential but fulfills important physiological fuctions in mammalian cell communication, immune defence, and vascodilation and in bacterial pathogenesis and defense against oxidative stress and antibiotics.

The heme group of P450 monooxygenases is directly involved in the oxidation process by activating $O_2$. According to their nicotine amide cofactor dependence, cytochrome P450 catalysis is directly coupled to central catabolic or anabolic pathways in living cells. Up to the present, the catalytic cycle (Fig. 4), by which cytochrome P450-mediated hydroxylation occurs, has been intensively studied (78, 126, 219, 225, 230, 231, 286, 296). According to the present understanding, substrate binding is followed by a first electron transfer from NAD(P)H via the electron transfer chain to the heme iron and reversible $O_2$ binding to give a superoxide–iron complex. A second reduction gives peroxo-iron, which is protonated to give hydroperoxo-iron. A second protonation either results in water abstraction and the formation of an iron-oxo species, the prototype oxidant in P450 catalysis, or gives iron-complexed hydrogen peroxide depending on whether the distal or the proximal oxygen atom is protonated. Thereby, cytochrome P450-catalyzed hydroxylation was proposed to involve multiple mechanisms and oxidants including hydroperoxo-iron, iron-complexed hydrogen peroxide, and two different spin states of the iron-oxo species. Hydrogen peroxide can dissociate at the (hydro)peroxo stage being one of the three possible uncoupling mechanisms (Fig. 4). This dissociation is reversible, and P450 enzymes can be shunted with hydrogen peroxide to give an active oxidant (see also peroxidases below). The efficiency of this hydrogen peroxide shunt has been improved by directed evolution (75, 158).

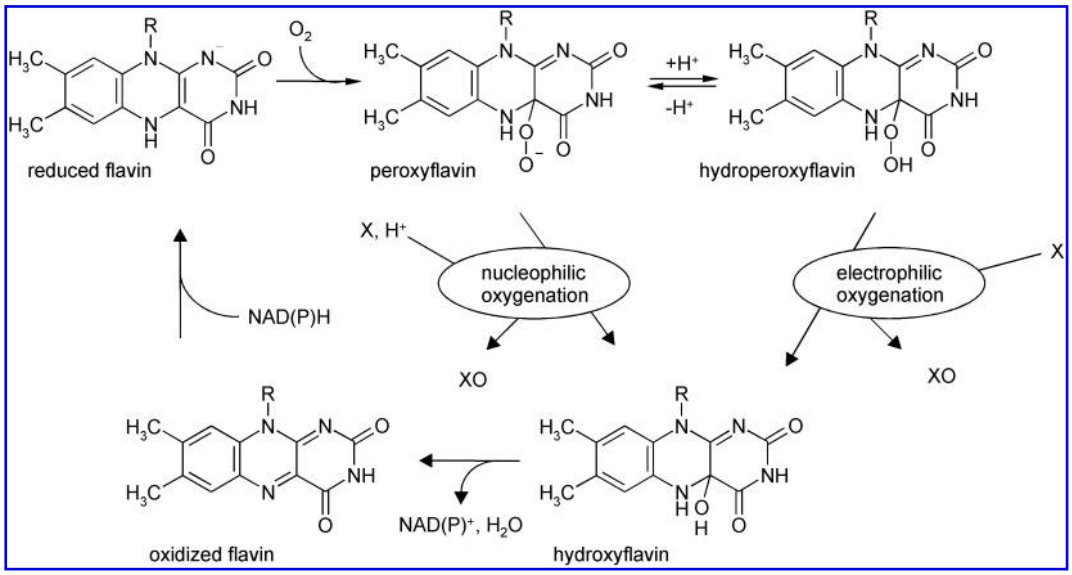


**FIG. 5. General mechanism of oxygenation reactions catalyzed by flavin dependent monooxygenases, for which NAD(P)H is delivering the necessary electrons.** Figure adapted from van Berkel *et al.* (330).

4. Flavin-dependent oxygenases. Flavin-dependent oxygenases also functionalize a wide variety of substrates (210, 330). Reactions catalyzed include epoxidations (165, 191, 241, 245, 246), aromatic hydroxylations (223), Bayer–Villiger oxidations (164, 220), and heteroatom oxyfunctionalizations (376), but no oxygenations of $sp^3$-hybridized carbons (see also Table 1). In contrast to flavin-dependent oxidases, the flavin is not covalently bound in flavoprotein monooxygenases. Depending on the type of enzyme, flavin is tightly (noncovalently) bound and reduced in the monooxygenase moiety itself or acts as an electron shuttle being reduced by a separate reductase component and then bound and stabilized by the monooxygenase component. In either case, the electrons are derived from NAD(P)H, thus involving a direct coupling to the redox metabolism of living cells. Peroxyflavin or hydroperoxyflavin are the activated oxygen species responsible for the nucleophilic or electrophilic attack of substrates, respectively (Fig. 5), and are formed via the reaction of reduced flavin (in most cases $FADH_2$) with $O_2$ in the following way (209, 330): Upon a one-electron transfer from reduced flavin to $O_2$, a complex of superoxide and the flavin radical is formed. Upon spin inversion, for most flavoprotein monooxygenases, a covalent adduct between the $C_{(4a)}$ of the flavin and dioxygen is formed yielding the above mentioned reactive $C_{(4a)}$-(hydro)peroxyflavin species. Such a peroxyflavin is unstable and typically decays to form hydrogen peroxide and oxidized flavin. However, flavoprotein monooxygenases are able to stabilize this species in such a way that it can oxygenate a substrate. As a result of nucleophilic or electrophilic attack on the substrate, a single oxygen atom is incorporated into the substrate, while the other oxygen atom is reduced to water. The specific type of oxygenation and selectivity depends on the shape and chemical nature of the active site of the specific enzyme.

### B. Peroxidases

The classical peroxidase reaction consists in a one-electron oxidation of the substrate with hydrogen peroxide or organic peroxides as electron acceptors. However, heme-dependent peroxidases also catalyze a large variety of oxygen transfer reactions, including olefin epoxidations, sulfoxidations, and allylic, propargylic, and benzylic hydroxylations; but no aliphatic hydroxylations have been reported (3, 320, 334, 337). As mentioned above, specific oxygen transfer reactions are of high synthetic interest. Thus, the mechanism of peroxidase-mediated oxygen transfer is described below in more detail. These reactions do not require the external addition of coenzymes or their regeneration (*e.g.*, by intracellular redox metabolism). In such two-electron oxidations, a peroxide serves as oxygen donor and electron acceptor and one molecule of water (or alcohol in the case of organic peroxide driven reactions) is produced as a co-product. In catalyzing these oxygen transfer reactions, heme-dependent peroxidases exhibit a reactivity more typical for cytochrome P450 monooxygenases than that of classical peroxidases, which typically catalyze oxidative dehydrogenation reactions via one-electron processes. Heme-dependent peroxidases are structurally and functionally related to P450 monooxygenases, which also catalyze substrate oxyfunctionalizations with hydrogen peroxide as oxygen source in the so-called peroxide shunt pathway (see above). In both, hydrogen peroxide enters the catalytic cycle at the hydroperoxo-stage coordinating as a hydroperoxoanion to Fe(III) (Fig. 4). The same oxidants and oxygen transfer mechanisms have been proposed for these two enzyme groups. However, oxygen transfer from oxidized peroxidase to the substrate is only possible when the heme iron is accessible for the substrates. In contrast to P450 enzymes, the fifth (proximal) ligand of the iron atom is a histidine, except in chloroperoxidase from *Caldariomyces fumago* (CPO), which belongs to the group of haloperoxidases (90, 142). With respect to oxygen transfer reactions, this heme-thiolate peroxidase with iron ligated to cysteine, similar to P450, is the most versatile enzyme of the known peroxidases.

An advantage of peroxidases is that they need no additional electron acceptor or donor and thus no regeneration of cofactors such as NAD(P/H). However, a major shortcoming

is the low operational stability of peroxidases, generally resulting from peroxide-induced deactivation (325). An example is the facile oxidative deterioration of the porphyrin ring in heme-dependent peroxidases such as CPO, necessitating the maintenance of low hydrogen peroxide concentrations, and/or the in situ generation of hydrogen peroxide from $O_2$ with a chemical reductant or an oxidase (247, 331).

### C. Oxidases

The most familiar oxidase enzymes are not involved in biosynthetic reactions, but play a pivotal role in metabolism, serving as terminal electron acceptors in energy storage pathways. There are, however, many oxidases that make use of the oxidizing potential of $O_2$ to promote biosynthetic reactions. Thereby, oxidases couple the one-, two-, or four-electron oxidation of substrates to the two- or four-electron reduction of $O_2$ to hydrogen peroxide or water and thus do not require the external addition or regeneration of coenzymes. Oxidases catalyze a variety of synthetically interesting oxidation reactions including the oxidation of amines (amino acid oxidases), the oxidation of alcohols, for example, in sugars, oxidative ring closure, oxidative decarboxylation, and hydroxylation reactions. The latter are rather atypical for oxidases, since $O_2$ only serves as electron acceptor and not as oxygen donor. Catalytic centers of oxidases typically contain flavin, iron, or copper. The respective characteristics and mechanisms are reviewed in the following three subsections.

1. Flavin-dependent oxidases. Among flavin-dependent enzymes, the vanillyl-alcohol oxidase (VAO) family forms a prominent and synthetically interesting group (197). For example, the flavin-dependent vanillyl-alcohol oxidase from *Penicillium simplicissimum* catalyzes both the benzylic desaturation and the benzylic hydroxylation of *para*-alkylphenols, depending on the nature of the aliphatic side chain (333, 334). The mechanisms include substrate oxidation by the flavin to *para*-quinone methides as common intermediates and differ in whether water attacks the methide. Thus, in contrast to flavin-dependent oxygenases (Fig. 5), the flavin is not reduced by NAD(P)H but directly by the substrate and the introduced oxygen atom in case of benzylic hydroxylation is derived from water as in the case of hydroxylating dehydrogenases (see below). The reduced flavin transfers the electrons to $O_2$, and, as another difference to flavin-dependent oxygenases, the resulting hydroperoxyflavin is not stabilized leading to hydrogen peroxide formation. A remarkable feature of this oxidase family is that it favors the covalent attachment of the flavin cofactor, which distinguishes them from flavin-dependent oxygenases. Remarkably, also some $O_2$-independent dehydrogenases such as *p*-cresol methylhydroxylase and eugenol hydroxylase (47, 145) (see below) belong to the VAO flavoprotein family (197). Interestingly, a gatekeeper residue was recently identified in the family member L-galactono-$\gamma$-lactone dehydrogenase, which prevents this enzyme from acting as an oxidase (198). When the alanine at position 113 was exchanged with a glycine, allowing $O_2$ to approach the isoalloxazine moiety of the flavin, the enzyme turned into an oxidase. Structurally equivalent positions in oxidases of this family are typically occupied by a glycine or a proline residue.

2. Iron-dependent oxidases. Several biosynthetic oxidases are known to belong to the mononuclear nonheme iron enzyme family featuring the 2-His-1-carboxylate facial triad (Fig. 3) introduced above in the oxygenase section (178, 183). The mechanisms of $O_2$ activation proposed for this subgroup are very diverse, but they contain elements of the mechanisms discussed above for the oxygenases of the same group. The general strategy appears to involve the binding of both the substrate and $O_2$ to the iron as in the extradiol and 2-oxo acid dioxygenases. This promotes electron transfer away from the substrate and (in most cases) the iron. The reduced dioxygen species then undergoes O-O bond cleavage to yield a molecule of water and leave an Fe(IV)=O species as in the 2-oxo acid-dependent oxygenases and pterin-dependent hydroxylases. Finally, the high-valent iron species is used as a reagent to complete a second part of the reaction, and in doing so accepts two more electrons to form the second molecule of water. Some well-studied examples of oxidases featuring the 2-His-1-carboxylate facial triad are isopenicillin N-synthase (IPNS, Fig. 3) (56, 268), fosfomycin synthase (FOS) (369), and 1-aminocyclopropane-1-carboxylate oxidase (ACCO) forming ethylene as a hormone in plants (221). These enzymes activate $O_2$ and ultimately form water using either four electrons from the substrate (IPNS), two from the substrate and two from NADH (FOS), or two from the substrate and two from ascorbate (ACCO).

3. Copper-dependent oxidases. Copper-containing oxidases catalyze the oxidation of a wide variety of substrates ranging from small molecules such as solvated $Fe^{2+}$ and methane to large peptides. Four different groups of copper-containing oxidases are distinguished: mononuclear enzymes containing sulfur-ligated copper (type 1), mononuclear copper sites with nonsulfur ligation (type 2), dinuclear copper oxidases (type 3), and multi-copper oxidases (216). Type 1 copper proteins, such as azurin, do not function as oxidases in the common sense but as electron transfer proteins.

Amine oxidases (AOs) are typical type 2 copper oxidases and catalyze the oxidative deamination of primary amines to produce the corresponding aldehydes, hydrogen peroxide, and ammonia (53, 356). The two-electron chemistry is carried out at a redox site that consists of a mononuclear Cu(II) ion and an organic cofactor, 2,4,5-trihydroxylphenylalanine quinone (TPQ), which is derived from the post-translational modification of an endogenous tyrosine. The reaction is initiated by the reductive half-reaction, in which the TPQ cofactor in the resting enzyme undergoes nucleophilic attack by the primary amine substrate to form a Schiff base followed by an aspartate-mediated proton abstraction resulting in a carbanionic intermediate (Fig. 6). Rearrangment and hydrolysis leads to the release of product aldehyde and the formation of aminoquinol. The oxidative half-reaction uses $O_2$ to regenerate the resting enzyme via a postulated iminoquinone intermediate to release hydrogen peroxide. Hydrolysis of the iminoquinone is presumed to release $NH_3$ and regenerate the resting enzyme.

Type 3 and multi-copper oxidases catalyze the four-electron reduction of $O_2$ to water coupled to the concomitant one-electron oxidation of a substrate (71). Tyrosinases are a prominent example for a type 3 copper oxidase and catalyze the oxidation of both monophenols (cresolase or monophenolase activity) and *o*-diphenols (catecholase or diphenolase activity) into reactive *o*-quinones (130). In the cresolase cycle, the four-electron reduction of one molecule of $O_2$ is coupled

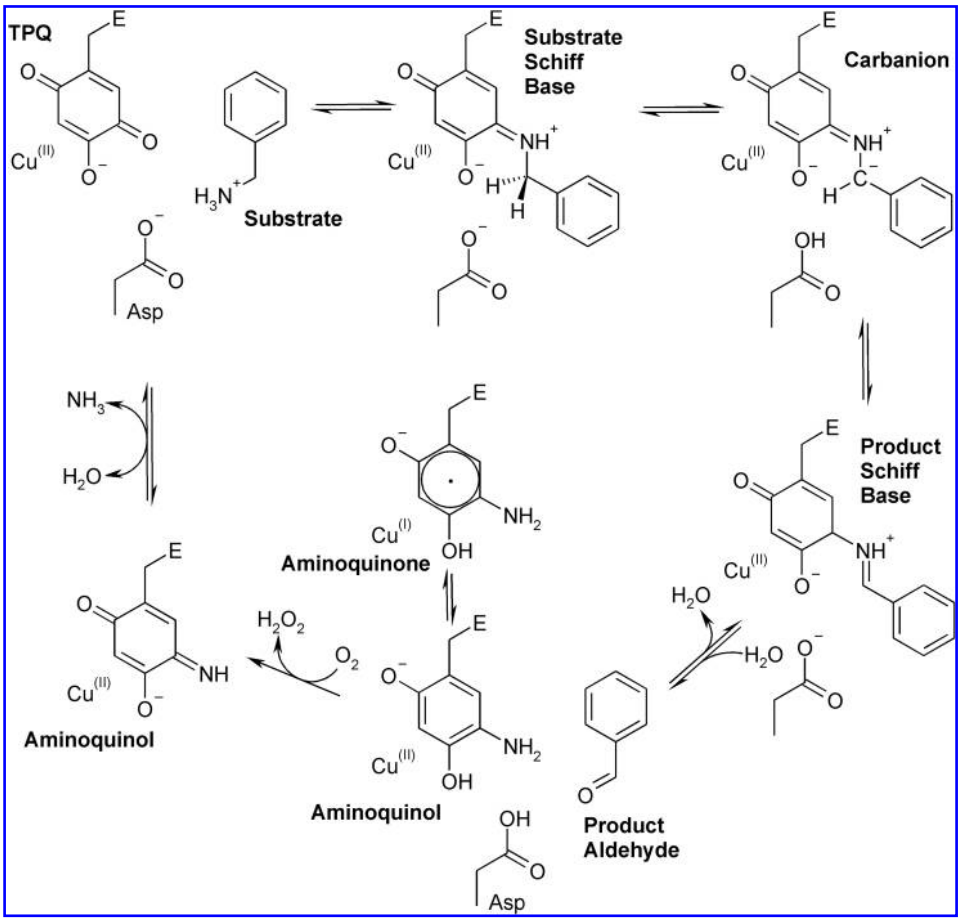


**FIG. 6. Proposed catalytic cycle of copper-containing amine oxidases (AOs).** TPQ is the cofactor, 2,4,5-trihydroxyphenylalanine quinone, which is derived from a constitutive Tyr that is part of the polypeptide of the enzyme (E). The substrate shown is the aromatic primary amine, benzylamine, a typical substrate of some amine oxidases, such as the AO from *E. coli*. Figure adapted from Brazeau *et al*. (53).

to the four-electron oxidation of one monophenol unit via diphenol to an *o*-quinon, whereas in the catecholase cycle, it is coupled to the secessive two-electron oxidation of two diphenol molecules (72). The active site of tyrosinases can exist in three intermediate states: deoxy (CuI–CuI), oxy (CuII–$O_2$–CuII) and met (CuII–CuII). The met-form is converted into the deoxy-form in a two-electron reduction with concomitant diphenol oxidation, and the resulting deoxy-form is able to reversibly fix $O_2$, leading to the oxy-form. The predominant (resting) met-form is not able to bind $O_2$ and thus does not act on monophenols, but has an important affinity for them and binds them through a dead-end pathway resulting in a lag period. This characteristic initial lag in the cresolase cycle can be abolished by addition of low amounts of *o*-diphenols. In fact, it is recognized that, *in vivo*, L-DOPA (3,4-dihydroxyphenylalanine) is responsible for the recruitment of the resting enzyme by reducing met-forms to deoxy-forms.

The active site of multi-copper oxidases, for which laccase is a prominent and versatile example, contains at least four copper atoms, which are one type 1 copper and a trinuclear cluster consisting of one type 2 and two type 3 coppers (358). The catalytic properties of such active sites have been attributed to the following three major steps (303, 305): Reduction of type 1 copper by electrons from the reducing substrate, electron transfer over ~13 Å from type 1 copper to the trinuclear cluster, and activation and reduction of $O_2$ to water at the trinuclear cluster.

Since oxidase and peroxidase catalysis typically is not dependent on an additional electron source such as NAD(P)H and thus does not require the addition of an organic cosubstrate for its regeneration, these enzymes are usually applied *in vitro*, where they are independent from cell metabolism. Thus, applications of these enzymes are not further discussed in this review. In this respect, enzyme deactivation by reactive oxygen species and the addition or removal of hydrogen peroxide are most critical.

### *D. Dehydrogenases*

Dehydrogenases typically catalyze reversible hydrogen transfer reactions. The synthetically most interesting dehydrogenase-catalyzed reactions include ketone reductions, reductive aminations, double bond reductions, alcohol oxidations, and aldehyde oxidations. The respective dehydrogenases can be classified into five distinct groups depending on their prosthetic group:

- Zinc-dependent enzymes
- Flavoprotein dehydrogenases
- Pterin-dependent enzymes
- Quinoprotein dehydrogenases
- Enzymes without prosthetic groups

1. Zinc-dependent dehydrogenases. Zinc-dependent dehydrogenases comprise mainly alcohol dehydrogenases (ADHs), which are grouped according to their substrate spec-

tra and structure into long-, medium-, and short-chain alcohol dehydrogenases (159). They catalyze the oxidation of primary and secondary alcohols to the corresponding aldehydes and ketones, respectively, utilizing the cofactor NAD(P)H for the transfer of the necessary hydride. Most Zn-dependent ADHs perform this redox reaction in a chemo-, regio-, and stereoselective way for a great variety of substrates and are exploited for the synthesis of building blocks for pharmaceuticals or specialty chemicals. As alcohol dehydrogenations typically are reversible reactions, Zinc-dependent ADHs also catalyze the reduction of ketones and aldehydes to the corresponding alcohols, which makes them flexible biocatalysts for a variety of redox reactions. Structure–function studies have mainly been accomplished for the Zinc-depending medium-chain horse liver alcohol dehydrogenase (HLADH), revealing a nucleotide binding domain and a catalytic domain, with the catalytically active zinc buried between them (14). In the absence of substrate, the zinc is coordinated to the three well conserved residues Cys-46, His-67, and Cys-174 of the active site and a water molecule, thus forming a tetrahedrical coordination shell (14, 99). The two main mechanisms proposed for alcohol oxidation by HLADH differ specifically in the coordination of the zinc during the redox reaction. One hypothesis proposes that the zinc ion also stays in tetrahedrical coordination during catalysis, as the water molecule bound in the inactive state is displaced upon substrate binding by the hydroxyl group of the alcohol (96, 99). In the subsequent redox reaction, two hydrogen atoms are removed from the substrate by coupled processes of proton abstraction and hydride ion transfer based on a proton relay system that is stabilized by the positive charge on the enzyme-bound zinc ion. Collapse of the intermediate to the ketone or aldehyde with the concomitant hydride transfer to $NAD(P)^+$ completes the reaction. Another possibility discussed is based on a change of the coordination symmetry of the zinc towards a pentacoordinated zinc, by the binding of the substrate in addition to the water molecule, followed by the same steps as described above. Recent studies on HLADH (21) and TbADH (*Thermoanaerobacter brockii*) (173) by X-ray crystal structure determination and time resolved X-ray absorption fine structure analyses (XAFS), respectively, revealed more evidence pointing in the direction of the latter mechanism, although both studies point towards pentacoordinated transient intermediates rather than a pentacoordinated Zinc during the whole reaction. The structural mechanism in the sourrounding of the catalytic zinc as proposed by Kleifeld and coworkers for TbADH are shown in Figure 7. The first coordination shell (without substrate) in TbADH differs from other described ADHs, as the catalytic Zinc is bound to three conserved residues, in this case Cys37, His59, and Asp150, and instead of water to a fourth amino acid, Glu60. There are strong indications that Glu60 is exchanged by a water molecule during catalysis involving the formation of a pentacoordinated intermediate. Substrate binding and conversion leads to further pentacoordinated intermediates.

For biocatalytic applications using whole cells, it has generally to be considered that reactions catalyzed by Zinc-dependent dehydrogenases are coupled to intracellular carbon and energy metabolism via nicotin adenine dinucleotide cofactors. Depending on the oxidative or reductive direction of catalysis, $NAD(P)^+$ or NAD(P)H have to be regenerated, respectively.

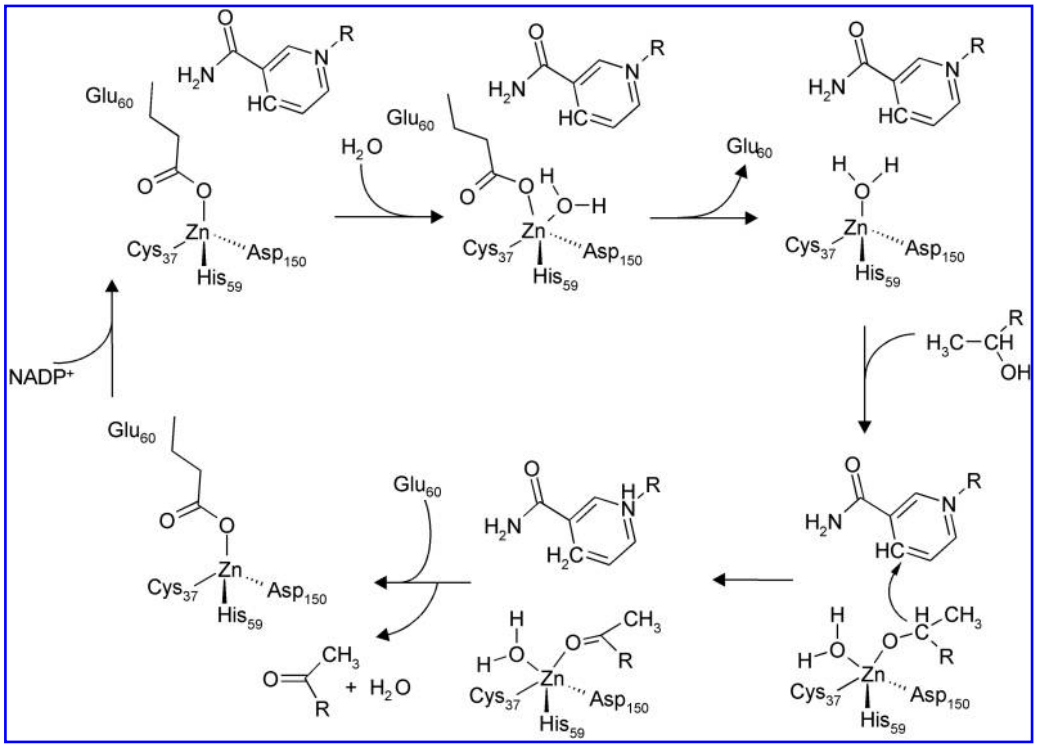


**FIG. 7. Reaction mechanism of TbADH as proposed by Kleifeld *et al.* (173).** Reaction occurs via transient pentacoordinated intermediates of the catalytic zinc (Zn). For details, see text.

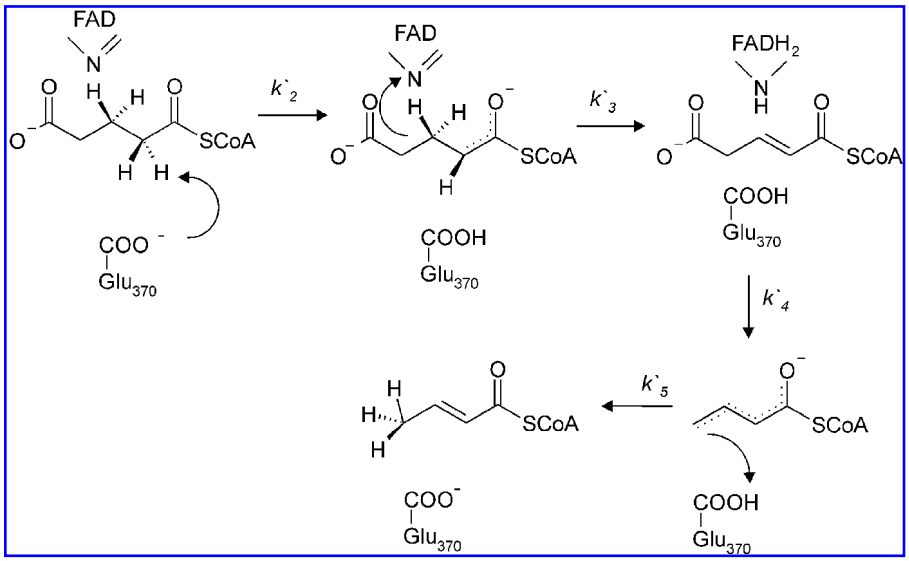


**FIG. 8. Covalent bond-breaking and forming reactions occurring within the active site of Glutaryl-CoA dehydrogenase during the conversion of glutaryl-CoA to crotonyl-CoA.** Neither substrate binding nor product release is shown. Figure adapted from Rao *et al*. (265).

2. Flavoprotein dehydrogenases. Enzymes containing FAD as prosthetic group either covalently or noncovalently bound are mostly involved in $O_2$ activation reactions. Flavin-containing dehydrogenases are important enzymes in the redox metabolism, but less used for synthetic applications. Acyl-CoA dehydrogenases compose a family whose members are highly conserved in sequence, structure, and function. They are important in the mitochondrial oxidation of lysine, hydroxylysine, and trypthophan. As in the case of flavin-dependent oxidases, FAD serves as an electron acceptor during the oxidation of the substrate and, in contrast to the oxidases, delivers the electrons to the respiratory chain and not directly to $O_2$. For glutaryl-CoA dehydrogenase (GCD), the enzymatic mechanism has been investigated in detail (265). GCD has a homotetrameric structure containing one noncovalently bound FAD per monomer. The reductive half-reaction of the dehydrogenase flavin generates the enzyme-bound intermediate glutaconyl-CoA, which is subsequently decarboxylated to yield crotonyl-CoA and $CO_2$ (Fig. 8). Upon binding of the substrate glutaryl-CoA, a glutamate residue functioning as a catalytic base (Glu370 in human GCD) abstracts an $\alpha$-proton from the substrate, followed by hydride transfer from the C-3 position of the substrate to the flavin yielding the $2e^-$-reduced form of FAD and the enzyme-bound desaturated intermediate glutaconyl-CoA (118, 199). Subsequently, the latter is decarboxylated by breaking the $C_\gamma$ - $C_\delta$ bond resulting in formation of a dienolate anion and $CO_2$. Protonation of the dienolate anion occurs via proton transfer to C-4 from the catalytic base Glu370, which can exchange its proton with solvent water (264). Finally, this protonation gives rise to the crotonyl-CoA product. The $2e^-$-reduced form of FAD is reoxidized in two consecutive oxidation steps, transferring the electrons to the respiratory chain.

Beside flavoproteins containing only the flavin in the catalytic center, there are two-component dehydrogenases, which have a covalently bound flavin in one subunit and a cytochrome in the other (84, 104). Examples for hydroxylating flavocytochromes include 4-cresol dehydrogenase (47, 146) and eugenol dehydrogenase (117) found in *Pseudomonas putida* strains or denitrifying bacteria. After fast electron transfer from the flavin to the cytochrome, 4-cresol dehydrogenase transfers the electrons to azurin or nitrate as physiological electron acceptors. The reaction mechanism was first described by Hopper *et al*. (144). During the reaction, a proton is removed from the hydroxyl group of the substrate *p*-cresol and a hydride ion is transferred from the methyl group to the N5 atom of the covalently bound flavin. The so-formed quinone methide intermediate then undergoes a nucleophilic attack of water at the methylene group, yielding *p*-hydroxybenzyl alcohol. For synthetic applications using whole cells, the physiological electron acceptor has to be made available via metabolism-linked regeneration. If regeneration is not feasible as in the case of nitrate, the reduced electron accepter (*e.g.*, nitrite) is further converted or excreted.

3. Pterin-dependent enzymes. Pteridin-dependent dehydrogenases also belong to the group of hydroxylating enzymes, which use water as electron donor. Molybdenum typically is coordinated to the two thiol groups of a pyranopterin-based cofactor, constituting the so-called molybdopterin cofactor (139). These enzymes can be composed of a variable number of subunits and contain different additional cofactors such as hemes, iron–sulfur clusters, and flavins, which transfer electrons from the molybdopterin cofactor to an electron acceptor. Such molybdoenzymes typically catalyze the hydroxylation of relatively activated carbon atoms (*e.g.*, heteroaromatic ring carbon). Furthermore, selenium has been reported to be involved in reactions catalyzed by xanthine dehydrogenase (238) and nicotinate dehydrogenases of anaerobic strains (119), for which $NAD^+$ and $NADP^+$ serve as electron acceptors, respectively. However, nicotinate dehydrogenases from aerobic strains have been reported to be selenium independent (150). The natural external electron acceptors for these enzymes are not known so far although membrane-bound dehydrogenases have been suggested to transfer electrons directly to the respiratory chain (10). Ethylbenzene dehydrogenase of *Azoarcus*-like strains is an especially interesting molybdoenzyme as it hydroxylates an unactivated benzylic carbon (157, 175). Kniemeyer *et al*. suggested that redox centers in this enzyme as well as the unknown natural electron acceptor should have high redox potentials to achieve reasonable oxidation rates with the ra-

ther inert hydrocarbon substrate (175). The reaction mechanism has been characterized best for xanthine dehydrogenase. A Mo(VI) in the resting state with a water-derived oxo- or hydroxyl-group in the ligand sphere is reduced to Mo(IV) during substrate oxidation and then is reoxidized by electron transfer to an iron–sulfur cluster. Hydroxylation might be initiated either by a nucleophilic attack by a hydroxy-ligand or by attack of a substrate cation on an oxo-ligand (139). Also here, the interaction with intracellular redox metabolism has to be considered for synthetic applications. For pterin-dependent enzymes, this interaction depends on the nature of the physiological electron acceptor of the employed enzyme.

4. Quinoprotein dehydrogenases. Quinoproteins function as primary dehydrogenases, which transfer reducing equivalents directly to the bacterial aerobic respiratory chain and are located in the periplasm. Thus, they are highly interesting regarding redox metabolism. They are involved mainly in the dehydrogenation of primary or secondary hydroxyl groups in alcohols and sugars and are applied mainly in biosensors (213). Quinoproteins contain an amino acid-derived *o*-quinone as a cofactor. Different kinds of quinone cofactors are known, but only pyrroloquinoline quinone (PQQ) is not covalently bound to the enzyme and is involved in oxido-reduction reactions (11). Mainly two dehydrogenases of this class, in which PQQ is the only cofactor, have extensively been studied. These are the membrane-bound glucose dehydrogenase (mGDH) and the soluble methanol dehydrogenase (MDH). The mechanisms of both enzymes have recently been reviewed (12, 88). MDH catalyzes the oxidation of methanol to formaldehyde. Upon substrate binding, the oxidation reaction is initialized by a base located in the active site (most likely an aspartate), which is mainly responsible for the abstraction of the proton from the alcohol group (4). $Ca^{2+}$ coordinated to the C-5 of the cofactor acts as a Lewis acid during substrate oxidation and stabilizes the C-5 carbonyl atom for the electrophilic attack by the hydride (150). The proton abstraction is directly followed by a direct hydride transfer from the methyl group of methanol to the C-5 of PQQ followed by tautomerization to $PQQH_2$ (375). The now oxidized product formaldehyde is released, while $PQQH_2$ is reoxidized by sequential single-electron transfer to a c-type cytochrome in the electron transport chain.

The membrane-bound glucose dehydrogenase oxidizes a wide range of pentoses and hexoses (83). In the cell, it is responsible for the direct oxidation of glucose to gluconate in the periplasm. The mechanism of substrate oxidation is very similar to the one described for methanol oxidation by MDH. The reaction is initiated by an aspartate, which abstracts a proton form the anomeric hydroxyl group of glucose, followed by a hydride transfer from the C-1 of the glucose molecule to the C-5 carbon of the PQQ cofactor, yielding the product gluconolactonate and $PQQH_2$. Subsequent oxidation of $PQQH_2$ involves either ubiquinon or *c*-type cytochromes as electron acceptors in the electron transport chain. mGDH from *E. coli* harbors two ubiquinone binding sites (102). One site is located near the active site and contains a tightly bound ubiquinone, which performs single electron transfer steps. The second site is situated in the amphiphilic segment of the membrane bound mGDH and reversibly binds ubiquinone from the membrane pool.

5. Dehydrogenases without prosthetic groups. Most oxidoreductases require metals or organic prosthetic groups for a successful hydride transfer. However, several dehydrogenases are known that have neither metal ions nor any other prosthetic group bound to their active site. These enzymes make good models to study the mechanism of hydride ion transfer in the active site because the reaction is devoid of proton transfer steps. The most prominent example of such enzymes is formate dehydrogenase (FDH), which is well known from an application point of view, as it is the basis for many established cofactor regeneration systems in synthetic biocatalysis (352, 374) (see also Section V.B). FDH catalyzes the oxidation of formate to $CO_2$, cleaving a single carbon–hydrogen bond in the substrate and concurrently forming a new one in the nicotinamide-coenzyme, which also accepts the electrons. It has been extensively reviewed (258, 318). In its natural host, FDH is an essential enzyme in the oxidation cycle of glyoxylate. Electrostatic effects are responsible for the correct hydrogen transfer during the FDH-catalyzed reaction. Multiple hydrogen bonds within a positively charged amino acid cluster direct the orientation of the anionic substrate formate, while a negatively charged amino acid cluster and hydrophobic side chains correctly orient the positively charged nicotinamide cofactor $NAD^+$, so that it is placed with one side facing a hydrophobic wall and the other facing the hydrophilic substrate binding site. During the reaction, various stabilizing and destabilizing interactions occur in the active site, including the improvement of the electrophilic properties of the nicotinamide moiety (C4N) of the coenzyme. The $NAD^+$ carboxamide group (C4N) is polarized via interaction with negatively charged ligands and perturbation of its ground state due to the twist of the carboxamide with respect to the pyridine plane. During catalysis, a hydride anion from the substrate formate attacks the electrophilic C4N of the positively charged nicotinamide moiety of $NAD^+$. Consequently, the two uncharged products $CO_2$ and NADH are formed (258).

## III. Microbial Redox Metabolism

Metabolism (metabole (gr.) = change) is the sum of the physical and chemical processes in an organism, by which its material substance is produced, maintained, and destroyed, and by which energy is made available (348a). Metabolism is usually divided into the two categories catabolism and anabolism. Catabolism is the degradation of molecules, yielding energy and the production of reducing agents. Anabolism, on the other hand, is the synthesis of molecules through the use of energy and consumption of reducing agents. Here, we introduce the additional term redox metabolism that we define as the sum of the biochemical modules, in which redox equivalents are produced or consumed. These modules are described in the following sections.

Most of the biological oxidations and reductions of organic substrates require redox cofactors which can be divided into three main classes: (i) dihydropyridines (*e.g.*, NAD/NADH, NADP/NADPH), (ii) flavins (*e.g.*, FMN/$FMNH_2$, FAD/$FADH_2$), and (iii) quinones (*e.g.*, ubiquinone UQ/$UQH_2$, menaquinone MQ/$MQH_2$, pyrroloquinoline quinone PQQ) (263). In the cellular biochemical network, the most abundant redox cofactors are NADH and NADPH. These cofactors serve two different purposes in cellular metabolism; NADH is

mainly used in catabolism and NADPH is the main electron donor in anabolism. More specifically, in aerobes, NADH is mainly involved in the generation of Gibbs free energy through the oxidative phosphorylation reaction (Section III.A.2), while, under anaerobic conditions, NADH is consumed in fermentative pathways (Section III.A.3). The cofactor NADPH is mainly used in the biosynthesis of biomass precursors (Section III.A.5). Both cofactors are reduced in the pathways of central carbon metabolism (Section III.A.1). Moreover, in some organisms, the cofactors are interconverted via nicotinamide nucleotide transhydrogenases, which catalyze the transfer of hydrogen from NADH to $NADP^+$ and *vice versa* (Section III.A.4).

### A. Modules of redox metabolism

1. Central carbon metabolism. Central carbon metabolism generates the energy, redox equivalents, and small-molecule building blocks that are necessary for all cellular functions. For example, the *E. coli* central carbon metabolism consists of approximately 40 reactions that are encoded by roughly 50 genes, including isoenzymes and protein complexes (Fig. 9). Notably, *E. coli* uses three major pathways to convert glucose into pyruvate: the Embden–Meyerhof–Parnas (EMP) pathway, commonly referred to as glycolysis; the pentose phosphate (PP) pathway; and the Entner–Doudoroff (ED) pathway. The major pathway downstream of pyruvate is, beside the fermetative pathways used during anaerobic growth, the oxidative tricarboxylic acid (TCA) cycle.

Genetic analyses of the most ancient archaea and bacteria indicate that the ED pathway, gluconeogenesis, and reductive TCA cycle reactions existed in the last common ancestor of all three domains of life (270). In fact, the reductive TCA cycle is proposed to be the metabolic core of all metabolism and originated before life existed (301). Notably, the catabolic EMP pathway most likely developed from an anabolic, gluconeogenic pathway and the oxidative TCA cycle arose from a reductive pathway.

In the *E. coli* central carbon metabolism, 7 NADH-, 4 NADPH-, and 1 $UQH_2$-dependent enzymes are responsible for the conversion of glucose to $CO_2$ (only the reduced redox cofactors are given; for directionality, see Fig. 9). The cofactor-

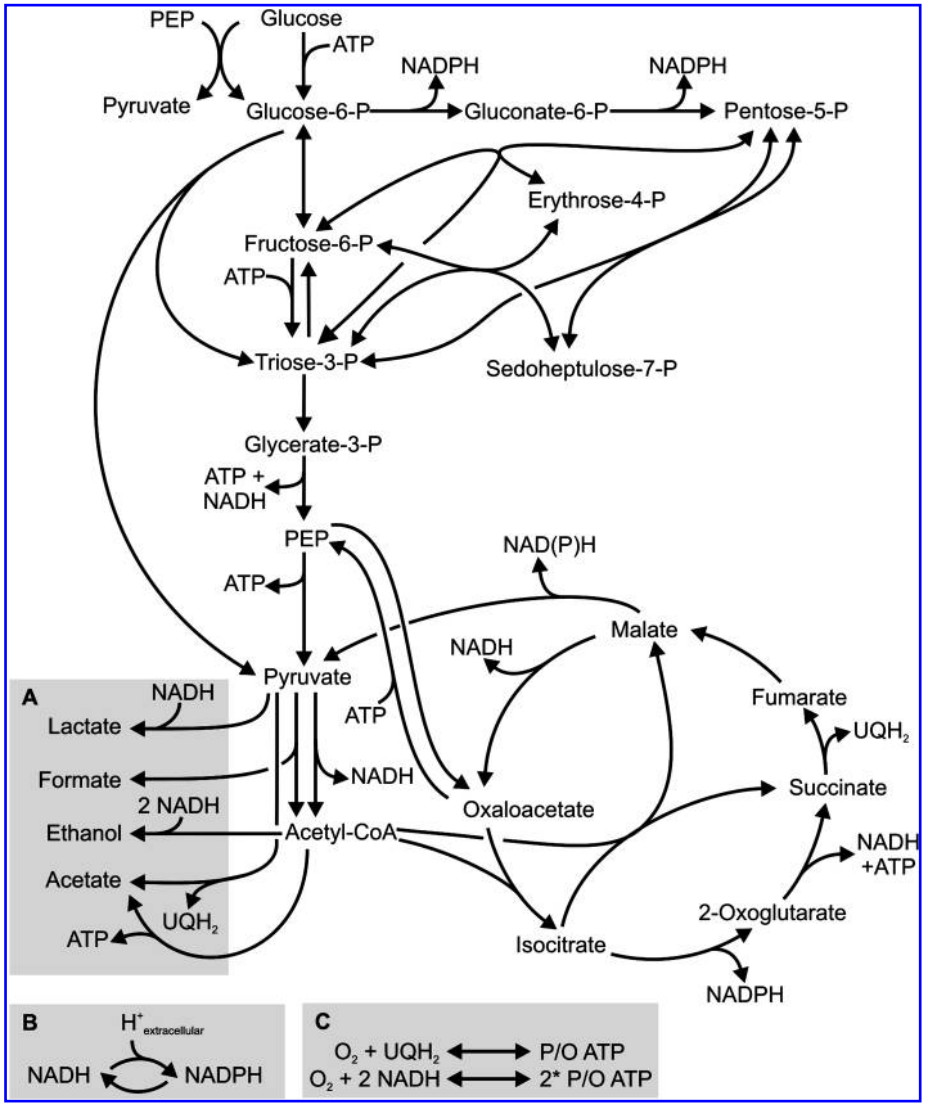


**FIG. 9. Central carbon metabolism of *E. coli*.** The redox cofactor-utilizing reactions are indicated. The fermentative pathways, the two transhydrogenase reactions, and the respiratory chain are shaded in *gray*. Only consumed or produced reduction equivalents (in the form of NADH, NADPH, $UQH_2$) and energy equivalents (in the form of ATP, $H^+_{extracellular}$ for proton gradient exploitation) are indicated. For simplicity, the corresponding reactants ($NAD^+$, $NADP^+$, UQ, ADP, $H^+_{intracellular}$) are omitted. Abbreviation: P, phosphate.

Table 2. Relative Rates of Redox Cofactor-Dependent Reactions During Growth on Minimal Medium with Glucose as Substrate

| *Reaction*[a] | *Enzyme* | *Redox cofactor*[b] | *E. coli aerobe, continuous culture, $D = 0.09\,h^{-1}$, (%)*[c,d] | *S. cerevisiae aerobe, continuous culture, $D = 0.1\,h^{-1}$, (%)*[e] | *S. cerevisiae anaerobe, continuous culture, $D = 0.1\,h^{-1}$, (%)*[f] | *S. cerevisiae respiro-fermentative batch (%)*[g] | *P. putida aerobe batch, (%)*[h] |
|---|---|---|---|---|---|---|---|
| 1 | Glucose-6-phosphate dehydrogenase | NADPH | 44 | 44 | 5 | 11 | 99 |
| 2 | 6-Phosphogluconate dehydrogenase | NADPH | 44 | 44 | 5 | 11 | 11 |
| 3 | Glyceraldehyde-3-phosphate dehydrogenase | NADH | 169 | 127 | 163 | 172 | 86 |
| 4 | Pyruvate dehydrogenase | NADH | 108 | 40 | 4 | 12 | 90 |
| 5 | Isocitrate dehydrogenase | NAD(P)H[i] | 93 | 60 | 3 | 6 | 68 |
| 6 | 2-Ketoglutarate dehydrogenase | NADH | 83 | 49 | 0 | 4 | 55 |
| 7 | Succinate dehydrogenase | $FADH_2$ | 83 | 49 | 0 | 3 | 55 |
| 8 | Malate dehydrogenase | NADH | 75 | 60 | 0 | <1 | 37 |
| 9 | Malic enzyme | NAD(P)H[j] | 7 | 7 | 0 | 0 | 10 |
| 11 | Transhydrogenase | NAD(P)H[k,l] | ca. 80 | - | - | - | ca. 60 |

[a]For corresponding reaction, see Figure 9.
[b]According to biochemistry text books. See (116) and Section III.B.2 for discussion.
[c]Flux normalized to the glucose uptake rate.
[d](103), [e](122), [f](160), [g](34), [h](38).
[i]NADH-dependent in *S. cerevisiae*.
[j]In *E. coli* a $NAD(P)^+$ and a $NADP^+$-dependent isoform exist (43).
[k]Transhydrogenases catalyze the hydrogen transfer from NADH to $NADP^+$ or *vice versa*.
[l]Here, NADPH is the reduced product.

dependent enzymes, the reactions they catalyze, and their relative activities (*i.e.*, flux normalized to glucose uptake rate) under different growth conditions are listed in Table 2 for three distinct microbes.

Glyceraldehyde-3-phosphate dehydrogenase has the highest contribution to NADH regeneration during aerobic growth of organisms with an active EMP pathway on glucose and other sugars (data not shown). This dominance is amplified during anaerobic growth, in which more than 90% of all NADH is formed in this single reaction. An alternate distribution of redox cofactor reduction is observed in organisms that do not use the EMP pathway, such as *P. putida* (Table 2, (115)). In many bacteria, glucose is catabolized primarily via the ED pathway, significantly lowering the flux through glyceraldehyde-3-phosphate dehydrogenase.

The reaction that connects pyruvate synthesis (via the ED, EMP, or PP pathway) with the TCA cycle is the NADH-dependent formation of acetyl-Coenzyme A (-CoA) that is catalyzed by the pyruvate dehydrogenase enzyme complex. Oxidative decarboxylation of pyruvate and acetyl-transfer to CoA involve the reduction of enzyme bound lipoic acid, of which the reoxidation is coupled to NADH formation. The activity of the pyruvate dehydrogenase enzyme complex is highly dependent on the electron donor (*i.e.*, carbon source) and acceptor (*i.e.*, respiratory substrate) that are used. During fermentative growth, this reaction only serves for the synthesis of biomass precursors; hence, the flux from pyruvate to acetyl-CoA is low (Table 2).

Of the many hundred reactions that occur in most cells, only few contribute significantly to redox cofactor reduction. During fermentative growth, these reduced cofactors must be strictly balanced, because no respiratory substrate such as $O_2$ is used as external electron acceptor. The specifics of the fermentative pathways that influence redox biocatalysis are briefly summarized in Section III.A.3.

2. Oxidative phosphorylation. Oxidative phosphorylation is a highly efficient energy-generating pathway composed of the electron transport chain (ETC) and ATP synthase. The ETC, which is located in the mitochondrial (eukaryotes) or cytoplasmic membrane (prokaryotes), is made up of complexes of different redox carriers including flavoproteins, quinones, and cytochromes. It catalyzes the oxidation of NADH, succinate, and a few other reduced substrates by passing electrons sequentially from one carrier to the next. Under aerobic conditions, the common final electron acceptor is $O_2$. Some bacteria use alternative final electron acceptors such as fumarate, nitrate, or nitrite when $O_2$ is absent (anaerobic respiration). Electron transfer in the ETC is coupled to the transfer of protons across the membrane. This efflux of protons creates both a transmembrane pH- and an electrochemical gradient, which is utilized by the ATP synthase to generate ATP. The ATP synthase acts as an ion channel that funnels protons back into the cytoplasm or into the mitochondrial matrix. During this reflux, energy is released, which is used to drive the phosphorylation of ADP to ATP.

Whereas the composition of the ETC in eukaryotic cells is more or less uniform, prokaryotic ETCs show a much greater diversity. Depending on the environmental conditions, bacteria synthesize different transmembrane complexes and produce different ETCs. As shown in Figure 10, *E. coli* possesses two different membrane bound NADH-dehydrogenases NDH-I (237) and NDH-II (31) and three ubiquinol oxidases [cytochromes *bd*-I, *bd*-II, and *bo* (86, 257)]. Due to the different $H^+/2e^-$ stoichiometries of these enzymes, the overall proton transfer per oxidized NADH molecule can vary between 2 and 8 $H^+/2e^-$. Assuming an $H^+$/ATP stoichiometry of 4, a 5-fold difference in ATP yield on glucose between these two extremes can be obtained (26). Bekker *et al.* observed a decrease in the specific $O_2$ consumption rate of 47% during glucose-limited growth of an *E. coli* mutant deficient in the cytochrome *bd*-II oxidase compared to the wild-type strain (26), indicating that, even under energy source limitation, the flux of electrons through the nonelectrogenic (no proton translocation) cytochrome *bd*-II oxidase is significant in wild-

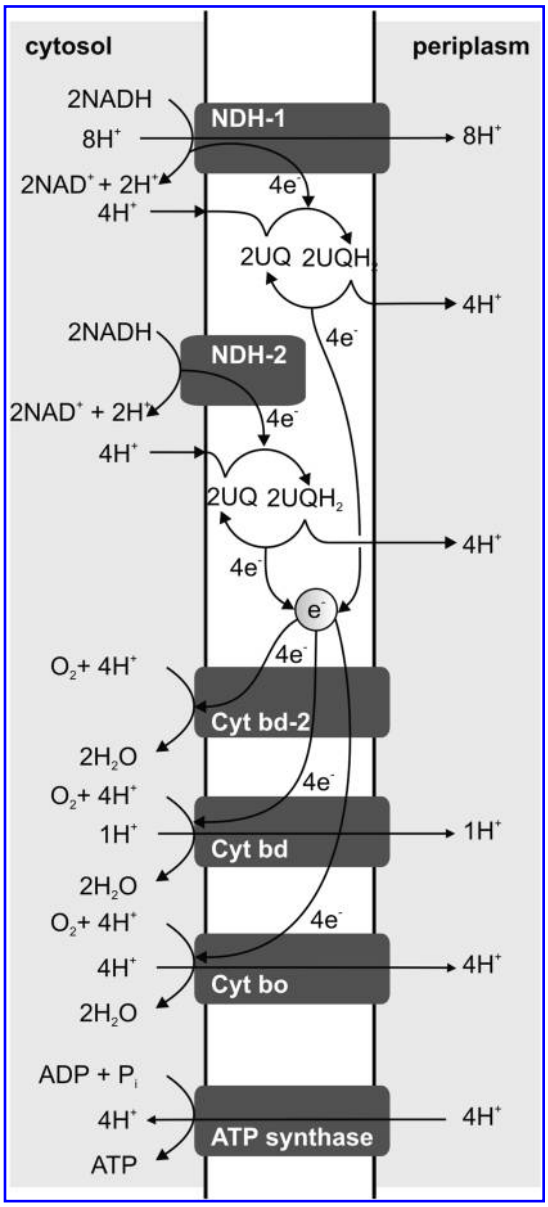


**FIG. 10. Scheme of the electron transport chain and its proton translocation properties in *E. coli*.** The electron pool is fictitious and only drawn for a better graphical presentation.

type *E. coli*. Noguchi *et al.* (235) determined that the nonelectrogenic NDH-2 activity constitutes around 40% of the total NADH oxidizing activity in *E. coli* during the early stationary phase after cultivation under glucose-unlimited and -limited conditions. Accordingly, the respiratory chain of *E. coli* is not optimized for ATP production under the tested conditions. *Prima facie*, this uncoupling of NADH oxidation from proton translocation is astonishing, but this mechanism enables the organism to respond appropriately to environmental changes (26).

For biotechnological process optimization, increasing the efficiency of the ETC is a promising metabolic engineering target. This strategy was followed by Zamboni *et al.* (372) to improve the riboflavin yield of *Bacillus subtilis* cultures. Riboflavin production depends on efficient ATP supply (87, 279). *Bacillus subtilis* also features a branched ETC consisting of quinol and cytochrome terminal oxidases with differing energetic efficiencies (267). Knockout of the *cydAB* genes, which code for the less efficient cytochrome *bd* oxidase, decreased the nongrowth-associated maintenance demand of the engineered *B. subtilis* strain by 40% and increased the riboflavin yield in fed-batch cultures. The *B. subtilis* mutant apparently could channel more ATP to the product formation pathway. Interestingly, respiration in *B. subtilis* appeared not to be driven directly by the energy demand, because similar specific $O_2$ consumption rates have been measured for the *B. subtilis* reference strain and its *cyd* knockout mutant that contrasts the behavior of *E. coli* as described above (26). That enhancing the coupling of electron transport to ATP synthesis is not a universally valid strain optimization strategy shall be exemplified by the behavior of *Zymomonas mobilis*. This organism has an exceptionally fast operating homoethanol fermentation pathway and completely satisfies its ATP demand through substrate phosphorylation. Nevertheless, *Z. mobilis* oxidizes NADH in the ETC if grown aerobically and deletion of the dissipatively operating NADH oxidase (type II NADH:CoQ oxidoreductase) leads to an increase of both aerobic growth rate and biomass yield (163).

Some of the redox enzymes of the ETC and the ATP synthase can operate in the opposite direction. In this mode the ATP synthase functions as an ATPase, consumes ATP, and translocates protons from the inside to the outside of the cell or mitochondrion. The increased proton gradient in turn can be used to regenerate NADH. This process of reverse electron flow is important in many chemolithotrophic bacteria that utilize ferrous iron ($Fe^{2+}$), nitrite ($NO_2^-$), or ammonia ($NH_3$) as electron- and thus energy source (23). Also fermenting bacteria, which do not possess an ETC use the ATP synthase as an ATPase to create a proton gradient, which is used for the transport of nutrients or the export of metabolic byproducts. Growth of *Lactococcus lactis* subsp. *cremoris* MG1363 on minimal salt medium, for instance, was shown to rely on the $H^+$-ATPase as a $H^+$-ATPase negative strain of this organism failed to grow on chemically-defined medium (177). Interestingly, addition of hemin to the *L. lactis* mutant restored growth on minimal salt medium in the presence of $O_2$, indicating that hemin complements a respiration-dependent proton transport system other than the $H^+$-ATPase (32). Indeed, Blank *et al*. showed that *L. lactis* is capable of forming cytochromes when hemin is provided in the growth medium and that the partially restored ETC is capable to couple NADH oxidation to the formation of a proton gradient. Also, Koebmann *et al.* (177) showed that the function of the $H^+$-ATPase is reversed towards an ATP synthase in hemin supplemented *L. lactis* cultures growing under energy limitation.

The presented examples show the complexity and diversity of bacterial ETCs and point out the difficulties to quantify NADH consumption and ATP production in this pathway. As NADH is the main electron donor for the redox cofactor dependent ETC, the ETC is a direct competitor for every biocatalytic redox reaction dependent on this redox cofactor. Consequently, a full understanding of the control of the distribution of electrons in the branched ETC is important, as it might open new possibilities for strain optimization for redox biocatalysis. Summarizing, oxidative phosphorylation, due to its high energetic efficiency in most aerobically grown organisms, enables the cells to grow with a high biomass yield. For redox biocatalysis, this pathway however exhibits a strong competition for reduced cofactors. Thus, for aerobic redox biocatalysis with growing cells, a trade off between high biomass yield and high biocatalytic performance has to be expected.

3. Fermentative pathways. During fermentation (*i.e.,* in the absence of extracellular electron acceptors), redox cofactors are balanced using central carbon metabolism intermediates as electron acceptors, such as pyruvate during homolactic fermentation of lactic acid bacteria and acetaldehyde during ethanol production by baker's yeast. In Figure 9, the fermentative pathways of *E. coli,* producing lactate and mixed acids (*i.e.,* formate, acetate, and ethanol), are depicted.

Since the 1860s and Pasteur's finding that fermentation products are produced by microbes, many alternative fermentative pathways have been described (Table 3). These pathways share certain properties: the redox balance is closed and the energy gain, typically given as the amount of ATP per consumed substrate molecule, is low. For example, under anaerobic conditions, *Saccharomyces cerevisiae* produces 2 mol ATP per mol glucose consumed and mixed acid fermentation by *E. coli* or lactic acid bacteria generates up to 3 ATP per mol glucose. This low energy yield is the reason why no organic acid can be produced as free acid during anaerobic fermentation below the pKa of the acid; transport under these conditions is active and costs an additional ATP per molecule produced (68, 336).

Some anaerobes compensate for this low yield by increasing energy availability by increasing carbon uptake (68). The sometimes extraordinarily high carbon uptake rates (*e.g.*, by *Z. mobilis*) result in high redox cofactor regeneration rates, which are comparable or higher than those during aerobic growth. This property renders anaerobic conditions attractive for redox biocatalysis, as long as $O_2$ is no biotransformation substrate as in the case of oxygenases.

Fermentation, however, must be redox-neutral (*i.e.,* no net oxidation or reduction of the substrate occurs considering all products formed). Ideally, the fermentation product is removed from the broth to avoid toxic effects and product inhibition. One often used system is formate dehydrogenase-mediated conversion of formate into $CO_2$, which delivers 1 NADH (see also Section V.B).

Alternatively, the acetone synthesis reactions in *Clostridium acetobutylicum* can be used, converting acetate into acetone, which can be removed simply by gas stripping. The successful

Table 3. Relative Rates of Redox Cofactor-Dependent Reactions During Growth on Minimal Medium with Glucose as Substrate

| *Fermentation product* | *Species* | *Enzymes involved in $NAD^+$ reduction* | *Enzymes involved in NADH oxidation* | *Redox cofactor regeneration flux (mmol $g_{CDW}h^{-1}$)* | *References* |
|---|---|---|---|---|---|
| Ethanol | *Saccharomyces cerevisiae* | Glyceraldehyde-3-phosphate dehydrogenase | Alcohol dehydrogenase | 34 | 137 |
| Acetate, ethanol, formate | *Escherichia coli* | Glyceraldehyde-3-phosphate dehydrogenase | Alcohol dehydrogenase | 9.5 | 253 |
| Ethanol | *Zymomonas mobilis* | Glucose-6-phosphate dehydrogenase, glyceraldehyde-3-phosphate dehydrogenase | Alcohol dehydrogenase | 115 | 115 |
| Lactate | *Lactococcus lactis* | Glyceraldehyde-3-phosphate dehydrogenase | Lactate dehydrogenase | 40 | 176 |
| Lactate, acetate, ethanol, formate | *Streptococcus zooepidemicus* | Glyceraldehyde-3-phosphate dehydrogenase | Lactate, acetaldehyde, and ethanol dehydrogenase | 50 | 36 |
| Ethanol, lactate | *Leuconostoc mesenteroides* | Glucose-6-phosphate dehydrogenase, P-gluconate dehydrogenase, glyceraldehyde-3-phosphate dehydrogenase | Lactate, acetaldehyde, and ethanol dehydrogenase | 30 | 91 |
| Succinate | *Mannheimia succiniciproducens* | Glyceraldehyde-3-phosphate dehydrogenase | Malate dehydrogenase | 25 | 236 |
| Acetone, butanol, ethanol | *Clostridium acetobutylicum* | Glyceraldehyde-3-phosphate dehydrogenase | Butanol, ethanol, butyraldehyde, butyryl-CoA, 3-hydroxy butyryl-CoA dehydrogenase | 100 | 131 |
| None | *Escherichia coli* during aerobic growth | See Table 1 | NADH dehydrogenase | 35 | 103 |

implementation of these reactions eliminates acetate from the fermentation broth in *E. coli* (27), but they have not been used to enable anaerobic redox biocatalysis. From an industrial perspective, low yields must be avoided, because the cost of the carbon and energy substrate (here: electron donor) contributes significantly to the overall cost of the biocatalytic process (211). Therefore, the produced fermentation product should also be valuable, if a commercially attractive redox biocatalysis setup is envisaged.

The necessity for a balancing of different redox cofactors (*i.e.* NADH and NADPH) is partially relieved by the presence of transhydrogenases in several bacteria and most higher organisms, because they catalyze electron transfer between NADPH and NADH and thus equilibrate the respective pools. The biology and impact of the presence and absence of transhydrogenases is discussed in the next section.

4. Transhydrogenase activities. For a balanced redox metabolism, the rates of redox cofactor reduction and oxidation must be highly similar. Hydride transfer between the two different nicotinamide dinucleotides NADH and NADPH increases the degree of freedom of cellular metabolism and allows on-demand delivery of redox cofactors. Two alternative transhydrogenases, the soluble, nonenergy-dependent transhydrogenase (EC 1.6.1.1) and the membrane-bound, proton-translocating transhydrogenase (EC 1.6.1.2), catalyze this interconversion summarized as $NADH + NADP^+ \leftrightarrow NAD^+ + NADPH$ (153).

The proton-translocating transhydrogenase consists of one (*e.g.*, in humans), two (*e.g.*, in *E. coli*), or three polypeptide chains (*e.g.*, in *Rhodospirillum rubrum*) with a total length of approximately 1000 amino acid residues, no prosthetic group, and homologies among the different species throughout the polypeptide chains (368). In *E. coli*, the protein complex features 13 trans-membrane-domains: four in the $\alpha$-subunit and nine in the $\beta$-subunit (218). The C-terminus of the $\alpha$-subunit and the N-terminus of the $\beta$-subunit face the cytosol and periplasm, respectively.

The soluble transhydrogenase is a flavoprotein that binds flavin adenine dinucleotide as a cofactor. The protein has approximately 470 amino acid residues and most likely functions as a homo-octamer (46), although filament-like structures that have an apparent weight of roughly 1000 kDa have been reported for the soluble transhydrogenase in *P. aeruginosa* (350).

Whereas the soluble transhydrogenase is found exclusively in certain bacteria, the proton-translocating transhydrogenase is expressed in some bacteria and in most mitochondria of all major groups of eukaryotes (312). Based on a sequence search of 648 bacterial genomes on the NCBI "microbes" BLAST website (www.ncbi.nlm.nih.gov/sutils/genom_table.cgi), the proton-translocating transhydrogenase is present in more phyla and species compared with the soluble transhydrogenase (Table 4).

The presence of both transhydrogenases in one organism, however, is not restricted to *E. coli* and close relatives within the order enterobacteriales; it is common in other *gamma* proteobacteria, such as the families Pseudomonadaceae and Vibrionaceae. In addition, nonclassified *gamma* proteobacteria, such as *Alteromonas macleodii* and *Psychromonas ingrahamii,* harbor genomic sequences that are highly similar to both transhydrogenases.

Table 4. Distribution of the Soluble and the Proton-Translocating Transhydrogenase in the Bacterial Kingdom

| *Phylum*[a] | *Class / order / family* | *Soluble transhydrogenase*[b] | *Proton-translocating transhydrogenase* | *Comments* |
|---|---|---|---|---|
| Actinobacteria | | some species | some species | both in *e.g., Rhodococcus, Mycobacterium* |
| Bacteroidetes | | none | some species | *e.g., Salinibacter rubber* |
| Chlamydiae | | none | none | exception: candidatus *Protochlamydia amoebophila*, ref\|NC_005861.1\| |
| Cyanobacteria | | none | some species | *e.g., Synechocystis* sp., *Acaryochloris marina* |
| Firmicutes | | none | none | exception: *Oenococcus oeni* |
| Proteobacteria | | | | |
| | *alpha* | many species | many species | both in many species, *e.g., Agrobacterium tumefaciens* |
| | *beta* | none | many species | |
| | *delta* | some species | some species | both in *Anaeromyxobacter* |
| | *epsilon* | none | none | |
| | *gamma* | many species | many species | |
| | Enterobacteriales | many species | many species | both in many species, *e.g., E. coli* |
| | Pasteurellaceae | none | many species | |
| | Pseudomonadaceae | many species | many species | both in many species, *e.g., P. putida* |
| | Vibrionaceae | many species | many species | both in many species |
| | Xanthomonadaceae | none | many species | |
| Spirochaetes | | none | some species | *Leptospira interrogans, Treponema denticola* |

[a]Only phyla with representative numbers of fully sequenced genomes are presented.
[b]Gene sequences were identified by tblastn using the UdhA and PntA sequences of *E. coli* as bait (www.ncbi.nlm.nih.gov/sutils/genom_table.cgi) and by using genome annotation.

The other phyla, in which species that have both transhydrogenases were identified in our sequence comparison, are actinobacteria and planctomycetes. This, however, does not exclude the existence of species in other phyla that also have both transhydrogenases. Homologs of the two transhydrogenases are not present in archaea (with the exception of a putative proton-translocating transhydrogenase in candidatus *Methanoregula boonei*, Genbank accession number ref|NC_009712.1|), yeast, and many bacteria (Table 4).

The existence of no, one, or two transhydrogenases in an organism raises interesting questions about their particular role in redox metabolism. Whereas a principal role of the proton-translocating transhydrogenase in the mitochondria of eukaryotes is to prevent oxidative stress by maintenance of reduced glutathione and systems that are linked to glutathione/NADPH (*e.g.*, thioredoxin and glutaredoxin) (275), the functions of the transhydrogenases in bacteria are less clear.

5. Anabolic pathways. Anabolism is the set of constructive metabolic processes where the energy released by catabolism is used to synthesize biomass constituents and secondary metabolites. In general, the complex molecules that make up cellular structures are constructed step-by-step from small and simple precursors. A total of 75–100 building blocks, coenzymes, and prosthetic groups are needed for cellular synthesis that are all synthesized from 12 precursor metabolites formed in the central carbon metabolism. The assembly of the macromolecular components of cell mass requires huge amounts of both energy (in the form of ATP) and the redox cofactor NADPH, which have to be supplied by the catabolic reactions. For example, the synthesis of 1 g of cell dry weight (CDW) of *E. coli* requires 41 mmol ATP and 18 mmol NADPH (317a).

Whereas the NADPH requirements for the production of one unit of biomass can be calculated from the stoichiometry of the biosynthetic reactions, determination of the ATP demand for biomass synthesis is more difficult as ATP is also consumed in nonmetabolic processes (*i.e.,* processes that do not contribute to net synthesis of biomass) such as maintenance of an electrochemical gradient across the plasma membrane (up to 50% of the ATP produced (310)), futile cycles such as ATPase-driven proton cycling through the membrane, and turnover of macromolecules. These ATP costs are generally termed maintenance demand and divided in a growth-dependent ($Y_{X/ATP}$) and a nongrowth-dependent term ($m_{ATP}$). The values of these parameters strongly depend on the strain and growth conditions. Values between 41 and 91 $g_{CDW}\ mol^{-1}$ and between less than 1 and 18.9 mmol $g_{CDW}\ h^{-1}$ have been reported for $Y_{X/ATP}$ and $m_{ATP}$, respectively (307). Moreover, especially when growth is limited by nutrients other than energy, energy generation is often uncoupled from growth demands and excess ATP is wasted in futile cycles (see Section III.B.2).

Obviously, redox biocatalysis coupled to cell growth is faced with a great drain of carbon as well as energy and reducing equivalents into biomass. In addition, high maintenance energy requirements also reduce the yield of redox equivalents available for the biocatalytic reaction (Fig. 11).

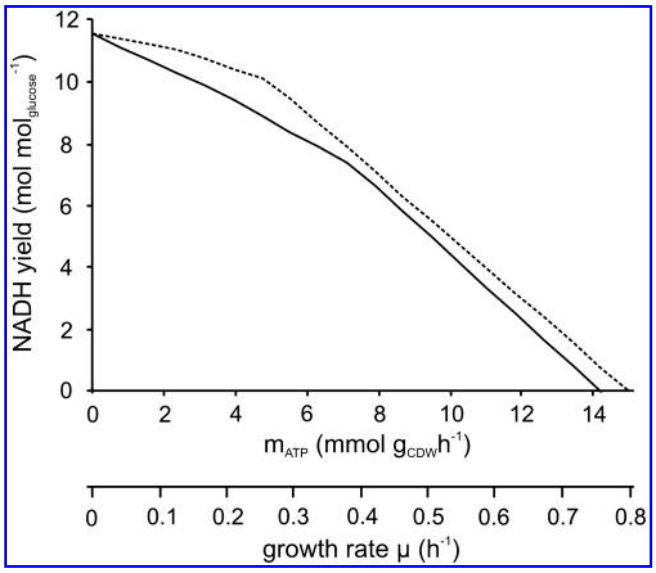


**FIG. 11. Maximal NADH yields of *E. coli* in dependence of maintenance energy demand (*dashed line*) and cell growth (*solid line*).** NADH yields were simulated by flux balance analysis (based on the reaction network shown in Figure 9) applying the objective 'maximize NADH regeneration'. The glucose uptake rate was set to 1 mmol $g_{CDW}h^{-1}$ and 10 mmol $g_{CDW}h^{-1}$ for the simulations with varying $m_{ATP}$ and growth rate, respectively. Solutions were computed with the MATLAB (The MathWorks Inc., Natick, MA) function 'linprog'.

Hence, for redox biocatalysis, the use of strains with a high energetic efficiency (or low maintenance demand) and/or nongrowing cells is preferable. However, biocatalysis with nongrowing cells faces other hurdles such as reduced metabolic activity and instability of the biocatalytic enzyme (63).

6. Hydrocarbon degradation pathways. Many of the above presented oxidoreductases interesting for biocatalysis are involved in degradation pathways of aliphatic and aromatic compounds, making these diverse molecules accessible for microbes as carbon and energy source [see (124) for a comprehensive review, and http://umbbd.msi.umn.edu/ for a comprehensive database]. As a figurative description, the catabolic funnel was introduced, containing all degradation pathways that ultimately "funnel" into the above described biochemical reactions of central carbon metabolism. More specifically, the activation of compounds by introducing oxygen from $O_2$, thereby forming the corresponding alcohol typically initiates the degradation of hydrocarbons, which proceeds via the aldehyde and the acid. Depending on the compound to be degraded, acids can subsequently be channeled into *ortho* or *meta* cleavage pathways (*i.e.*, aromatic hydrocarbons) or esterified with CoA and further degraded for example via *β*-oxidation (*i.e*, aliphatic hydrocarbons), eventually flowing into the common central carbon metabolism. The degradation pathways do not *per se* consume redox cofactors as the electrons needed for alcohol synthesis by, for example, a monooxygenase typically are recovered during subsequent dehydrogenations to, for example, aldehydes and acids. Finally, the complete oxidation of the compounds in the TCA cycle allows regeneration of redox cofactors needed for all cellular processes (see Section III.A.1). An interesting concept not yet discussed in this review is the so called co-metabolism (*i.e.*, the partial degradation of substrates that cannot sustain growth) (155). Co-metabolism (*i.e.*, the degradation of a co-substrate, also named auxiliary substrate) causes an increase in biomass yield by providing additional electrons for energy generation via cell metabolism (17). This concept was intensively discussed in the context of bioremediation for increasing degradation rates of xenobiotics, which are man-made chemicals not easily accessible by enzymes involved in degradation. Using a growth substrate (*e.g.*, glucose) in the presence of a xenobiotic that can be (partially) degraded will result in higher biomass yields and growth rates, compared to xenobiotic degradation alone. The concept of co-metabolism was not explicitly discussed for increasing yields during biocatalysis, although the concepts of artificial redox regeneration systems presented in Section V.B take advantage of such an auxiliary substrate as an additional electron donor. This concept, however, was applied to produce dead end metabolites (*e.g.*, 5-methyl-2-pyrazinecarboxylic acid from 2,5-dimethylpyrazine with wild-type *P. putida* mt-2 growing on *p*-xylene and using the same xylene degradation pathway for both growth and biotransformation) (171, 172).

Having discussed the biochemical inventory of a cell that can be used for redox biocatalysis, we present in the following how these metabolic modules operate and how this operation can be monitored.

### *B. Operation of metabolic modules*

In this section, we discuss how redox cofactors are regenerated in metabolic networks fulfilling the constraints of mass and redox conservation.

1. Introduction to the balancing concept and the resulting stoichiometric models. In the preceding section, we introduced the different modules of microbial metabolism. The array of active reactions within these modules cannot operate independently but have to obey conservation principles with respect to elements, mass, enthalpy, and charge. Thus, elemental or mass balance equations can be employed to relate conversion rates that describe the metabolic system. In the beginning of the use of mathematical models in bioengineering science, a black-box approach was applied, in which the cell was treated as a black-box that exchanges material from its environment and processes it through many cellular

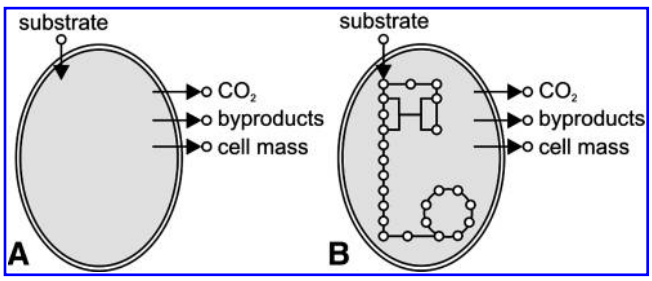


**FIG. 12. Graphical presentation of the two modeling approaches black-box modeling (A) and stoichiometric modeling (B).**

reactions, which are lumped into one for the overall cell biomass growth (Fig. 12).

As atomic species are conserved in the overall conversion of substrates to metabolic products and biomass, the elements flowing into the system must balance the elements flowing out of the system. Hence, each element considered in the black-box obviously yields one constraint as for each an elemental balance can be written. Considering, for example, the elements C, H, O, and N yield a linear equation system with four rows and a number of variables equal to the number of substrate uptake and product formation rates. The system can be solved if it is determined, that is if the number of independent variables—the unknown reaction rates—equals the number of elemental balances. The system is overdetermined if less unknown rates exist than constraints and the redundancies can be used to check the consistency of the data and improve the accuracy and credibility of the measured rates by balancing and gross error diagnosis, respectively (338). Gross measurements errors in yeast cultures due to evaporation of ethanol have, for example, been detected by this approach (232). Furthermore, black-box models have frequently and successfully been used to determine maximal biomass yields on $O_2$ and different carbon sources (269), to determine unmeasured rates [*e.g.*, with respect to $CO_2$ evolution or $O_2$ uptake (79)], and for process control (348).

The black-box approach is very useful when the aim is to check the overall balance of carbon or any other element flowing into and out of the cell, but it does not supply any information about the processes occurring inside the cell. Intracellular reaction rates (fluxes) are however of utmost importance in metabolic engineering with the aim not (only) to improve the bioprocess by adapting process parameters but by improving the performance of the microbial cell itself (*i.e.*, by engineering the cell metabolism). Intracellular fluxes cannot be measured directly but can be calculated by solving the mass balances of the intracellular metabolites. This concept is referred to as metabolite balancing in contrast to elemental balancing in the black-box approach. Assuming that the metabolism resides in a (pseudo)-steady state, that is, no metabolite concentration changes occur over time, establishing the mass balances of all metabolites of the system under consideration yields the equation system given by Eq. (1).

$$\begin{pmatrix} \frac{dc_1}{dt} \\ \frac{dc_2}{dt} \\ \vdots \\ \frac{dc_m}{dt} \end{pmatrix} = \begin{pmatrix} s_{11} & s_{12} & \cdots & s_{1n} \\ s_{21} & s_{22} & \cdots & s_{2n} \\ \vdots & \vdots & \ddots & \vdots \\ s_{m1} & s_{m2} & \cdots & s_{mn} \end{pmatrix} \cdot \begin{pmatrix} r_1 \\ r_2 \\ \vdots \\ r_n \end{pmatrix} = \begin{pmatrix} 0 \\ 0 \\ \vdots \\ 0 \end{pmatrix}$$

$$\mathbf{S} \cdot \mathbf{r} = 0 \qquad \text{Eq.(1)}$$

In this equation $c_i$ is the concentration of metabolite i, $s_{ij}$ the stoichiometric coefficient of metabolite i in reaction j, and $r_j$ the rate of reaction j. c is the vector of the m metabolite concentrations, S is the stoichiometric matrix, and r the vector of the n reaction rates.

Modeling the system in a (pseudo)-steady state has the great advantage that this appoach solely relies on the—generally well determined—stoichiometries of the underlying biochemistry and does not require data on reaction kinetics, of which most have not been determined, yet. Certainly, construction of explicit kinetic models is highly desirable for predictive metabolic modeling as these models allow for the most detailed and quantitative description of the dynamics and function of the metabolic system. However, use of large-scale kinetic models, required, for example, to describe whole cells, is not only hampered by the lack of reliable kinetic parameters but also by the inevitable computational complexity of such models and the hard interpretability of large-scale simulations, which is still a matter of dissent. Due to these hindrances, kinetic modeling is currently often limited to smaller (sub)-systems or individual pathways but has, nevertheless, contributed significantly to the understanding of metabolic regulation principles (106, 344). In this review, we focus on stoichiometric modeling and its contribution to unravel and improve redox biocatalysis and refer the reader to references (154, 308) for comprehensive reviews about kinetic modeling.

To compute intracellular reactions rates at steady state, the equation system given by Eq. (1) has to be solved. However, since the number of reactions n in real metabolic networks mostly is much larger than the number m of internal metabolites, the equation system is underdetermined and an infinite number of flux distributions r would usually be generated with the linear equation system (Eq. (1)).

Several methods for the analysis of the space of feasible flux distributions, which describe the metabolic capabilities of the organism, and methods to infer a single flux distribution for specific conditions exist. These methods shall briefly be described in the following. For an in-depth description the reader is referred to (260, 307).

*a. Constraint-based modeling.* The basic idea of constraint-based modeling is to shrink the solution space by applying additional constraints besides the steady-state constraint given by Eq. (1). Such constraints are, for instance, imposed by thermodynamics (irreversibility of reactions), enzyme capacity constraints (maximal uptake/reaction rates), or regulatory mechanisms (set of active reactions in dependence of environmental conditions). The addition of these constraints results in a bounded solution space. By analysis of the constrained system, it is thus possible to dissect between feasible and infeasible flux distributions.

*b. Flux balance analysis.* Flux balance analysis (FBA) identifies extreme patterns in the constrained solution space that maximize a particular linear objective function. The optimal flux distribution is calculated by linear programming. Whereas the optimal value is unique, the calculated flux distribution itself might not be unique, especially in large-scale networks (194, 207). Thus, even when optimality is assumed, it may happen that only little can be said about the flux distribution inside the cell; only some reaction rates can be specified that are fixed in the optimal solution. Addition of, for example, regulatory constraints (81) or application of thermodynamic feasibility or performance analysis (134, 366) have proven useful to reduce the number of optimal flux distributions. For example, Beard and coworkers have conducted studies aimed at eliminating internal flux cycles (24) (*i.e.*, sets of reactions for which the overall reaction is zero, such as A → B → C → A). According to the first law of thermodynamics, the overall thermodynamic driving force

through this cycle must be zero, meaning that no net flux through this cycle is possible. Through the introduction of appropriate constraints, flux distributions from FBA did no longer involve any flux through such cycles, thereby substantially reducing the flux solution space. In another approach, Henry *et al.* investigated the thermodynamic feasibility of reactions by calculating the Gibbs free energy change for all reactions of the genome-scale metabolic network of *E. coli* (133). According to thermodynamics, the occurrence of a reaction is only possible if the Gibbs free energy change of reaction is negative. As the analysis relies on data of Gibbs energy of formation and intracellular metabolite concentrations that are mostly unknown, the authors used a group contribution method to estimate Gibbs energies and allowed metabolite concentrations in the range of 20 m*M* to $10^{-2}$ m*M*. Due to these uncertainties, only five reactions (of 873) were identified to be strictly irreversible, indicating the need for more accurate data for the assignment of reaction directions. Indeed, improvements of the group contribution method (134, 156) have recently been reported. This progress and the continuously increasing quality and performance of quantitative metabolome analyses will increase accuracy and applicability of this approach.

FBA has successfully been applied for the determination of maximal product yields (339) or the identification of gene knockout or gene insertion targets for strain improvement (6, 55). The limitations of FBA can be illustrated by means of a study of Blank *et al*. (37), in which maximal NADH regeneration rates available for redox biocatalysis were estimated by applying FBA on a central carbon metabolism model of *E. coli*. While the predicted dependency of the NADH regeneration rate on the metabolic networks was reflected in the rates achieved for oxygenase catalysis with isogenic single gene knockout mutants, the calculated NADH regeneration rates exceeded about 3-fold the NADH demand for the oxygenation reaction. This discrepancy points out that the applicability of this method is restricted to the exploration of the capacities of a metabolic network, but that these calculated maximal values might not readily be achievable as microbes are typically not evolved for a maximal NADH regeneration rate.

To calculate flux distributions that are more consistent with the metabolic state of an organism, an objective function that reflects the true biological objective has to be chosen. Frequently used optimality criteria for this purpose are maximization of growth rate or ATP production and the minimization of the sum of squares (44, 98, 284). In a recent study, Sauer and coworkers compared flux ratios calculated by applying 11 different optimality criteria and 9 additional constraints (yielding 99 objective/constraint combinations) and compared them to flux ratios determined from $^{13}$C-based metabolic flux analysis (see Section IV.C) experiments (292). No single objective described the flux states under all conditions, but the study showed that unlimited growth on glucose in $O_2$ or nitrate respiring batch cultures is best described by nonlinear maximization of the ATP yield per flux unit whereas under nutrient scarcity in continuous cultures, linear maximization of the overall ATP or biomass yields achieved the highest predictive accuracy. Although FBA-predicted flux ratios showed a high congruence with the experimentally determined ratios for the carefully chosen objectives, the predictive fidelity was only tested for a limited set of growth conditions and it is unclear whether the same constraints hold true for other organisms than *E. coli.*

Metabolic flux analysis, which is described in the following section, is better suited for the determination of the metabolic state of an organism under specific conditions.

*c. Metabolic flux analysis.* Metabolic flux analysis (MFA) tries to shrink the possible solution space of Eq. (1) by measuring some of the reaction rates in a steady state experiment (307). Ideally, enough reaction rates can be measured to render the equation system determined or even overdetermined so that one unique solution remains for the actual flux distribution in the respective experiment. This solution then describes the *in vivo* metabolic state of the investigated system. In large complex networks, however, the measured extracellular reaction rates are often insufficient to render the system determined. A special problem is that of reaction dependencies; these reduce the rank of the stoichiometric matrix, and hence the calculability of fluxes. Reaction dependency occurs particularly in cyclic pathways, which are abundantly present in metabolic networks. To solve these underdetermined or rank deficient systems, additional constraints have to be found.

One possibility is the addition of cofactor balances (*e.g.*, of ATP, NADH, or NADPH). Addition of the ATP balance increases the rank of the stoichiometric matrix by one unit and equally the number of calculable fluxes. However, to close the ATP balances, estimates for the ATP yield and the ATP requirements for maintenance processes have to be made. As mentioned in Sections III.A.2 and III.A.5, both factors are difficult to determine and vary with growth conditions (283, 335). Furthermore, the calculated flux distribution is very sensitive to changes in these estimates (45).

Separate balancing of NADH and NADPH is often complicated as many organisms balance their ratios via transhydrogenases or transhydrogenase-like metabolic cycles (see Section III.A.4). In these cases, only a mass balance that lumps the two cofactors can be used. Additionally, NADH balancing in respiring organisms is sensitive to the estimated value for the efficiency of oxidative phosphorylation ($H^+$/ATP stoichiometry) and the accuracy of the measured $O_2$ uptake rate (278).

Restricting the reaction directionality of irreversible reactions is a means to enhance the quality of MFA. Although this information does not increase the calculability of metabolic reactions, it constrains the solution space, in which all possible flux distributions are situated, and thus allows to fine tune the calculated flux distribution. To assess the directionality of reactions, a thermodynamic feasibility analysis can be applied (134, 189).

Due to the aforementioned limitations of flux distribution calculations, especially for the determination of NAD(P)H formation rates, $^{13}$C-based metabolic flux analysis is used to overcome some of these limitations. This method, which will be described in detail in Section IV.C, uses information on the incorporation patterns of $^{13}$C atoms into biomass components as additional constraints and allows a significantly higher resolution of intracellular fluxes. The predominance of this method is also reflected in the examples given below, in which mostly $^{13}$C-based metabolic flux analysis has been applied to elucidate the redox metabolism of different organisms.

2. Stoichiometric constraints on redox metabolism. To sustain growth, accumulation of the reduced cofactors NADPH and NADH and the depletion of their oxidized form have to be avoided (*i.e.,* the cell has to adjust supply and demand of these cofactors precisely). Subject to the available metabolic pathways, the organisms achieve this balance through different metabolic modes.

*a. Function of transhydrogenases.* In *E. coli* having both transhydrogenases, divergent functions of the soluble and proton-translocating transhydrogenases in NAD(P)H metabolism have been described (281). The soluble pyridine nucleotide transhydrogenase (UdhA) was found to be essential during growth with excess formation of NADPH (281), as observed on acetate (from isocitrate dehydrogenase) and in a phosphoglucoisomerase mutant on glucose (from the glucose-6-phosphate and 6-phosphogluconate dehydrogenases), implicating NADPH oxidation as a major function of UdhA. Under standard laboratory conditions, using glucose as the carbon and energy source, it was estimated that the proton-translocating transhydrogenase contributed 35%–45% of the NADPH required for biomass synthesis (281); thus, UdhA has a major function in $NADP^+$ reduction.

Cirino and colleagues attempted to increase NADPH availability for the biocatalytic synthesis of xylitol from xylose by manipulating transhydrogenase activity. Notably, the absence of UdhA or presence of PntAB failed to influence biocatalytic performance (74), necessitating additional studies on the role of transhydrogenases in *E. coli* and bacteria in general. In addition, Sauer *et al.* (281) reported that transcription of the two transhydrogenase genes is regulated by the demand in enzymatic activity and raised the issue of how organisms that lack one or both transhydrogenases close the redox cofactor balances. Studies that have pursued the elucidation of transhydrogenase-like activities explain how organisms overcome this limitation. Examples are briefly summarized in the following section.

*b. Transhydrogenase-like metabolic cycles.* The absence of transhydrogenases constrains the rates of cofactor reduction and oxidation, because they have to be carefully balanced for both NADH and NADPH. In *S. cerevisiae*, these restrictions lead to the production of the reduced byproduct glycerol during growth on glucose, balancing surplus NADH that originates from biomass synthesis (33, 137).

Alternatively, transhydrogenase-like cycles were proposed to relieve these stringent constraints. For example, a phosphoglucoisomerase deletion in *S. cerevisiae* resulted in increased NADPH regeneration via the two PP pathway reactions through glucose-6-phosphate dehydrogenase and 6-phosphogluconate dehydrogenase, leading to $NADP^+$-depletion and cease of growth. This phenotype was suppressed in a mutant that had increased NADH- and NADPH-dependent glutamate dehydrogenase activities. The parallel activity of the two alternative enzymes resulted in a net conversion of NADPH to NADH.

Because the phosphoglucoisomerase deletion is not lethal in *Kluyveromyces lactis*, similar transhydrogenase-like cycles were proposed to exist in this yeast. A compartmented cycle that involves NADH- and NADPH-dependent alcohol dehydrogenases (242) and a phosphorylating glyceraldehyde-3-phosphate dehydrogenase that has dual cofactor specificity (342) has been described. However, Siso and colleagues reported that these transhydrogenase-like cycles are insignificant in *K. lactis* (317); rather, the external mitochondrial dehydrogenases that accept cytosolic NADPH as an electron donor and, to a lesser extent, the enzymes that are involved in the oxidative stress response are the sinks for the excess NADPH that is formed in the PP pathway.

Although many bacteria and all reported yeast species do not express transhydrogenases (Table 3), little information exists on NADPH balancing. Recently, textbook material on cofactor specificity has been shown to be limited to *E. coli* and not to be appropriate for other bacteria. In particular, the PP pathway does not rely exclusively on $NADP^+$ in most species and can accept $NAD^+$, thereby avoiding redox cofactor imbalances (116).

*c. Organism-specific redox cofactor balancing.* Under aerobic conditions, $O_2$ serves as a final electron acceptor in respiration, which enables the continuous oxidation of the reduced cofactor NADH and can be coupled to or decoupled from ATP formation, as has been described in Section III.A.2. ATP produced in excess to the microbial energy demand can be dissipated in futile cycles. The $C_3$–$C_4$ metabolite interconversions at the anaplerotic node (Fig. 13) constitute potential futile cycles. The microbe *Corynebacterium glutamicum* is endowed with all decarboxylation and carboxylation reactions shown in Figure 13. Petersen *et al.* (255) showed by $^{13}C$-based MFA that this organism exhibits an intensive cyclic flux catalyzed by pyruvate carboxylase, PEP carboxykinase, and pyruvate kinase, exceeding the anaplerotic flux required for biomass synthesis 3-fold wasting 1 ATP per cycle. This wastage was discussed to be relevant for operation of metabolism under excess resource conditions. In contrast, under highly energy-demanding conditions the pyruvate

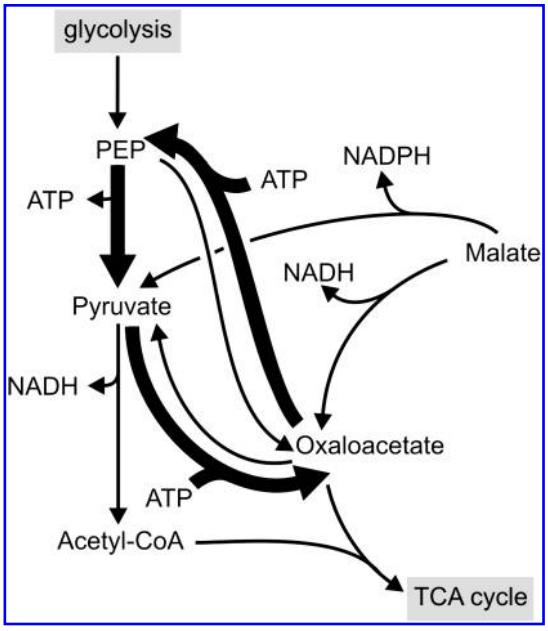


**FIG. 13. ATP dissipating futile cycle in *C. glutamicum*.** This cycle, which has been detected by $^{13}C$-based MFA, consumes one ATP per turn (255).

carboxylase of *C. glutamicum* is inhibited and the $C_3$–$C_4$ futile cycle is reduced.

Consequently, as long as $O_2$ supply and the capacity of the ETC do not get limiting, $NAD^+$ regeneration is easily accomplished in aerobically growing cells. If one of these factors limits NADH oxidation, the cells achieve a closed redox balance only if they reduce the NADH yield per catabolized unit of carbon source via incomplete oxidation of the substrate. This aerobic excretion of byproducts, which is observed for example in *E. coli* as acetate accumulation or in *S. cerevisiae* as ethanol formation, is called overflow metabolism or the Crabtree effect.

Likewise, under anaerobic conditions, microorganisms achieve a redox balance by reduction of pyruvate or acetyl-CoA, as described in Section III.A.3. To sustain growth, some pyruvate or phosphoenolpyruvate (PEP) has to be channeled into the TCA cycle to produce the biomass precursors oxaloacetate, 2-oxoglutarate, and succinyl-CoA. However, cyclic operation of the TCA cycle would lead to significant NADH accumulation under anaerobic conditions. To enable the allocation of biomass precursors, the TCA cycle operation is shifted from a cyclic mode to a branched pathway, in which the cycle is split into a reductive and an oxidative part with the end products succinyl-CoA and 2-oxoglutarate, respectively. In this mode, the enzyme fumarate reductase with fumarate as a terminal electron acceptor is used instead of succinate dehydrogenase. The electron donor is menaquinol, which commonly serves as a membrane-soluble, mobile electron carrier between respiratory complexes under anaerobic conditions (152). Menaquinol is regenerated via oxidation of NADH by NADH dehydrogenase that accepts menaquinone as electron acceptor in the absence of $O_2$, nitrate, or nitrite (319). In total, the reduction of 1 mol pyruvate or 1 mol PEP to 1 mol succinate consumes 2 mol NADH.

The overproduction of the fermentative byproduct succinate is a suitable example to illustrate how redox cofactor balancing can constrain maximal product yields. The maximum theoretical succinate yield from glucose derived solely from a carbon balance is 2 mol $mol^{-1}$ or 1.31 g $g^{-1}$. However, if a closed redox balance is forced, the succinate yield significantly drops. The actual achievable yield thus is limited by the supply of reduction equivalents. Moreover, the yield depends on the metabolic network as has been shown in several studies (82, 196, 341), in which maximal succinate yields have been calculated by stoichiometric analyses.

Two principal routes for the production of succinate have been described: The anaerobic reductive TCA cycle branch described above and the aerobic glyoxylate shunt (Fig. 14). The succinate yield of both pathways is the same (1 mol $mol^{-1}$). Whereas the aerobic route produces 5 mol NADH and 2 mol ATP per mol succinate produced, the anaerobic production of succinate via the reductive TCA cycle branch is limited by the supply of NADH (also see the net equations in Fig.14). The NADH limitation of the latter route can be alleviated by the addition of a $NAD^+$-dependent formate dehydrogenase, which couples the reduction of $NAD^+$ to the oxidation of formate to $CO_2$ and thus leads to an increase of the theoretical succinate yield on glucose to 1.33 mol $mol^{-1}$. More promising, however, is a combination of the two production pathways, which allows for a maximal theoretical succinate yield of 1.71 mol $mol^{-1}$ (1.21 g $g^{-1}$). Indeed, the simultaneous activity of these pathways can be achieved by dual-phase fermentations, with an aerobic growth phase followed by an anaerobic production phase. Applying this approach, Vemuri *et al.* (341) reached a succinate yield of 1.5 mol $mol^{-1}$, which is appr. 88% of the theoretical yield achievable. The example nicely demonstrates the importance of redox cofactor balancing for the design of metabolic engineering strategies.

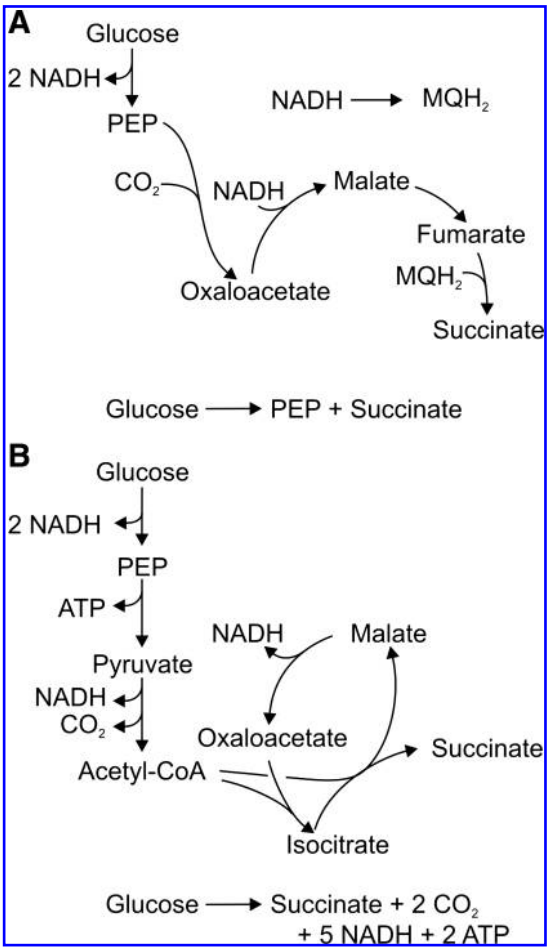


**FIG. 14. Anaerobic (A) and aerobic (B) succinate production pathways in *E. coli*.**

The reduced cofactor NADPH is mainly used in biosynthetic reactions. Organisms that do not possess other possibilities to reoxidize this cofactor have to strictly adjust the NADPH formation to the biosynthetic demand. In a recent study, the intracellular flux distributions of 14 hemiascomycetous yeast species have been determined, revealing a linear correlation between the relative PP pathway flux and the biomass yield and implying that the PP pathway flux is driven by the NADPH demand for biomass synthesis and that NADPH production and NADPH consumption are strictly balanced (35). Analogously, Jouhten (160) could show that this correlation also exists for *S. cerevisiae* growing at $pO_2$ levels varying between 20.9% and 0% in glucose-limited continuous cultures.

*Escherichia coli* has several alternative glucose oxidation pathways that differ in their NADH, NADPH, and/or ATP yield. As has been shown previously (109), this organism

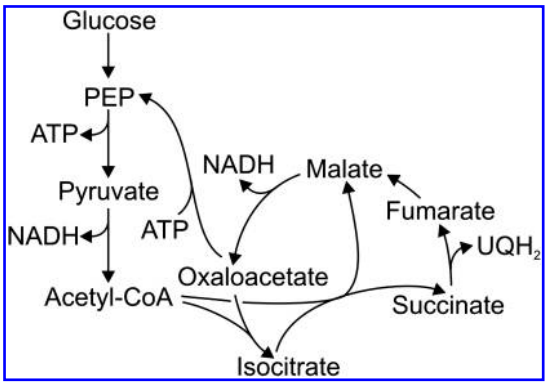


**FIG. 15. The PEP-glyoxylate shunt in *E. coli*.** Figure adopted from Fischer and Sauer (109).

exploits this redundancy to flexibly adjust its NADPH yield to biosynthetic needs. Fischer *et al.* detected a bifunctional anabolic and catabolic pathway that is characterized by the conjoint activity of glyoxylate shunt and PEP carboxykinase for complete oxidation of PEP to $CO_2$ (Fig. 15) and thus constitutes an alternative to the TCA cycle. The net reaction of this cycle reads PEP $\rightarrow$ 3 $CO_2$ + 4 NADH + $UQH_2$ + ATP. Use of this PEP-glyoxylate cycle prevents the formation of NADPH, albeit at the expense of one ATP. The PEP-glyoxylate shunt was identified in slow-growing, strictly glucose-limited chemostat cultures of *E. coli* and in glucose excess batch cultures of a phosphoglucoisomerase-deficient mutant. As the latter mutant is known to overproduce NADPH due to the exclusive use of the PP pathway, PEP-glyoxylate shunt activity in this strain might function as a means to balance this redox cofactor. Equivalently, the slow-growing *E. coli* culture might also be faced with an NADPH formation exceeding the biosynthetic NADPH demand.

On the other hand, deletion of the *zwf* gene encoding the glucose-6-phosphate dehydrogenase leads to a reduction in the NADPH yield in *E. coli*. However, deletion of *zwf* neither alters maximal growth rate nor yield. This is due to the flexibility of the *E. coli* metabolism that counteracts the deletion of the PP pathway by doubling the TCA cycle flux and activating the $NADP^+$-dependent malic enzyme, thereby ensuring the formation of 46% of the NADPH demand for biomass synthesis. As in the wild-type strain that synthesizes the same fraction via PP pathway and TCA cycle, the residual NADPH is generated via the transhydrogenase PntAB.

*d. Redox cofactor specificity of enzymes.* Organisms with less redundant metabolic pathways or lacking transhydrogenases can use isoenzymes with different cofactor specificity or enzymes that accept both cofactors to balance the redox cofactors.

The organisms *Pseudomonas fluorescens* and *Z. mobilis*, for example, break down glucose exclusively via the Entner–Doudoroff pathway. Calculation of NADPH regeneration in these organisms, assuming the commonly accepted exclusive cofactor use of the dehydrogenases, that is $NADP^+$-dependence of the glucose-6-phosphate dehydrogenase, 6-phosphogluconate dehydrogenase, and isocitrate dehydrogenase as well as $NAD^+$-dependency of the glyceraldehyde 3-phosphate dehydrogenase and malate dehydrogenase, the NADPH formation rates in these two organisms exceed the biosynthetic NADPH demand by 25% and 35%, respectively (116). Due to the absence of transhydrogenase activity in these strains, Fuhrer and Sauer questioned the reported cofactor specificities. Indeed, *in vitro* enzyme activity studies confirmed that these strains contain PP pathway dehydrogenases without any apparent preference for either cofactor at saturated *in vitro* conditions or two isoenzymes with different cofactor specificities. Albeit the cofactor preference at quasi *in vivo* conditions shifted to NADPH, the remaining activity with $NAD^+$ is sufficient to yield a closed NADPH balance for *P. fluorescens*, while, in *Z. mobilis*, an even NADPH balance can only be achieved if the glucose 6-phosphogluconate dehydrogenase is completely $NAD^+$-specific. In *Z. mobilis*, balancing of NADPH might be achieved by a non-exclusive NADH specificity of dehydrogenases, for which relaxed cofactor specificities have been reported in the literature (163).

Differential expression of isoenzymes with different redox cofactor specificities has been reported for *S. cerevisiae*. Above, we depicted that the PP pathway flux in *S. cerevisae* correlates positively with the biomass yield and thus is driven by the demand for NADPH and biomass precursors. Similarly, Frick and Wittmann (113) observed a decrease of the relative PP pathway flux with increasing growth rate in *S. cerevisiae* cells grown in glucose-limited chemostats. Frick and Wittmann ran chemostats at dilution rates between 0.15 and 0.40 $h^{-1}$, at which the yeast switched from fully respiratory via respiro-fermentative to mainly fermentative growth. With increasing growth rate, the contribution of the PP pathway to NADPH formation decreased significantly from 113% to 51% of the NADPH demand for biomass synthesis. The authors assumed that under respiro-fermentative and fermentative growth conditions, the reduced NADPH supply via the PP pathway is compensated by a switch to the $NADP^+$-dependent isoforms of the isocitrate dehydrogenase and the acetaldehyde dehydrogenase.

Several other examples of isoenzymes with different cofactor specificities exist, for example, $NAD^+$- and $NADP^+$-dependent malic enzymes in *E. coli* or *Rhizobium meliloti* or

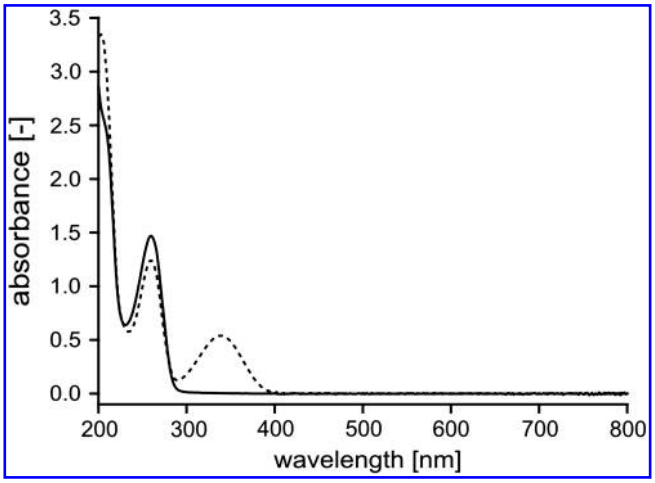


**FIG. 16. Absorption spectra of the reduced (*dashed line*) and oxidized (solid line) nicotinamide adenine dinucleotides.** NADH and $NAD^+$ (0.1 m*M*) were dissolved in 1.25 m*M* Tris-buffer having a pH of 8.0.

6-phosphogluconate dehydrogenases in *B. subtilis* (373). These enzymes have been studied in detail (43, 94, 200), but their respective physiological functions and their potential role in cofactor balancing have not been further investigated.

## IV. Quantitative Analysis of Redox Metabolism

In this section, we introduce methods for the quantitative determination of concentrations and regeneration rates of redox cofactors in cells.

### A. Regeneration rate vs. concentration of redox cofactors

Based on regeneration rates, one can directly deduce maximal biocatalytic rates that are critical for optimizing whole-cell redox biocatalysis. Complementarily to the regeneration rate, redox cofactor concentrations indicate, for example, which enzymes operate effectively under given conditions. Assuming simple Michaelis–Menten kinetics described by the classic rate equation $v = V_{max} * [S] / (K_m + [S])$, in which the observed rate depends on the maximum rate of catalysis by the enzyme ($V_{max}$), the substrate concentration ([S]), and the Michaelis–Menten constant ($K_m$), it can be emphasized that intracellular redox cofactor availability for biocatalysis not only depends on cofactor concentration and regeneration but also on the two enzyme-specific parameters $V_{max}$ and $K_m$.

Considering a functional metabolic network in a living cell with over 100 redox cofactor-dependent reactions, the redox cofactor concentrations directly define the achievable reaction rate of each enzyme. Enzymes that have a low $K_m$ will be saturated under most conditions that a cell encounters. For example, the NADH-dependent dehydrogenases of the electron transport chain have very low Michealis–Menten constants, highlighting their central role in NADH oxidation. To efficiently couple an NADH-dependent enzyme to cellular redox metabolism, the chosen enzyme should have a low $K_m$ for NADH and, ideally, a high $V_{max}$ challenging the metabolic capacitiy of the cell. To investigate these coherences and to optimize whole cells for redox biocatalysis, strategies to increase either the concentration of the total redox cofactor pool or the regeneration of reduced cofactors (*i.e.*, the rate) have been proposed, as discussed in the following sections.

NADH concentrations in mammalian cells are reported to be in the high micromolar range (*e.g.*, 300 $\mu M$ in mouse erythrocytes, (367)), 1 m$M$ in yeast, and between 0.6 and 1.1 m$M$ in bacteria (116). Notably, the majority of redox cofactors is not freely accessible, but approximately 80% of the redox cofactor pool is bound to enzymes (39, 370).

To increase total redox cofactor concentrations, Wubbolts *et al.* (363) overexpressed the *E. coli* nicotinic acid phosphoribosyl-transferase gene, which caused a 5-fold increase in the intracellular concentration of NAD(H) when the recombinant strain grew in the presence of nicotinamide, a precursor of $NAD^+$. Further, an *E. coli* strain that contained a higher total pool of reduced/oxidized nicotinamide adenine dinucleotides exhibited an identical flux distribution as the control strain during growth in a glucose-limited chemostat at a dilution rate of 0.2 $h^{-1}$, suggesting that NAD(H) availability is not limiting under these conditions (30).

During redox biocatalysis, the deletion of pathways that degrade nicotinamide adenine dinucleotides was investigated for its stabilizing effect on catalytic activity. However, cofactor loss through damaged cellular membranes caused by harsh reactions conditions and not intracellular cofactor degradation was found to be the chief reason that nicotinamide adenine dinucleotide concentrations decreased (136). This could partially be overcome by using an alternative redox cofactor regeneration system (289).

The rate of redox cofactor regeneration is intrinsically linked with the intracellular carbon flux distribution and the rate of carbon substrate uptake. While intracellular flux analysis, mainly by $^{13}C$-tracer based experiments, is becoming a routine technique (282), first studies report the use of this method to estimate redox cofactor regeneration rates during biocatalysis (37, 38, 67). Comparing maximal theoretical NADH regeneration rates sustained by the *E. coli* metabolic network under resting cell (*i.e.*, no growth) conditions with biocatalytic oxygenation rates in wet lab experiments under the same conditions, the latter rates were found to be 3- to 4-fold lower than the former, considering ideal oxygenation stoichiometry (37). Similarly, during the NADPH-dependent conversion of xylose to xylitol, Cirino and coworkers reported a maximal yield of 4 $mol_{xylitol}\ mol_{glucose}^{-1}$ (74), which is more than 2-fold lower than the theoretical yield. The observed discrepancies between theoretical redox cofactor regeneration rates and biocatalytic performance were discussed in the context of competing redox cofactor utilizing reactions (*e.g.*, electron transport chain) dissipating energy in futile cycles, nonoptimal flux distribution in the metabolic network (*e.g.*, synthesis of byproducts), and nonefficient redox cofactor/product coupling (*i.e.*, nonproduct targeted electron transfer), or a combination thereof (37, 74). Strategies to improve the rate of redox cofactor regeneration for redox biocatalysis are discussed in Section V.C.

As a reminder, the two alternative nicotinamide adenine dinucleotides serve very distinct cellular functions, while NADH mainly is involved in aerobic energy generation, NADPH is the electron donor in biomass synthesis pathways. To serve as an effective reductant, the $NADP^+$/NADPH pool must be kept in a sufficiently reduced state. Independently from the carbon source used, a $NAD^+$/NADH ratio of about 10 was reported for *E. coli* under aerobic conditions, while the phosphorylated nicotinamide adenine dinucleotide pool was more reduced at an $NADP^+$/NADPH ratio of 1 (8). Since *E. coli* posseses both the proton-translocating and the soluble transhydrogenase, an additional level of regulation is required to prevent equilibration of the more reduced NADP(H) pool with the more oxidized NAD(H) pool. The strong allosteric regulation of the soluble transhydrogenase [activation by NADPH, inactivation by $NADP^+$; reported for the *P. aeruginosa* enzyme (354)] might be part of this additional level of regulation. Interestingly, Fuhrer and Sauer (116) reported recently that the difference in reducing power of the two nicotinamide adenine dinucleotides was species dependent and, with a 3- to 5-fold difference in oxidized to reduced species rather low and in *Rhodobacter sphaeroides* surprisingly even identical, indicating significant differences in redox metabolism between species.

Results from an engineered *E. coli* strain with an increased nicotinamide adenine dinucleotide pool resulting in a higher $NAD^+$/NADH ratio suggest that the redox cofactor ratio *per se* is not a determining factor for the regulation of fluxes through central carbon metabolism (30). Instead, the intra-

cellular availability of NADH might play a more critical role (30). This was proposed previously upon studying NADH and total $NAD^+$/NADH levels during growth of several bacteria, including *E. coli* (357). Under the tested growth conditions, NADH levels were constant and independent of species and carbon source, while the total pool of nicotinamide adenine dinucleotides varied considerably between species and growth conditions. Matin and Gottschal (212) confirmed these results in chemostat experiments of a *Pseudomonas* sp. strain with different limiting carbon sources, under nitrogen limitation, and with different dilution rates. Once more, the NADH and in addition the NADPH concentration were constant, while the total pool sizes changed depending on the dilution rate.

In summary, the information content of redox cofactor concentrations and regeneration rates are highly complementary. It is therefore desirable to quantify both values during analysis and optimization of the host metabolism for redox-biocatalysis. The state-of-the-art analytical methods for respective quantifications are presented in the next paragraphs.

### *B. Quantification of nicotinamide adenine dinucleotides*

The investigation of the roles of the redox cofactors $NAD(P)^+$/NAD(P)H in cellular metabolism and whole-cell biocatalysis necessitates reliable methods for their quantification. Although analytical platforms for redox cofactors have become increasingly sophisticated (29, 208, 367) and have been specifically adapted for quantification during whole-cell biocatalysis (291), quantification of these cofactors remains complicated. Parameters that have to be taken into account independently of the analytical assay are the presence of interfering substances, the stability of the redox cofactors, and the rapid turnover inside the cell. The latter two items are elaborated and the removal of interfering substances is discussed in the following description of the analytical methods, wherever it is appropriate.

Because redox cofactors are frequently used to monitor enzymatic activities through changes in absorbance at 340 nm (Fig. 16), the impact of assay conditions on their stability, especially of pH and the buffer system, has been examined in detail (204, 273). The stabilities of oxidized and reduced cofactors show inverse pH dependences. While oxidized cofactors are stable at an acidic pH, the reduced forms are stable at basic pH values (i.e., $NADP^+$ and NADPH are stable at pH values below 9 and above 6.5, respectively) (205). Not only the pH, but also the combination of pH and temperature influences nicotinamide adenine dinucleotide stability. For example, the optimal pH for NADPH stability shifts to more basic values above 8 at higher temperatures (205).

The frequently used phosphate buffer (buffering range between pH 4.8 and 8.8) lowers the stability of reduced nicotinamide adenine dinucleotides, most likely by transferring electrons from the pyridine group to the inorganic phosphate (5). Alternative buffer systems, such as 0.1 *M* PIPES, stabilize NADH at pH 6.5 at 25°C, while a higher pH of 7.8 and a higher temperature of 30°C caused NADH degradation in a 40-minute-long spectrophotometric assay (273). Other buffer components, such as acetate, are as unfavorable as phosphate (362). The difference in pH sensitivity of the reduced and oxidized forms is used to remove the reduced forms at pH values of approximately one (*e.g.*, by $HClO_4$) and oxidized forms at pH 12 (*e.g.*, by KOH) (204, 205). It was reported that the respective redox cofactors to be isolated were stable for at least 2 hours under these conditions (208).

Notably, little information exists on nicotinamide adenine dinucleotide stability during whole-cell biotransformations. One can envision that organic solvents, which are frequently used as substrate/product and in situ extractants, influence the stability of redox cofactors. To this end, Schroer and coworkers (291) reported decreased stabilities of the reduced and oxidized forms of NAD(H) and NADP(H) in the presence of methyl acetoacetate and 2-propanol. A resting cell assay without an additional carbon source for cell maintenance was used, however, suggesting that the cells were not metabolically active but rather that they were used as a simple form of an enzyme immobilizate with a regenerating enzyme and a cosubstrate in place. In summary, developing a method to quantify nicotinamide adenine dinucleotides requires careful design of the buffer conditions that will introduce a compromise, because the optimal stabilities of reduced versus oxidized and phosphorylated versus nonphosphorylated cofactors differ.

The "stability" of the reduced cofactors is significantly lowered in cells under conditions at which enzymes can operate, because the consumption rate is high compared with the intracellular concentration (for most cells, between 1 m*M* and 1 $\mu M$ total $NAD^+$/NADH). Assuming a maximum NADH concentration of 1 m*M* and an NADH regeneration rate of 15 mmol $g_{CDW}h^{-1}$, as reported for *P. putida* during growth on minimal medium with glucose as the carbon and energy source (38), the half-life is approximately 4 minutes. Because intracellular NADH is often present in the $\mu$molar range and the redox regeneration rate during redox-dependent biocatalysis can reach up to 100 mmol $g_{CDW}$ $h^{-1}$ (38), even shorter half-lives must be assumed.

Rapid sampling procedures that allow microbial metabolism to be quenched in subseconds were developed to account for the fast turnover of central carbon metabolism metabolites [see (285) for a comprehensive review]. The methods are primarily based on a combination of valves with minimized dead volumes and a quenching solution (*e.g.*, −40°C methanol, liquid nitrogen, etc.). Sample treatment after quenching wholly depends on the analytical method that is used for quantification. In the next paragraphs, simple spectroscopic techniques up to sophisticated liquid chromatography-mass spectrometry (LC-MS) methods are summarized.

In the 1960s, enzymatic cycling methods to determine $NAD^+$, NADH, $NADP^+$, and NADPH concentrations were developed (205, 233). The improved assays use changes in color of thiazolyl blue tetrazolium bromide (MTT) to monitor concentration (29, 202, 233). This cycling assay is highly sensitive, but reproducibility is difficult to achieve, because enzyme stability and reagent handling influence the outcome of the assay, in addition to other aspects. More specifically, in our experience, alcohol dehydrogenase instability demands a new calibration curve for each experiment. Minimizing light exposure of MTT is crucial, because the color can change in minutes when MTT is exposed to direct sunlight. Some studies opine that samples are neutralized after acid/base treatment, although a pH of approximately 7 can alter cofactor concentrations. Following the protocols, the samples are

not neutralized, but roughly half of the corresponding acid/base that is necessary for neutralization is added. In addition, as in any enzymatic assay, the linearity of the substrate to the quantity to be measured must be considered. Therefore, rather a low amount of crude extract is generally used. It is important to state that laboratories in which the cycling assay is carefully established can generate high quality data. Nevertheless, the myriad possible pitfalls ask for alternative methods that are potentially simpler, are less prone to error, and deliver additional information, such as the concentrations of other cofactors (*e.g.*, ATP) or intracellular metabolites (*e.g.*, glucose-6-phosphate).

The simplest assay for measuring reduced redox cofactors is spectrophotometry at 340 nm, as discussed above (see Fig. 13). This method is suitable only for samples that have high concentrations ($\mu M$ and higher) and low complexity, however, because reduced cofactors and other compounds absorb at this wavelength. To improve specificity and sensitivity, high-pressure liquid chromatography (HPLC), which allowed analytes to be separated, was coupled with a UV detector (208). Mailinger *et al.* distinguished between oxidized and reduced redox cofactors using acidic and alkaline sampling conditions to remove the reduced and oxidized forms, respectively, as explained above. However, only the oxidized redox cofactors were quantified with high accuracy, because interfering substances were present in the alkaline samples. Therefore, the reduced redox cofactors were oxidized by a glutamate dehydrogenase (208).

Mass spectrometers (MS) are more sophisticated detectors for HPLC systems because they do not only quantify but also enrich signals and confirm analytes. Yamada *et al.* reported detection limits for the quantification of $NAD^+$ and its related compounds to be as low as 0.1 pmol using HPLC-tandem mass spectrometry (LC-MS/MS) (367). Recently, Schroer *et al.* modified their metabolome method (206) to quantify $NAD^+$, NADH, $NADP^+$, and NADPH during the biotransformation of methyl acetoacetate to methyl 3-hydroxybutyrate, using 2-propanol as the substrate for redox cofactor regeneration. The limit of detection was below 6 fmol and the limit of quantification below 25 fmol, with a short analysis time of 35 min (291).

Although the recent developments towards quantitative, highly sensitive, and robust LC-MS/MS methods are promising, also here, the intrinsic and different instabilities of redox cofactors have to be considered, especially with respect to pH and buffer composition (273). Most HPLC methods operate at a pH [*e.g.*, pH 6.5 (208)], which can result in analyte degradation. The impact of elution buffers also have to be considered, as phosphate and acetate enhance redox cofactor degradation (273). Most likely, however, sample preparation will limit the widespread use of these methods, because fast sampling and sample conditions (*e.g.*, temperature, buffer, pH) will influence the outcome significantly; NADH degradation of more than 50% was observed during sample preparation (291).

Alternatives based on miniaturization of the cycling assay (365), measurements of *in vivo* NADH concentrations by 2-photon autofluorescence dynamics imaging (166), and $^{13}$C-nuclear magnetic resonance (NMR) (229) may overcome some or all of the above mentioned limitations. The *in vivo* approaches are particularly attractive, because they allow real-time and non-cell-destructive analysis of NAD(P)H. In addition, cumbersome sample preparation is eliminated. Two-photon autofluorescence dynamics imaging has not been used to investigate microbial metabolism, most likely due to the small size of many bacteria, which is on the order of the wavelength of visible light. In addition, this technique does not allow determination of the ratio of reduced to oxidized cofactor.

In contrast, $^{13}$C-NMR has been used extensively to examine sugar metabolism in *L. lactis* and other microbes (229). During aerobic glucose metabolism of *L. lactis*, $NAD^+$ and NADH concentrations of 3 and 0 m$M$ were measured, respectively, while 1 and 2 m$M$ were observed in the first hour after glucose depletion (228). Although $^{13}$C-NMR is highly potent, the expensive instrumentation, need for expert knowledge, and the low sensitivity limit its general applicability for the analysis of redox metabolism. The latter makes it especially difficult to determine redox cofactor levels during growth, because the required cell concentrations (*i.e.*, the required metabolite concentrations) are hardly achievable; instead, high-cell density resting cell assays are routinely used.

In summary, reliable determination of redox cofactor concentrations requires careful establishment of analytical and sample preparation methods as well as careful data interpretation.

### C. Metabolic flux analysis for redox cofactor regeneration rate estimation

As mentioned in Section III.B.1, $^{13}$C-based MFA is currently the best approach for the quantification of the *in vivo* flux distribution and the unique technique for the calculation of cofactor regeneration rates. With $^{13}$C-based MFA, the limitations of classical MFA can be overcome and a higher flux resolution can be achieved by complementing the stoichiometric constraints used in MFA with isotope isomer (isotopomer) constraints gained from a carbon labeling experiment. In such an experiment, a substrate containing the stable isotope tracer $^{13}$C is fed to the biological system. The labeled carbon atoms are then distributed over the metabolic network and the labeling patterns of intracellular metabolites or amino acids located in proteins can be measured by NMR or MS instruments.

The rationale behind these $^{13}$C tracer experiments is that the carbon backbones of the metabolites often are manipulated differently by alternative pathways, leading to distinct $^{13}$C-labeling patterns of the metabolites. Thus, constraints to fluxes complementary to the basic stoichiometric constraints can be derived by measuring the mass isotope distribution of metabolites, that is, the relative abundances of molecules only differing in the number of heavy isotopes. Currently, two main approaches exist for the interpretation of the determined $^{13}$C-labeling patterns and the inference of intracellular fluxes. In the global isotopomer balancing approach, the problem of estimating metabolic fluxes from the isotopomer measurements is formulated as a nonlinear optimization problem, where candidate flux distributions are iteratively generated until they fit well enough to the experimental $^{13}$C-labeling patterns (288, 355). The second method is metabolic flux ratio analysis, coined by Sauer as METAFoR (280), which relies on the local interpretation of labeling data using probabilistic equations which constrain the ratios of fluxes producing

the same metabolite. The approach is essentially independent of the global flux distribution in the entire metabolic network (108, 280), meaning that flux ratios can be calculated without knowing the uptake and production rates of external metabolites and the biomass composition. If enough independent flux ratios can be identified, it is possible to use them to constrain the metabolic network equation system and to calculate the full flux distribution within the network (110).

Due to the great sensitivity of gas chromatography-mass spectrometry (GC-MS) instruments as compared to NMR, GC-MS analysis is today the most popular technique for detecting $^{13}$C-labeling patterns of metabolites. Highly sensitive and high-resolution mass spectrometers enable the analysis of proteinogenic amino acids from only 0.3 mg CDW so that experiments can be scaled down to deep-well microplate format, allowing high-throughput $^{13}$C-labeling experiments at significantly reduced costs for the expensive isotopically labeled substrate (34, 110).

$^{13}$C MFA based on the measurement of proteinogenic amino acid labeling pattern has the disadvantage that the time to reach an isotopically steady state (no change of the labeling pattern over time) necessitates running the experiments significantly longer than the doubling time ($\mu^{-1}$). Chemostat experiments are, for example, generally run for at least three complete volume exchanges before sampling. To overcome this disadvantage, endeavors exist for measuring at nonstationary conditions the labeling patterns of intracellular metabolites that have turnover rates in the second to subsecond scale. The simultaneous measurement of intracellular metabolite concentrations and labeling patterns poses high challenges to the analytics because metabolite concentrations are about 500-fold lower than that of proteinogenic amino acids. Due to the rapid turnover of the metabolites, the sampling technique has to ensure an immediate stop of the metabolic activity (see Section IV.B for details). However, tackling these difficulties is worthwhile as central metabolite-based MFA not only reduces experiment duration but also increases the resolution of intracellular fluxes and extends the scope of $^{13}$C-MFA to nonstationary conditions, such as fed-batch fermentations or transients in batch cultures, and to resting cells. See Ref. (316) for a review of the recent advances in $^{13}$C-based MFA.

## V. Coupling of Redox Biocatalysis with Redox Metabolism

In this section, we present examples for applied redox biocatalysis that couple a redox reaction of synthetic interest (*i.e.*, a redox cofactor dependent enzyme) to the host metabolism. In addition, strategies to increase redox cofactor regeneration rates by using a second electron donor substrate or by modifying the host's central carbon metabolism are presented.

### A. Examples from industry and academia

The presented examples cover five oxygenase enzyme classes and one dehydrogenase class (see also Fig. 1). Where possible, the interplay of redox metabolism and biocatalytic performance of the whole-cell biocatalysts is discussed. For detailed analyses on energetics of fermentation and biocatalysis examples, we refer to a recent summary article (68).

As an example of a mononuclear nonheme oxygenase, we chose the 2-oxoglutarate dependent proline 4-hydroxylase from *Dactylosporangium* sp. strain RH1, a bacterium of the class actinobacteria. The enzyme catalyzes the production of *trans*-4-hydroxy-L-proline from L-proline. Two alternative whole-cell biocatalysts have been constructed for this product by the company Kyowa Hakko Kogyo Co. Ltd. (Tokyo, Japan), which differed in the substrate used. For the one step biotransformation of L-proline to *trans*-4-hydroxy-L-proline, only the gene for the proline 4-hydroxylase was expressed in *E. coli* (297). The catabolized carbon and energy source glucose delivered the 2-oxoglutarate, which is a cosubstrate and electron donor of the proline 4-hydroxylase. The products of this reaction are succinate, $CO_2$, and *trans*-4-hydroxy-L-proline. This reaction running in parallel to the conversion of 2-oxoglutarate to succinate in the TCA cycle costs one NADH and one ATP, which would otherwise be generated by 2-oxoglutarate dehydrogenase and succinyl-CoA ligase, respectively. Interestingly, *E. coli* expressing proline 4-hydroxylase showed an increased growth rate in the presence of L-proline as compared to cells lacking this enzyme. As 2-oxoglutarate dehydrogenase is repressed during growth of *E. coli* under excess glucose, most likely by high NADH levels, the bypass from 2-oxoglutarate directly to succinate via the proline 4-hydroxylase might overcome the limiting rate of succinate formation and hence of the TCA cycle. To make the addition of the biotransformation substrate obsolete, an *E. coli* strain carrying a deregulated proline synthesis pathway was engineered. The nonfeedback controlled genes of the *gamma*-glutamylphosphate reductase (*proA*) and the *gamma*-glutamyl kinase (*proB*) were introduced (298). To increase proline synthesis and subsequently *trans*-4-hydroxy-L-proline formation, the first gene (*i.e.*, *putA*) of the proline degradation pathway was deleted. The engineered strain produced up to 25 g/L *trans*-4-hydroxy-L-proline within a rather long fermentation time of 96 h. Improvements with respect to rate and titer were not reported, but targets for improvements are numerous, including the rate of proline synthesis and the utilization of succinate. The synthesis of *trans*-4-hydroxy-L-proline represents a good example for biocatalysis-directed strain engineering, starting with the choice of substrate and not ending with the interplay with (redox) metabolism.

The heme-dependent P450 monooxygenases are a very interesting class of enzymes with members highly specialized for a certain substrate, while others are highly promiscuous (*e.g.*, P450s of the human liver). Bureik and co-workers established several whole-cell biocatalysts based on heterologous expression of human P450 encoding genes using the yeast *Schizosaccharomyces pombe*. These NADPH-dependent enzymes were used for the synthesis of the designer drug 4′-hydroxymethyl-*alpha*-pyrrolidinohexanophenone using P450 2D6 (254, 255), the synthesis of the designer drug N-(1-phenylcyclohexyl)-2-hydroxyethanamine using P450 2B6 (254), and the synthesis of hydrocortisone from 11-deoxycortisol using P450 11B1 (129), besides others. The low rates and final titers reported for most of the substrates asked for the elucidation of possible limitations. Production of these heme-containing proteins appears to be efficient in *S. pombe*. The supply of the cosubstrates $O_2$ and NADPH was shown not to be limiting by quantitative physiology and $^{13}$C-tracer based MFA (92), leaving the intrinsic reaction

rates and the mass transfer of the relatively large and hydrophobic substrates as the most likely limitations of P450 whole-cell biocatalysis.

The company Cognis (Monheim, Germany) reported on engineered *Candida tropicalis* strains for the production of long-chain dicarboxylic acids (161), which are important raw materials for polymer synthesis in the chemical industry. The strains overexpressed the native P450 monooxygenase and the corresponding NADPH-cytochrome reductase genes and in addition contained a deletion of the gene for the first enzyme in the $\beta$-oxidation pathway. Aliphatic molecules with chain lengths ranging from 12 to 22 carbons are substrates of this P450, allowing the synthesis of a wide range of saturated and unsaturated dicarboxylic acids. Actually, *C. tropicalis* engineered in this way is the most efficient P450 based whole-cell biocatalyst with respect to achieved rate (up to 1.9 g $L^{-1}$ $h^{-1}$) and titer (up to 166 g $L^{-1}$) (161). In a pathway engineering project, P450 enzymes were used for the multistep synthesis of hydrocortisone from glucose. In engineered *S. cerevisiae*, the pathway to ergosterol was composed of one native P450 monooxygenase and four P450s of mammalian origin (315). Although the reported production rate and final titers were rather low, the chemical reactions carried out in one reaction compartment are remarkable, indicating the potential of P450 and biocatalysis in general for the synthesis of fine chemicals (95).

The biocatalytic potential of the nonheme, binuclear xylene monooxygenase was studied in great detail by Bühler *et al.* (59, 60, 62). The enzyme originates from *P. putida* mt-2 and was used in growing cells of recombinant *E. coli.* The synthesis of alcohols, aldehydes, and acids from aromatic substrates was shown to be possible with this single enzyme. The application of the two-liquid phase concept (*i.e.*, the use of an additional organic solvent phase to increase substrate/product solubility and to reduce cell toxicity) allowed the targeted production, for example, of 3,4-dimethylbenzaldehyde from pseudocumene (61). It was shown that the initial pseudocumene concentration was important for the exclusive production of 3,4-dimethyl-benzaldehyde. For example, further oxidation of the product to 3,4-dimethylbenzoic acid was inhibited by pseudocumene or 3,4-dimethylbenzyl alcohol, letting the authors conclude that only the careful use of the two-liquid phase system allowed the exploitation of the complex kinetics of the multistep oxygenation catalyzed by xylene monooxygenase. Maximal productivities of up to 1.6 g $L^{-1}$ $h^{-1}$ have been reported. The impact on redox metabolism differs depending on the product formed with one NADH consumed per alcohol, two per aldehyde, and three per acid molecule produced. Furthermore, the NADH-dependent back reaction from aldehyde to alcohol had to be considered. This reaction was catalyzed by host dehydrogenases and counteracted aldehyde synthesis, albeit to low extent. The influence of NADH availability on the reaction rates was further analyzed *inter alia* on the basis of a mathematical process model for the two-step oxygenation of pseudocumene to the corresponding aldehyde, which consumes a least two NADH molecules per product molecule formed. Surprisingly, a pH shift from 7.1 to 7.4 significantly reduced growth rates and doubled specific biotransformation rates but had no effect on single-step bioconversion rates in short-term experiments based on resting cells (61, 66). This observation and process simulation provided evidence for a pH-influenced competition for NADH between XMO and the respiratory chain with its consequential impact on bioconversion and cell growth. For the simulation of such differential NADH limitation, a pH-dependent feedback inhibition of the NADH consuming bioconversions was introduced as a modeling tool, which allowed good simulations of biotransformation experiments performed at varying pH, scale, and initial substrate concentration. A change in the pH influences the proton gradient and thus the proton motive force over the cytoplasmic membrane (300, 377), where the enzyme systems competing for NADH, namely XMO and the enzymes involved in oxidative phosphorylation, are located. Therefore, a rise in the pH might promote the flow of NADH to XMO at the expense of the flow to the electron transport chain. This might cause additional stress for the cells and interfere with cell growth. In fact, this was reflected by lower biomass yields and growth rates at higher biotransformation rates. The same enzyme was used by Lonza Group Ltd. (Basel, Switzerland) for the selective oxidation of a methyl group of heteroarenes to the corresponding carboxylic acids utilizing wild-type *P. putida* mt-2. The activity of the xylene monooxygenase was induced by growing the cells on *p*-xylene. The required redox cofactor regeneration was carried out by the xylene degradation pathways and especially the catabolism of the resulting products in the TCA cycle (295). The process runs at a $m^3$-scale with multi tons of product produced per year (201).

The flavin-dependent styrene monooxygenase from *Pseudomonas sp.* strain VLB120 catalyzing the enantioselective epoxidation of styrene to (*S*)-styrene oxide was investigated in great detail by our group. We chose this enzyme for studying its interplay with redox metabolism in whole-cell biocatalysts, as high enzyme production above 20% of total protein, activities of up to 100 U $g_{CDW}^{-1}$, and productivities of up to 13 g $L_{aq}^{-1}$ $h^{-1}$ have been achieved with recombinant *E. coli* (241, 243). The stoichiometry of the catalyzed reaction involves one NADH per product molecule formed, although slightly higher NADH consumption was reported for the isolated enzymes *in vitro* (241), which was explained by uncoupling of NADH oxidation from product formation, a mechanism also postulated to be present during biocatalysis in whole cells (37, 67). Substrate, product, and/or $O_2$ mass transfer and *in vivo* enzyme activity were found not to limit the production rate. In fact, NADH supply was postulated to limit oxygenase catalysis at high rates (65). For example, a 50% higher specific styrene epoxidation activity was observed for resting (*i.e.*, nongrowing) cells as compared to growing cells, suggesting that the competition for redox cofactors during biomass synthesis lowers the rate of the epoxidation reaction. This hypothesis was confirmed by decreasing the redox cofactor regeneration rate and/or yield in styrene monooxygenase containing resting cells using single gene deletion mutants of *E. coli*'s central carbon metabolism (37). Indeed, the rate of redox biocatalysis was dependent on the metabolic network structure. For (*S*)-styrene epoxide production, growing recombinant *E. coli* cells are routinely used in our group in an optimized two-liquid phase system to maximize substrate addition and minimize substrate/product toxicity (244). Thereby, the growing state ensures constant oxygenase levels. Although partition coefficients for both substrate and product were high in the solvent–water system used, high concentrations of (*S*)-styrene epoxide caused acetic acid formation, membrane permeabilization, and cell lysis (246). Under these

conditions, specific epoxidation, $CO_2$ evolution, $O_2$ uptake, and glucose uptake rates decreased simultaneously. Since $CO_2$ evolution is directly proportional to the generation of reduction equivalents in the form of NAD(P)H and $FADH_2$ during aerobic glucose catabolism (141), the simultaneous decrease of glucose uptake rates, specific $CO_2$ evolution rates, and specific styrene monooxygenase activities suggested that decreasing cofactor regeneration rates may have reduced biotransformation performance.

Solvent-tolerant *P. putida* DOT-T1E were able to increase glucose uptake rates and redox cofactor regeneration rates on demand (38). This strain, employed as a recombinant, allowed (*S*)-styrene epoxide formation also in the presence of the toxic low $logP_{ow}$ organic solvent octanol. However, 3-times lower specific activities and up to 10-times lower yields of (*S*)-styrene epoxide per NADH regenerated were observed, when compared to biotransformations in the presence of a nontoxic solvent. This reduced biocatalytic activity combined with increased glucose uptake rates and some additional detailed analyses lead to the conclusion that, under these harsh growth conditions, the redox cofactors are used for energy generation to enable solvent tolerance rather than redox biocatalysis. As possible reasons for low yields of (*S*)-styrene epoxide formed per NADH regenerated, product toxicity, uncoupling, cell maintenance, and regulatory phenomena have been discussed (37, 38, 67).

Another group of flavin dependent enzymes, the Baeyer–Villiger monooxygenases, catalyze the stereoselective oxidation of linear and cyclic ketones to the corresponding esters and lactones, respectively (7). Recently, pilot-scale production of a lactone employing cyclohexanone monooxygenase was reported (22). The racemic substrate bicyclo[3.2.0] hept-2-en-6-one was converted to an equimolar mixture of (-)-(1R,5S)-3-oxabicyclo[3.3.0]oct-6-en-2-one and (-)-(1S,5R)-2-oxabicyclo-[3.3.0]-oct-6-en-3-one. Limited substrate feed that guaranteed nonlimiting $O_2$ levels and the avoidance of substrate accumulation turned out to be important for the scale up. The authors point out that, for an efficient downstream processing, the substrate feed should be stopped before harvesting as the chromatographic separation of the products is simple when no or only trace amounts of substrate are present (22). In this example, a maximal productivity of $0.6\,g\,L^{-1}\,h^{-1}$ and a final product titer of $4.5\,g\,L^{-1}$ were reported.

The toluene dioxygenase belonging to the mononuclear, nonheme Rieske type dioxygenases (Table 1) was used to produce toluene *cis*-glycol from toluene. In order to prevent toxification of the whole-cell biocatalyst by toluene, a tetradecane based two-liquid phase system was used. In this system, the *cis*-dihydrodiol dehydrogenase deficient *P. putida* UV4 allowed the accumulation of the toluene degradation intermediate toluene *cis*-glycol at volumetric productivities of $9.5\,g\,L_{aq}^{-1}\,h^{-1}$ (77, 203). The nontoxic, rather polar product accumulated in the aqueous phase. The high activity of $120\,U\,g_{CDW}^{-1}$ for this NADH consuming reaction suggests efficient NADH regeneration by the cell metabolism on the carbon and energy source glucose.

For 3-methylcatechol production, the toluene dioxygenase was coupled to the *cis*-dihydrodiol dehydrogenase in a two-step reaction that is redox neutral (*i.e.*, NADH oxidation by the dioxygenase and $NAD^+$ reduction by the dehydrogenase). Hence, the reaction sequence should add limited or no redox burden to the cell. However, as the highly toxic product is poorly soluble in both water and organic solvents with a high $logP_{OW}$, the toxic low $logP_{OW}$ solvent octanol was chosen as second phase. Using solvent-tolerant *P. putida* S12 as the host strain (351), productivities of $0.067\,g\,L_{aq}^{-1}\,h^{-1}$ were achieved. As reported for the epoxidation of styrene in an octanol–water two-phase system (38), the low activities suggest that the presence of octanol add a major burden on cellular metabolism, reducing the capacities for redox biocatalysis.

ICI (Imperial Chemical Industries, Slough, UK) and others previously used a benzoate dioxygenase from *P. putida* for the production of *cis*-dihydrodiols, which are intermediates in the synthesis of *β*-lactams. The natural host was used for gene expression and cofactor regeneration via its central carbon metabolism. Although the *P. putida* strain used tolerated high substrate/product concentrations, cell growth (biocatalyst production) and redox biocatalysis were separated in two steps, as the *cis*-dihydrodiols inhibit growth at low concentrations (201). The reviewed benzoate and toluene dioxygenase examples highlight the competition between biomass (*i.e.*, biocatalyst) synthesis and biocatalysis, as both biochemical processes depend on energy and redox cofactors generated during catabolism. The proposed separation of the two processes is valid as long as the biocatalytic activity is stable. As an outlook, the concept of "zero growth" can be mentioned here that aims at the uncoupling of biomass and product formation (40).

Dehydrogenases are frequently used in industry for the synthesis of fine chemicals (*e.g.*, chiral alcohols). Here, we present academic results and an industrial example for the zinc-dependent NADPH requiring alcohol dehydrogenase of *Lactobacillus brevis* (LBADH). LBADH was identified in a screen for oxidoreductases with low substrate specificity (148). This enzyme showed interesting catalytic activities (149) and, importantly, was highly stable. This stability was recently used by Schroer *et al.* in the whole-cell biotransformation of methylacetoacetate to *(R)*-methyl 3-hydroxybutanoate, reporting high space time yields for up to 7 weeks (289). In this example, the redox cofactor dependent enzyme was not connected to cellular metabolism and NADPH was regenerated via the oxidation of 2-propanol to acetone catalyzed by the very same LBADH (refer also to Section V.B). This example is especially remarkable, as a maximal space time yield of $29\,g\,L^{-1}\,h^{-1}$ and a very low catalyst consumption of $0.0168\,g_{catalyst}\,g_{product}^{-1}$ were reported, indicating the potential of whole-cell redox biocatalysis. As the electron donor 2-propanol was added in only slight excess, a redox cofactor regeneration rate in the order of the product formation rate can be assumed.

The same enzyme was used by Codexis Inc (Redwood City, CA) as a basis for generating a variant that efficiently catalyzes the transformation of 4-chloro-3-oxobutyrate-ethylester to *(S)*-4-chloro-3-hydroxybutyrate-ethylester, an intermediate for the synthesis of a hydroxynitril ester. The latter compound is a precursor of Lipitor (Pfizer Inc., New York, NY), a cholesterol-lowering agent with a yearly production exceeding 100 tons. The redox cofactors were supplied by glucose dehydrogenase in an *in vitro* system based on isolated enzymes. The applicability of this two enzyme reaction was achieved by selecting variants of the enzymes that showed high activities in the presence of 20% (w/v) substrate and butyl acetate as solvent.

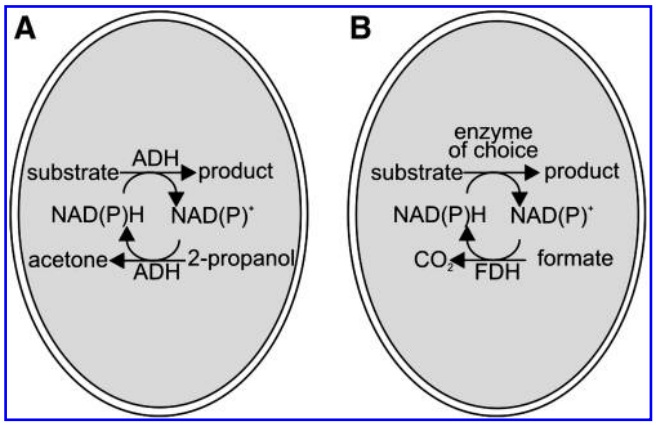


**FIG. 17. Strategies for artificial redox cofactor regeneration.** (**A**) A dual-substrate enzyme is used that reduces the redox cofactor using an auxiliary substrate while oxidizing the cofactor in the target reaction. Here the most frequently used system based on an alcohol dehydrogenase is shown. (**B**) Alternatively, two enzymes are used for biotransformation and redox cofactor regeneration, respectively. Here, the well-described formate dehydrogenase regeneration system is shown.

The reviewed dehydrogenase examples indicate the potential of artificial redox cofactor regeneration systems, which are independent of the cellular redox metabolism (see next section). Such systems, however, only are applicable to stable enzymes and whole-cell biocatalysts (which, for example, do not lose the redox cofactors due to permeabilization).

### B. Artificial redox cofactor regeneration systems

For thoroughness, concepts for metabolism-independent artificial redox cofactor regeneration systems are briefly introduced with a focus on whole-cell biocatalysts. Explicitly, we do not provide a comprehensive summary of such artificial cofactor regeneration systems, because a recent comprehensive review is available (353).

For whole-cell biocatalysis, two different artificial cofactor regeneration strategies have been developed, both making use of a second enzymatic reaction [Fig. 17, (353)], in analogy to the substrate coupled and enzyme coupled cofactor regeneration strategies for *in vitro* biocatalysis. Using a dual-substrate enzyme for parallel oxidation of an auxiliary substrate (electron donor) and reduction of the target substrate (electron acceptor), direct coupling of the rate of redox cofactor regeneration and biocatalysis can be guaranteed. The organic solvent-resistant alcohol dehydrogenase from *Rhodococcus ruber*, which catalyzes the synthesis of valuable alcohols using 2-propanol as the auxiliary substrate, is a prominent example for this approach (180). 2-Propanol concomittantly is oxidized to acetone (121, 289).

In the second approach, the auxiliary substrate is oxidized by an additional enzyme, generating the reduced form of the redox cofactors. A salient example is the formate dehydrogenase (187, 293). Both enzymatic reaction systems that are depicted in Figure 14 profit from the volatile products acetone and $CO_2$, which have limited (121) or no inhibitory effect on biocatalytic rates, respectively. Formate dehydrogenase is frequently used in the industrial production of fine chemicals, such as L-*tert*-leucine (185).

### C. Network redesign

We have shown in Section III.B how redox cofactor balances constrain metabolic network operation and have pointed out the flexibility of microorganisms to adjust the metabolic fluxes to environmental or genetic perturbations. This flexibility is exploited when performing whole-cell redox biotransformations: The enhanced cofactor demand induced by the biotransformation reaction is compensated for by the host strain adequately adapting its metabolism. This interrelation between redox biocatalysis and host metabolism and the possible limitation of redox biocatalysis by the host metabolism have long been overlooked when optimizing redox biocatalytic processes. Instead, optimization strategies focused on enzyme activity, selectivity, and specificity as well as process design.

In contrast, in fermentation processes, in which the product (*e.g.*, amino acid, ethanol, lactate, or antibiotic) is produced from the growth substrate by exploiting native metabolic pathways, the necessary shift of carbon fluxes from biomass to product formation pathways makes the interaction of biocatalysis and cell metabolism directly obvious. Optimization of fermentation processes therefore included intensive pathway engineering to relieve carbon limitation imposed by metabolic bottlenecks. Moreover, systemic metabolic analyses revealed that certain processes, which require large amounts of reduced cofactors (*e.g.*, amino acid or antibiotics production) are not carbon limited but rather constrained by redox cofactor supply. Such processes could be improved by redirecting fluxes towards pathways with higher redox cofactor yields (25, 335).

In the last decades, the advances in molecular biology paved the way for synthetic biology that aims to design and construct new biological components, such as enzymes, genetic circuits, and cells, and to redesign existing biological systems (169). This targeted and immense interventions in the cell metabolism by, for example, *de novo* pathway design and transfer to alternate hosts, clarified the importance of balancing heterologous pathways with the host metabolism—both in terms of carbon as well as redox balance—not only for fermentation but also for biotransformation processes. Thus, today the potential of boosting the availability of redox cofactors for biocatalysis improvement has generally been recognized.

The ultimate aim of synthetic biology is the accurate predictive modeling of microbial chemical factories by computer-aided-design (CAD) systems. But due to the complexity of biological systems, such design tools still do not exist or are in their infancy. Stoichiometric metabolic models fall into this category and—as discussed in Section III.B.1—have only limited predictive capability. Therefore, most of the currently applied tools (encompassing metabolic flux analysis, transcriptomics, proteomics, etc.) are analytical and allow only an inverse engineering of the cell that is the determination of the genetic and/or environmental factors conferring a desired phenotype (emerged by natural evolution or by for example random mutagenesis or other nontargeted strain optimization techniques) and endowing that phenotype on another strain or organism by directed genetic or environmental manipulation (19).

Despite such limitations, these methods have proven useful in engineering the redox metabolism of diverse microorganisms. In the remainder of this section we will discuss strategies for the rational redesign of host metabolism that could alleviate redox cofactor limitation and ameliorate process performance.

Constraint-based models have been used to tackle the metabolic engineering problem of predicting gene knockouts or insertions for strain optimization. The first to report a rational modelling framework for suggesting gene knockouts leading to the overproduction of a desired metabolite were Burgard *et al.* (69, 70). They developed OptKnock, an algorithm that identifies reactions in a metabolic network that enable the decoupling of cellular growth from product formation. Knockout of the corresponding genes results in a strain, in which growth is strictly linked to product formation.

OptKnock is implemented by formulating a bi-level linear optimization problem in which both biomass and product formation are optimized. The problem is solved using mixed integer linear programming (MILP) that guarantees to find the global optimal solution. The algorithm was applied to identify in an *E. coli* metabolic network gene knockout targets suitable for enhanced overproduction of succinate, lactate, and 1,3-propanediol. The obtained *in silico* mutants were in good agreement with engineered strains reported in literature. The same authors developed OptStrain, a computational framework aimed at guiding pathway modifications for the overproduction of a target compound through reaction deletions from and insertions to a metabolic network. OptStrain also affords to solve a MILP problem.

Bro *et al.* (55) applied a less comprehensive but substantially less computationally demanding reaction insertion analysis to score strategies for the metabolic engineering of the *S. cerevisiae* redox metabolism with the aim to a shift from glycerol to ethanol formation under anaerobic conditions without affecting the biomass yield. This was achieved by applying FBA with the objective to minimize the glucose uptake rate at a fixed growth rate equal to the maximum specific growth rate of the wild type *S. cerevisiae* strain under anaerobic conditions ($\mu = 0.27\,h^{-1}$) and adding—one at a time—3800 reactions of a metabolic reaction database. The performance of these 3800 modified reaction networks was evaluated. One of the best strategies was the addition of the irreversible conversion of glyceraldehyde 3-phosphate and $NADP^+$ into 3-phosphoglycerate and NADPH catalyzed by a non-phosphorylating $NADP^+$-dependent glyceraldehyde-3-phosphate dehydrogenase, thereby completely eliminating glycerol formation and boosting the ethanol yield by 10%.

*In vivo* testing of this strategy by expressing *gapN* of *Streptococcus* mutants yielded a strain that produced 40% less glycerol and 3% more ethanol under anaerobic conditions. The maximal growth rate of this strain was not impaired and biomass yield was slightly enhanced. The residual glycerol formation was attributed to a limited glyceraldehyde-3-phosphate dehydrogenase activity as a simulation with a glycerol flux constrained to the experimentally determined value precisely predicted the increased biomass and ethanol yield.

Several other examples of successful implementation of *in silico* derived gene deletion strategies exist in the literature (13, 143, 170). Although these studies intended to redirect fluxes towards product formation pathways, it turned out in some cases that the process was rather limited by redox cofactor availability than by carbon supply. In contrast, a study of Blank *et al.* (37) focused directly on the estimation of the maximal NADH regeneration capacity of *E. coli* considering supply of this reduced cofactor as the limiting factor of the NADH-dependent styrene epoxidation in recombinant *E. coli* cells.

Besides the estimation of maximal NADH regeneration rates, which can serve as target values for redox cofactor dependent biocatalysis, the study showed the importance of the PP pathway flux and transhydrogenase activity for efficient NADH regeneration during growth on glucose. These findings can guide future strategies for the rational design of superior redox biocatalysts. Indeed, overexpression of transhydrogenases and several PP pathway enzymes have already been identified as metabolic engineering targets to improve the rate of redox cofactor-dependent enzymes.

One example is the production of L-lysine in *C. glutamicum*. The synthesis of one mol lysine requires 4 mol NADPH; to satisfy this high redox cofactor demand, Becker *et al.* (25) suggested an amplification of the PP pathway flux as a promising target to improve lysine formation. They pursued this strategy by overexpressing a *zwf* gene in a *C. glutamicum* lysine overproducer and measured a significant increase of the lysine yield by 30%. Additional overproduction of fructose-1,6-bisphosphatase resulted in an overall yield increase of 70%. $^{13}C$-based MFA performed with the different strains unraveled that the genetic modifications indeed resulted in a higher PP pathway flux and that this flux correlated with lysine production. However, in this case, the metabolic engineering strategy did not originate from a computational metabolic analysis but from a metabolic flux profiling study of five successive generations of lysine-producing *C. glutamicum* strains. Wittmann and Heinzle (359) showed in this study that the relative PP pathway flux successively increased from generation to generation, clearly corresponding to the product yield. This inverse engineering—albeit not the ultimate goal of synthetic biologists—has proven useful to identify new, nonintuitive metabolic engineering targets (54, 138).

An alternative strategy to increase NADPH supply for lysine production is the expression of the proton-translocating transhydrogenase genes of *E. coli*. Depending on the carbon source, an up to 300% higher titer and thus yield on carbon source could be achieved, indicating that lysine production is strongly NADPH limited (162).

Overexpression of transhydrogenases as a means to ameliorate cofactor supply has been applied in several other processes. For example, improved synthesis of chiral alcohols in a one-step biotransformation from the corresponding ketones was reported with a recombinant *E. coli* strain overproducing the proton-translocating transhydrogenase, an NADPH-dependent alcohol dehydrogenase, and a $NAD^+$-dependent formate dehydrogenase (349). An $NADP^+$-dependent gluconate:NADP-5-oxidoreductase was engineered into *Gluconobacter oxydans* to produce 5-keto-D-gluconate from glucose. The coexpression of *udhA* significantly increased the productivity of this whole-cell biocatalyst (135). Furthermore, an *E. coli* strain containing genes from *Alcaligenes eutrophus* for polyhydroxybutyrate (PHB) production and overexpressing the gene encoding the soluble transhydrogenase UdhA was constructed (277). This modified strain accumulated significantly higher amounts of PHB compared

with the strain lacking the additional UdhA activity. Because PHB demands copious NADPH, the authors concluded that recombinant UdhA delivered the additional NADPH. This engineering strategy contrasts the proposed natural role of UdhA (281), oxidizing excess NADPH, thereby guaranteeing a closed NADPH/$NADP^+$ balance. Because the enzyme catalyzes a reversible reaction, the direction of the reaction is highly influenced by the intracellular substrate and product concentrations, as recently discussed for several bacteria (116).

As discussed in Section III.B.2, the biocatalytic performance of *E. coli* transhydrogenase deletion mutants did not differ compared with that of the reference strain during fed-batch and resting cell assays for NADPH-dependent transformation of xylose to xylitol (74). This finding indicates the necessity of additional studies to clarify the function of the two transhydrogenases in *E. coli* and other bacteria.

As described in Section III.B.1, regulatory constraints may restrict the fluxes in a metabolic network. Thus, deregulation of specific pathways can also be a good strategy in strain optimization. As an example, we present here the effect of TCA deregulation on the metabolic fluxes in *E. coli*. It is well known that this organism produces acetate in the so-called overflow metabolism during aerobic growth on glucose and it is assumed that this overflow metabolism occurs due to a repression of the TCA cycle (340). Since the TCA cycle is the main source of energy and reducing equivalents, the enhancement of TCA cycle activity is of practical interest for redox biocatalysis. Two approaches that successfully deregulated this pathway have been reported. Veit *et al.* relieved transcriptional control of the *sdhCDAB–b0725–sucABCD* operon by chromosomal promoter exchange mutagenesis, yielding a strain with increased specific activities of the TCA cycle enzymes succinate dehydrogenase, 2-oxoglutarate dehydrogenase, and succinyl-CoA synthetase, which are encoded by this operon (340). The resulting strain produced less acetate and directed more carbon towards carbon dioxide formation than the parent strain *E. coli* MG1655, indicating a higher flux through the TCA cycle. As the strain maintained high growth and glucose consumption rates, it might be a good candidate for redox biocatalysis. In the second approach, the global regulator ArcAB, a two component system, that *inter alia* regulates the TCA cycle genes in response to the $O_2$ level or redox state, has been deleted by knockout of the genes *arcA* and *arcB* (234). Investigation of the effects of these gene deletions on the *E. coli* metabolism under aerobic growth conditions showed a derepression of the TCA cycle related genes *glt*A, *fum*A, *mdh*, and *ace*A and a consequential activation of the respective TCA cycle enzymes.$^{13}$C-based MFA revealed that this activation also induced an increase of the TCA cycle flux.

Both examples highlight the influence of regulatory mechanisms on the metabolic fluxes, stressing the importance to take regulatory constraints into account when designing biocatalysts. Indeed, many engineering efforts have been moderately successful due to the interference of regulatory systems with the introduced genetic or environmental modifications. Thus, efficient engineering of whole-cell (redox) biocatalysts requires an improved ability to predictably regulate these biological systems (50).

As pointed out above, one of the aims strived by synthetic biologists is the accurate predictive modeling of microbial chemical factories by computer-aided-design systems for which high-quality kinetic models are essential. Yet, due to the difficulties discussed in Section III.B.1, those models are currently very scarce. The last example, the engineering of a methanol oxidation pathway in *Pichia pastoris*, may therefore be seen as an outlook. In this study, NADH regeneration rates were calculated with a kinetic model that correctly predicted the limitation of the methanol oxidation pathway by the activity of formaldehyde dehydrogenase (290). *P. pastoris* is a methylotrophic yeast that efficiently uses methanol as carbon and energy source. Methanol is dissimilated via alcohol oxidase, formaldehyde dehydrogenase, and formate dehydrogenase yielding 2 mols of NADH per mol of methanol. Schroer *et al.* determined the kinetics of these three enzymes *in vitro* and used these data to construct a kinetic model of the methanol oxidation pathway. To elucidate the impact of overexpressing the genes of this pathway on the NADH regeneration rates, they calculated theoretical NADH regeneration rates using the compiled model with varying $V_{max}$ values of every individual enzyme. Model results indicated that formaldehyde dehydrogenase is the main bottleneck of the pathway. To confirm these results, strains overproducing the highly active model oxidoreductase butanediol dehydrogenase and one of the three enzymes of the methanol oxidation pathway where tested for their catalytic capabilities. In compliance with model predictions, the strain overexpressing the formaldehyde dehydrogenase gene showed an improved catalytic activity for the NADH-dependent reduction of acetoin to 2,3-butanediol, whereas overexpression of the alcohol oxidase or the formate dehydrogenase genes was not advantageous for the NADH-dependent bioconversion. Clearly, the kinetic model used in this study is an intense abstraction of the metabolism as it only encompasses three enzymes and only indirectly accounts for alternative formaldehyde utilizing reactions via a reduction of the experimentally determined $V_{max}$ value of the alcohol oxidase. Nevertheless, the model could successfully be used for model-guided design of a whole-cell biocatalyst with an increased cofactor regeneration rate. Moreover, identification of formaldehyde dehydrogenase as the bottleneck of the linear pathway could not have been predicted by stoichiometric modeling as this approach does not account for kinetics (*e.g.*, substrate inhibition), again stressing the necessity of kinetic model development.

## VI. Conclusions

The increasing biochemical knowledge on oxidoreductases in combination with the ever advancing tools of recombinant DNA technology promotes the exploitation of the synthetic potential of redox enzymes for a growing number of applications. Although highly productive biocatalysts based on isolated enzymes or nonliving cells have been developed for the synthesis of fine chemicals, most applications in industry and academia make use of self-regenerating (*i.e.*, growing or nongrowing but metabolizing) whole-cell biocatalysts often due to the limited stability of oxidoreductase systems. In metabolically active cells, the enzyme activity is connected to the redox metabolism of the host, providing the redox cofactors necessary for catalysis. Hence, operation of host metabolism is crucial for highly productive and stable redox biocatalysis. This central role of host metabolism typically is

not considered during traditional biocatalyst and bioprocess engineering, which focuses on the optimization of the enzyme of interest (*i.e.*, gene expression, activity, specificity) and reaction engineering considering the cell as a black box. However, recent advances in our understanding of the complex metabolic network operation and the interplay of redox cofactor-dependent enzymes leads to increasing interest regarding the synthetic potential of oxidoreductase-based whole-cell biocatalysts. The application of the flavin-dependent styrene monooxygenase provides an illustrative example of an oxidoreductase used for productive biocatalysis. The metabolic network structure and its operation were identified to be crucial for high biocatalytic activities of the styrene monooxygenase containing whole-cell biocatalysts. Furthermore, the complex regulation of metabolism may in itself be a target for the optimization of redox cofactor availability. Instead of single enzyme optimization that often has been disappointing, considering and optimizing the enzyme of choice as part of the entire metabolic network may be more promising. Indeed, several successful network optimization strategies have recently been published, highlighting the potential of this approach. Further investigations on the detailed mechanisms of oxidoreductases and their functionality and interplay within the metabolic network of living cells, using the described ideas of synthetic bio(techno)logy, should provide the basis for designing efficient (*i.e.*, in respect to rate, yield, and/or titer) whole-cell based biocatalytic processes for the synthesis of high-value added products for the chemical and pharmaceutical industries.

## Acknowledgments

We are grateful to all colleagues who shared manuscripts and thoughts. We are grateful to Andreas Schmid for fruitful discussions and his ongoing support. We thank Jochen Lutz for contributing Figure 16 and Mattijs Julsing for fruitful discussion regarding redox cofactor quantification. This work was supported by the Deutsche Bundesstiftung Umwelt (DBU) and by the German Ministry of Science and Education (BMBF, Project ERA-NET SysMO, No. 0313980A) (VAPMdS).

## References

1. This reference has been deleted.
2. Abu–Omar MM, Loaiza A, and Hontzeas N. Reaction mechanisms of mononuclear nonheme iron oxygenases. *Chem Rev* 105: 2227–2252, 2005.
3. Adam W, Lazarus M, Saha–Möller CR, Weichold O, Hoch U, Häring D, and Schreier P. Biotransformations with peroxidases. *Adv Biochem Eng/Biotech* 63: 73–108, 1999.
4. Afolabi PR, Mohammed F, Amaratunga K, Majekodunmi O, Dales SL, Gill R, Thompson D, Cooper JB, Wood SP, Goodwin PM, and Anthony C. Site-directed mutagenesis and X-ray crystallography of the PQQ-containing quinoprotein methanol dehydrogenase and its electron acceptor, cytochrome c(L). *Biochemistry* 40: 9799–9809, 2001.
5. Alivisatos SG, Ungar F, and Abraham G. Nonenzymatic interactions of reduced coenzyme I with inorganic phosphate and certain other anions. *Nature* 203: 973–975, 1964.
6. Alper H, Jin YS, Moxley JF, and Stephanopoulos G. Identifying gene targets for the metabolic engineering of lycopene biosynthesis in *Escherichia coli*. *Metab Eng* 7: 155–164, 2005.
7. Alphand V, Carrea G, Wohlgemuth R, Furstoss R, and Woodley JM. Towards large-scale synthetic applications of Baeyer–Villiger monooxygenases. *Trends Biotechnol* 21: 318–323, 2003.
8. Andersen KB and von Meyenburg K. Charges of nicotinamide adenine nucleotides and adenylate energy charge as regulatory parameters of the metabolism in *Escherichia coli*. *J Biol Chem* 252: 4151–4156, 1977.
9. Andersen OA, Stokka AJ, Flatmark T, and Hough E. 2.0 angstrom resolution crystal structures of the ternary complexes of human phenylalanine hydroxylase catalytic domain with tetrahydrobiopterin and 3-(2-thienyl)-L-alanine or L-norleucine: Substrate specificity and molecular motions related to substrate binding. *J Mol Biol* 333: 747–757, 2003.
10. Andreesen JR and Fetzner S. The molybdenum-containing hydroxylases of nicotinate, isonicotinate, and nicotine. *Met Ions Biol Syst* 39: 405–430, 2002.
11. Anthony C. Quinoprotein-catalysed reactions. *Biochem J* 320: 697–711, 1996.
12. Anthony C. The quinoprotein dehydrogenases for methanol and glucose. *Arch Biochem Biophys* 428: 2–9, 2004.
13. Asadollahi MA, Maury J, Patil KR, Schalk M, Clark A, and Nielsen J. Enhancing sesquiterpene production in *Saccharomyces cerevisiae* through *in silico* driven metabolic engineering. *Metab Eng* 11: 328–334, 2009.
14. Auld D. Zinc coordination sphere in biochemical zinc sites. *Biometals* 14: 271–313, 2001.
15. Austin RN, Buzzi K, Kim E, Zylstra GJ, and Groves JT. Xylene monooxygenase, a membrane-spanning nonheme di-iron enzyme that hydroxylates hydrocarbons via a substrate radical intermediate. *J Biol Inorg Chem* 8: 733–740, 2003.
16. Austin RN, Luddy K, Erickson K, Pender–Cudlip M, Bertrand E, Deng D, Buzdygon RS, van Beilen JB, and Groves JT. Cage escape competes with geminate recombination during alkane hydroxylation by the di-iron oxygenase AlkB. *Angew Chem Int Ed* 47: 5232–5234, 2008.
17. Babel W, Brinkmann U, and Muller RH. The auxiliary substrate concept. An approach for overcoming limits of microbial performances. *Acta Biotechnol* 13: 211–242, 1993.
18. Baik MH, Newcomb M, Friesner RA, and Lippard SJ. Mechanistic studies on the hydroxylation of methane by methane monooxygenase. *Chem Rev* 103: 2385–2419, 2003.
19. Bailey JE, Sburlati A, Hatzimanikatis V, Lee K, Renner WA, and Tsai PS. Inverse metabolic engineering: A strategy for directed genetic engineering of useful phenotypes. *Biotechnol Bioeng* 79: 568–579, 2002.
20. Bailey LJ, Mccoy JG, Phillips GN, and Fox BG. Structural consequences of effector protein complex formation in a diiron hydroxylase. *Proc Natl Acad Sci USA* 105: 19194–19198, 2008.
21. Baker PJ, Britton KL, Fisher M, Esclapez J, Pire C, Bonete MJ, Ferrer J, and Rice DW. Active site dynamics in the zinc-dependent medium chain alcohol dehydrogenase superfamily. *Proc Natl Acad Sci USA* 106: 779–784, 2009.
22. Baldwin CVF, Wohlgemuth R, and Woodley JM. The first 200-L scale asymmetric Baeyer–Villiger oxidation using a whole-cell biocatalyst. *Org Process Res Dev* 12: 660–665, 2008.
23. Barton L. Reverse electron flow. In: *Structural and Functional Relationships in Prokaryotes*, edited by Barton L. New York: Springer, 2005, pp. 447–448.

24. Beard DA, Babson E, Curtis E, and Qian H. Thermodynamic constraints for biochemical networks. *J Theor Biol* 228: 327–333, 2004.
25. Becker J, Klopprogge C, Zelder O, Heinzle E, and Wittmann C. Amplified expression of fructose 1,6-bisphosphatase in *Corynebacterium glutamicum* increases *in vivo* flux through the pentose phosphate pathway and lysine production on different carbon sources. *Appl Environ Microbiol* 71: 8587–8596, 2005.
26. Bekker M, de Vries S, Ter Beek A, Hellingwerf KJ, and de Mattos MJT. Respiration of *Escherichia coli* can be fully uncoupled via the nonelectrogenic terminal cytochrome bd-II oxidase. *J Bacteriol* 191: 5510–5517, 2009.
27. Bermejo LL, Welker NE, and Papoutsakis ET. Expression of *Clostridium acetobutylicum* ATCC 824 genes in *Escherichia coli* for acetone production and acetate detoxification. *Appl Environ Microbiol* 64: 1079–1085, 1998.
28. Bernhardt R. Cytochromes P450 as versatile biocatalysts. *J Biotechnol* 124: 128–145, 2006.
29. Bernofsky C and Swan M. An improved cycling assay for nicotinamide adenine dinucleotide. *Anal Biochem* 53: 452–458, 1973.
30. Berrios–Rivera SJ, San KY, and Bennett GN. The effect of NAPRTase overexpression on the total levels of NAD, the $NADH/NAD^+$ ratio, and the distribution of metabolites in *Escherichia coli*. *Metab Eng* 4: 238–247, 2002.
31. Bjorklof K, Zickermann V, and Finel M. Purification of the 45 kDa, membrane bound NADH dehydrogenase of *Escherichia coli* (NDH-2) and analysis of its interaction with ubiquinone analogues. *FEBS Lett* 467: 105–110, 2000.
32. Blank LM, Koebmann BJ, Michelsen O, Nielsen LK, and Jensen PR. Hemin reconstitutes proton extrusion in an $H^+$-ATPase-negative mutant of *Lactococcus lactis*. *J Bacteriol* 183: 6707–6709, 2001.
33. Blank LM and Sauer U. TCA cycle activity in *Saccharomyces cerevisiae* is a function of the environmentally determined specific growth and glucose uptake rates. *Microbiology* 150: 1085–1093, 2004.
34. Blank LM, Kuepfer L, and Sauer U. Large-scale $^{13}C$-flux analysis reveals mechanistic principles of metabolic network robustness to null mutations in yeast. *Genome Biol* 6: R49, 2005.
35. Blank LM, Lehmbeck F, and Sauer U. Metabolic flux and network analysis in fourteen hemiascomycetous yeasts. *FEMS Yeast Res* 5: 545–558, 2005.
36. Blank LM, McLaughlin RL, and Nielsen LK. Stable production of hyaluronic acid in *Streptococcus zooepidemicus* chemostats operated at high dilution rate. *Biotechnol Bioeng* 90: 685–693, 2005.
37. Blank LM, Ebert BE, Bühler B, and Schmid A. Metabolic capacity estimation of *Escherichia coli* as a platform for redox biocatalysis: Constraint-based modeling and experimental verification. *Biotechnol Bioeng* 100: 1050–1065, 2008.
38. Blank LM, Ionidis G, Ebert BE, Bühler B, and Schmid A. Metabolic response of *Pseudomonas putida* during redox biocatalysis in the presence of a second octanol phase. *FEBS J* 275: 5173–5190, 2008.
39. Blinova K, Carroll S, Bose S, Smirnov AV, Harvey JJ, Knutson JR, and Balaban RS. Distribution of mitochondrial NADH fluorescence lifetimes: Steady-state kinetics of matrix NADH interactions. *Biochemistry* 44: 2585–2594, 2005.
40. Boender LG, de Hulster EA, van Maris AJ, Daran–Lapujade PA and Pronk JT. Quantitative physiology of *Saccharomyces cerevisiae* at near-zero specific growth rates. *Appl Environ Microbiol* 75: 5607–5614, 2009.
41. Bollinger JM and Krebs C. Stalking intermediates in oxygen activation by iron enzymes: Motivation and method. *J Inorg Biochem* 100: 586–605, 2006.
42. Bollinger JM and Broderick JB. Frontiers in enzymatic C-H-bond activation. *Curr Opin Chem Biol* 13: 51–57, 2009.
43. Bologna FP, Andreo CS, and Drincovich MF. *Escherichia coli* malic enzymes: Two isoforms with substantial differences in kinetic properties, metabolic regulation, and structure. *J Bacteriol* 189: 5937–5946, 2007.
44. Bonarius HPJ, Hatzimanikatis V, Meesters KPH, deGooijer CD, Schmid G, and Tramper J. Metabolic flux analysis of hybridoma cells in different culture media using mass balances. *Biotechnol Bioeng* 50: 299–318, 1996.
45. Bonarius HPJ, Schmid G, and Tramper J. Flux analysis of underdetermined metabolic networks: The quest for the missing constraints. *Trends Biotech* 15: 308–314, 1997.
46. Boonstra B, French CE, Wainwright I, and Bruce NC. The *udhA* gene of *Escherichia coli* encodes a soluble pyridine nucleotide transhydrogenase. *J Bacteriol* 181: 1030–1034, 1999.
47. Bossert ID, Whited G, Gibson DT, and Young LY. Anaerobic oxidation of *p*-cresol mediated by a partially purified methylhydroxylase from a denitrifying bacterium. *J Bacteriol* 171: 2956–2962, 1989.
48. Boyd DR, Sharma ND, Bowers NI, Brannigan IN, Groocock MR, Malone JE, McConville G, and Allen CCR. Biocatalytic asymmetric dihydroxylation of conjugated mono- and poly-alkenes to yield enantiopure cyclic *cis*-diols. *Adv Synth Catal* 347: 1081–1089, 2005.
49. Boyd DR and Bugg TDH. Arene *cis*-dihydrodiol formation: From biology to application. *Org Biomol Chem* 4: 181–192, 2006.
50. Boyle PM and Silver PA. Harnessing nature's toolbox: Regulatory elements for synthetic biology. *J R Soc Interface* 6: S535–S546, 2009.
51. Brazeau BJ, Austin RN, Tarr C, Groves JT, and Lipscomb JD. Intermediate Q from soluble methane monooxygenase hydroxylates the mechanistic substrate probe norcarane: Evidence for a stepwise reaction. *J Am Chem Soc* 123: 11831–11837, 2001.
52. Brazeau BJ and Lipscomb JD. Key amino acid residues in the regulation of soluble methane monooxygenase catalysis by component B. *Biochemistry* 42: 5618–5631, 2003.
53. Brazeau BJ, Johnson BJ, and Wilmot CM. Copper-containing amine oxidases. Biogenesis and catalysis; a structural perspective. *Arch Biochem Biophys* 428: 22–31, 2004.
54. Bro C, Regenberg B, and Nielsen J. Genome-wide transcriptional response of a *Saccharomyces cerevisiae* strain with an altered redox metabolism. *Biotechnol Bioeng* 85: 269–276, 2004.
55. Bro C, Regenberg B, Forster J, and Nielsen J. *In silico* aided metabolic engineering of *Saccharomyces cerevisiae* for improved bioethanol production. *Metab Eng* 8: 102–111, 2006.
56. Brown CD, Neidig ML, Neibergall MB, Lipscomb JD, and Solomon EI. VTVH-MCD and DFT studies of thiolate bonding to $\{FeNO\}^7/\{FeO_2\}^8$ complexes of isopenicillin *N* synthase: Substrate determination of oxidase versus oxygenase activity in nonheme Fe enzymes. *J Am Chem Soc* 129: 7427–7438, 2007.
57. Bruijnincx PCA, van Koten G, and Gebbink RJMK. Mononuclear nonheme iron enzymes with the 2-His-1-carboxylate

facial triad: Recent developments in enzymology and modeling studies. *Chem Soc Rev* 37: 2716–2744, 2008.
58. Bugg TD and Ramaswamy S. Nonheme iron-dependent dioxygenases: Unravelling catalytic mechanisms for complex enzymatic oxidations. *Curr Opin Chem Biol* 12: 134–140, 2008.
59. Bühler B, Schmid A, Hauer B, and Witholt B. Xylene monooxygenase catalyzes the multistep oxygenation of toluene and pseudocumene to corresponding alcohols, aldehydes, and acids in *Escherichia coli* JM101. *J Biol Chem* 275: 10085–10092, 2000.
60. Bühler B, Witholt B, Hauer B, and Schmid A. Characterization and application of xylene monooxygenase for multistep biocatalysis. *Appl Environ Microbiol* 68: 560–568, 2002.
61. Bühler B, Bollhalder I, Hauer B, Witholt B, and Schmid A. Use of the two-liquid phase concept to exploit kinetically controlled multistep biocatalysis. *Biotechnol Bioeng* 81: 683–694, 2003.
62. Bühler B, Bollhalder I, Hauer B, Witholt B, and Schmid A. Chemical biotechnology for the specific oxyfunctionalization of hydrocarbons on a technical scale. *Biotechnol Bioeng* 82: 833–842, 2003.
63. Bühler B and Schmid A. Process implementation aspects for biocatalytic hydrocarbon oxyfunctionalization. *J Biotechnol* 113: 183–210, 2004.
64. Bühler B and Schmid A. Selective enzymatic hydroxylations. In: *Handbook of C-H Transformations*, edited by Dyker G. Weinheim. Germany: Wiley-VCH, 2005, pp. 516–529.
65. Bühler B, Straathof AJJ, Witholt B and Schmid A. Analysis of two-liquid-phase multistep biooxidation based on a process model: Indications for biological energy shortage. *Org Process Res Dev* 10: 628–643, 2006.
66. Bühler B, Straathof AJJ, Witholt B, and Schmid A. Analysis of two-liquid-phase multistep biooxidation based on a process model: Indications for biological energy shortage. *Org Process Res Dev* 10: 628–643, 2006.
67. Bühler B, Park JB, Blank LM, and Schmid A. NADH availability limits asymmetric biocatalytic epoxidation in a growing recombinant *Escherichia coli* strain. *Appl Environ Microbiol* 74: 1436–1446, 2008.
68. Bühler B, Blank LM, Ebert BE, Buehler K, and Schmid A. Energy and cofactor issues in fermentation and oxyfunctionalization processes. In: *The Metabolic Pathway Engineering Handbook: Tools and Applications*, edited by Smoke CD. Boca Raton, FL: CRC Press (Taylor & Francis Group), 2009, 21: 1–32.
69. Burgard AP and Maranas CD. Probing the performance limits of the *Escherichia coli* metabolic network subject to gene additions or deletions. *Biotechnol Bioeng* 74: 364–375, 2001.
70. Burgard AP, Pharkya P, and Maranas CD. OptKnock: A bilevel programming framework for identifying gene knockout strategies for microbial strain optimization. *Biotechnol Bioeng* 84: 647–657, 2003.
71. Burton SG. Oxidizing enzymes as biocatalysts. *Trends Biotech* 21: 543–549, 2003.
72. Cabanes J, Chazarra S, and Garcia–Carmona F. Tyrosinase kinetics: A semi-quantitative model of the mechanism of oxidation of monohydric and dihydric phenolic substrates. Reply. *J Theor Biol* 214: 321–325, 2002.
73. Carballeira JD, Quezada MA, Hoyos P, Simeo Y, Hernaiz MJ, Alcantara AR, and Sinisterra JV. Microbial cells as catalysts for stereoselective redox reactions. *Biotechnol Adv* 27: 686–714, 2009.
74. Chin JW, Khankal R, Monroe CA, Maranas CD, and Cirino PC. Analysis of NADPH supply during xylitol production by engineered *Escherichia coli*. *Biotechnol Bioeng* 102: 209–220, 2009.
75. Cirino PC and Arnold FH. A self-sufficient peroxide-driven hydroxylation biocatalyst. *Angew Chem Int Ed* 42: 3299–3301, 2003.
76. Clifton IJ, Hsueh LC, Baldwin JE, Harlos K, and Schofield CJ. Structure of proline 3-hydroxylase. Evolution of the family of 2-oxoglutarate dependent oxygenases. *Eur J Biochem* 268: 6625–6636, 2001.
77. Collins AM, Woodley JM, and Liddell JM. Determination of reactor operation for the microbial hydroxylation of toluene in a 2-liquid phase process. *J Ind Microbiol* 14: 382–388, 1995.
78. Coon MJ. Cytochrome P450: Nature's most versatile biological catalyst. *Annu Rev Pharmacol* 45: 1–25, 2005.
79. Cooney CL, Wang HY, and Wang DIC. Computer-aided material balancing for prediction of fermentation parameters. *Biotechnol Bioeng* 19: 55–67, 1977.
80. Costas M, Mehn MP, Jensen MP, and Que L. Dioxygen activation at mononuclear nonheme iron active sites: Enzymes, models, and intermediates. *Chem Rev* 104: 939–986, 2004.
81. Covert MW and Palsson BO. Transcriptional regulation in constraints-based metabolic models of *Escherichia coli*. *J Biol Chem* 277: 28058–28064, 2002.
82. Cox SJ, Shalel Levanon S, Sanchez A, Lin H, Peercy B, Bennett GN, and San KY. Development of a metabolic network design and optimization framework incorporating implementation constraints: A succinate production case study. *Metab Eng* 8: 46–57, 2006.
83. Cozier GE, Salleh RA, and Anthony C. Characterization of the membrane quinoprotein glucose dehydrogenase from *Escherichia coli* and characterization of a site-directed mutant in which histidine-262 has been changed to tyrosine. *Biochem J* 340: 639–647, 1999.
84. Cunane LM, Chen ZW, Shamala N, Mathews FS, Cronin CN, and McIntire WS. Structures of the flavocytochrome *p*-cresol methylhydroxylase and its enzyme-substrate complex: Gated substrate entry and proton relays support the proposed catalytic mechanism. *J Mol Biol* 295: 357–374, 2000.
85. Cunane LM, Chen ZW, McIntire WS, and Mathews FS. *p*-Cresol methylhydroxylase: Alteration of the structure of the flavoprotein subunit upon its binding to the cytochrome subunit. *Biochemistry* 44: 2963–2973, 2005.
86. D'Mello R, Hill S, and Poole RK. The cytochrome bd quinol oxidase in *Escherichia coli* has an extremely high oxygen affinity and two oxygen-binding haems: Implications for regulation of activity *in vivo* by oxygen inhibition. *Microbiology* 142: 755–763, 1996.
87. Dauner M, Sonderegger M, Hochuli M, Szyperski T, Wuthrich K, Hohmann HP, Sauer U, and Bailey JE. Intracellular carbon fluxes in riboflavin-producing *Bacillus subtilis* during growth on two-carbon substrate mixtures. *Appl Environ Microbiol* 68: 1760–1771, 2002.
88. Davidson V. Electron transfer in quinoproteins. *Arch Biochem Biophys* 428: 32–40, 2004.
89. Decker A and Solomon EI. Dioxygen activation by copper, heme and nonheme iron enzymes: Comparison of electronic structures and reactivities. *Curr Opin Chem Biol* 9: 152–163, 2005.
90. Dembitsky VM. Oxidation, epoxidation and sulfoxidation reactions catalysed by haloperoxidases. *Tetrahedron* 59: 4701–4720, 2003.

91. Dols M, Chraibi W, Remaud–Simeon M, Lindley ND, and Monsan PF. Growth and energetics of *Leuconostoc mesenteroides* NRRL B-1299 during metabolism of various sugars and their consequences for dextransucrase production. *Appl Environ Microbiol* 63: 2159–2165, 1997.
92. Dragan CA, Blank LM, and Bureik M. Increased TCA cycle activity and reduced oxygen consumption during cytochrome P450-dependent biotransformation in fission yeast. *Yeast* 23: 779–794, 2006.
93. Drauz K and Waldmann H. *Enzyme Catalysis in Organic Synthesis*. Weinheim, Germany: Wiley-VCH, 2002, p. 1559.
94. Driscoll BT and Finan TM. Properties of NAD(+)- and NADP(+)-dependent malic enzymes of *Rhizobium* (*Sinorhizobium*) *meliloti* and differential expression of their genes in nitrogen-fixing bacteroids. *Microbiology* 143: 489–498, 1997.
95. Dumas B, Brocard–Masson C, Assemat–Lebrun K, and Achstetter T. Hydrocortisone made in yeast: metabolic engineering turns a unicellular microorganism into a drug-synthesizing factory. *Biotechnol J* 1: 299–307, 2006.
96. Dunn MF, Biellmann JF, and Branlant G. Roles of zinc ion and reduced coenzyme in horse liver alcohol dehydrogenase catalysis. Mechanism of aldehyde activation. *Biochemistry* 14: 3176–3182, 2002.
97. Earhart CA, Vetting MW, Gosu R, Michaud–Soret I, Que L, and Ohlendorf DH. Structure of catechol 1,2-dioxygenase from *Pseudomonas arvilla*. *Biochem Bioph Res Co* 338: 198–205, 2005.
98. Edwards JS, Ibarra RU, and Palsson BO. *In silico* predictions of *Escherichia coli* metabolic capabilities are consistent with experimental data. *Nature Biotech* 19: 125–130, 2001.
99. Eklund H, Plapp BV, Samama JP, and Branden CI. Binding of substrate in a ternary complex of horse liver alcohol dehydrogenase. *J Biol Chem* 257: 14349–14358, 1982.
100. Elango N, Radhakrishnan R, Froland WA, Wallar BJ, Earhart CA, Lipscomb JD, and Ohlendorf DH. Crystal structure of the hydroxylase component of methane monooxygenase from *Methylosinus trichosporium* OB3b. *Protein Sci* 6: 556–568, 1997.
101. Elgren TE, Orville AM, Kelly KA, Lipscomb JD, Ohlendorf DH, and Que L. Crystal structure and resonance Raman studies of protocatechuate 3,4-dioxygenase complexed with 3,4-dihydroxyphenylacetate. *Biochemistry* 36: 11504–11513, 1997.
102. Elias MD, Nakamura S, Migita CT, Miyoshi H, Toyama H, Matsushita K, Adachi O, and Yamada M. Occurrence of a bound ubiquinone and its function in *Escherichia coli* membrane-bound quinoprotein glucose dehydrogenase. *J Biol Chem* 279: 3078–3083, 2004.
103. Emmerling M, Bailey JE, and Sauer U. Glucose catabolism of *Escherichia coli* strains with increased activity and altered regulation of key glycolytic enzymes. *Metab Eng* 1: 117–127, 1999.
104. Ernst M, Kaup B, Muller M, Bringer–Meyer S, and Sahm H. Enantioselective reduction of carbonyl compounds by whole-cell biotransformation, combining a formate dehydrogenase and a (*R*)-specific alcohol dehydrogenase. *Appl Microbiol Biotechnol* 66: 629–634, 2005.
105. Eser BE, Barr EW, Frantorn PA, Saleh L, Bollinger JM, Krebs C, and Fitzpatrick PF. Direct spectroscopic evidence for a high-spin Fe(IV) intermediate in tyrosine hydroxylase. *J Am Chem Soc* 129: 11334–11335, 2007.
106. Fell D. Understanding the Control of Metabolism. London: Portland, 1997, p. 301.
107. Ferraro DJ, Gakhar L, and Ramaswamy S. Rieske business: Structure–function of Rieske nonheme oxygenases. *Biochem Bioph Res Co* 338: 175–190, 2005.
108. Fischer E and Sauer U. Metabolic flux profiling of *Escherichia coli* mutants in central carbon metabolism using GC-MS. *Eur J Biochem* 270: 880–891, 2003.
109. Fischer E and Sauer U. A novel metabolic cycle catalyzes glucose oxidation and anaplerosis in hungry *Escherichia coli*. *J Biol Chem* 278: 46446–46451, 2003.
110. Fischer E, Zamboni N, and Sauer U. High-throughput metabolic flux analysis based on gas chromatography-mass spectrometry derived $^{13}C$ constraints. *Anal Biochem* 325: 308–316, 2004.
111. Fitzpatrick PF. Mechanism of aromatic amino acid hydroxylation. *Biochemistry* 42: 14083–14091, 2003.
112. Flitsch SL, Schmid A, Hollmann F, Bühler B, Grogan G, and van Pée K–H. Oxidation reactions. In: *Enzyme Catalysis in Organic Synthesis*, edited by Drauz K and Walsmann H. Weinheim, Germany: Wiley-VCH, 2002, pp. 1065–1280.
113. Frick O and Wittmann C. Characterization of the metabolic shift between oxidative and fermentative growth in *Saccharomyces cerevisiae* by comparative C-13 flux analysis. *Microb Cell Fact* 4: 30, 2005.
114. Fu H, Newcomb M, and Wong C–H. *Pseudomonas oleovorans* monooxygenase catalyzed asymmetric epoxidation of allyl alcohol derivatives and hydroxylation of a hypersensitive radical probe with the radical ring opening rate exceeding the oxygen rebound rate. *J Am Chem Soc* 113: 5878–5880, 1991.
115. Fuhrer T, Fischer E, and Sauer U. Experimental identification and quantification of glucose metabolism in seven bacterial species. *J Bacteriol* 187: 1581–1590, 2005.
116. Fuhrer T and Sauer U. Different biochemical mechanisms ensure network-wide balancing of reducing equivalents in microbial metabolism. *J Bacteriol* 191: 2112–2121, 2009.
117. Furukawa H, Wieser M, Morita H, Sugio T and Nagasawa T. Purification and characterization of eugenol dehydrogenase from *Pseudomonas fluorescens* E118. *Arch Microbiol* 171: 37–43, 1998.
118. Ghisla S and Thorpe C. Acyl-CoA dehydrogenases. *Eur J Biochem* 271: 494–508, 2004.
119. Gladyshev VN, Khangulov SV, and Stadtman TC. Properties of the selenium- and molybdenum-containing nicotinic acid hydroxylase from *Clostridium barkeri*. *Biochemistry* 35: 212–223, 1996.
120. Glickman MH and Klinman JP. Lipoxygenase reaction mechanism: Demonstration that hydrogen abstraction from substrate precedes dioxygen binding during catalytic turnover. *Biochemistry* 35: 12882–12892, 1996.
121. Goldberg K, Edegger K, Kroutil W, and Liese A. Overcoming the thermodynamic limitation in asymmetric hydrogen transfer reactions catalyzed by whole cells. *Biotechnol Bioeng* 95: 192–198, 2006.
122. Gombert AK, Moreira dos Santos M, Christensen B, and Nielsen J. Network identification and flux quantification in the central metabolism of *Saccharomyces cerevisiae* under different conditions of glucose repression. *J Bacteriol* 183: 1441–1451, 2001.
123. Gorren ACF and Mayer B. Nitric oxide synthase: A cytochrome P450 family foster child. *Biochim Biophys Acta* 1770: 432–445, 2007.
124. Gottschalk G and Knackmuss HJ. Bacteria and the biodegradation of chemicals achieved naturally, by combina-

tion, or by construction. *Angew Chem Int Ed* 32: 1398–1408, 1993.
125. Green MT, Dawson JH, and Gray HB. Oxoiron(IV) in chloroperoxidase compound II is basic: Implications for P450 chemistry. *Science* 304: 1653–1656, 2004.
126. Green MT. C-H bond activation in heme proteins: The role of thiolate ligation in cytochrome P450. *Curr Opin Chem Biol* 13: 84–88, 2009.
127. Guengerich FP. *Mammalian cytochromes P450*. Boca Raton, FL CRC Press, 1987, p. 484.
128. Guengerich FP. Cytochrome P450 oxidations in the generation of reactive electrophiles: Epoxidation and related reactions. *Arch Biochem Biophys* 409: 59–71, 2003.
129. Hakki T, Zearo S, Dragan CA, Bureik M, and Bernhardt R. Coexpression of redox partners increases the hydrocortisone (cortisol) production efficiency in CYP11B1 expressing fission yeast *Schizosaccharomyces pombe*. *J Biotechnol* 133: 351–359, 2008.
130. Halaouli S, Asther M, Sigoillot JC, Hamdi M, and Lomascolo A. Fungal tyrosinases: new prospects in molecular characteristics, bioengineering and biotechnological applications. *J Appl Microbiol* 100: 219–232, 2006.
131. Harris LM, Blank L, Desai RP, Welker NE, and Papoutsakis ET. Fermentation characterization and flux analysis of recombinant strains of *Clostridium acetobutylicum* with an inactivated *solR* gene. *J Ind Microbiol Biot* 27: 322–328, 2001.
132. Hausinger RP. Fe(II)/α-ketoglutarate-dependent hydroxylases and related enzymes. *Crit Rev Biochem Mol* 39: 21–68, 2004.
133. Henry CS, Jankowski MD, Broadbelt LJ, and Hatzimanikatis V. Genome-scale thermodynamic analysis of *Escherichia coli* metabolism. *Biophys J* 90: 1453–1461, 2006.
134. Henry CS, Broadbelt LJ, and Hatzimanikatis V. Thermodynamics-based metabolic flux analysis. *Biophys J* 92: 1792–1805, 2007.
135. Herrmann U, Merfort M, Jeude M, Bringer–Meyer S, and Sahm H. Biotransformation of glucose to 5-keto-D-gluconic acid by recombinant *Gluconobacter oxydans* DSM 2343. *Appl Microbiol Biotechnol* 64: 86–90, 2004.
136. Heuser F, Schroer K, Lutz S, Bringer–Meyer S, and Sahm H. Enhancement of the NAD(P)(H) pool in *Escherichia coli* for biotransformation. *Eng Life Sci* 7: 343–353., 2007.
137. Heyland J, Fu J, and Blank LM. Correlation between TCA cycle flux and glucose uptake rate during respiro-fermentative growth of *Saccharomyces cerevisiae*. *Microbiology* 155: 3827–3837, 2009.
138. Hibi M, Yukitomo H, Ito M, and Mori H. Improvement of NADPH-dependent bioconversion by transcriptome-based molecular breeding. *Appl Environ Microbiol* 73: 7657–7663, 2007.
139. Hille R. Molybdenum enzymes containing the pyranopterin cofactor: An overview. *Met Ions Biol Syst* 39: 187–226, 2002.
140. Himes RA and Karlin KD. Copper–dioxygen complex mediated C-H bond oxygenation: Relevance for particulate methane monooxygenase (pMMO). *Curr Opin Chem Biol* 13: 119–131, 2009.
141. Hoffmann F and Rinas U. On-line estimation of the metabolic burden resulting from the synthesis of plasmid-encoded and heat-shock proteins by monitoring respiratory energy generation. *Biotechnol Bioeng* 76: 333–340, 2001.
142. Hofrichter M and Ullrich R. Heme-thiolate haloperoxidases: Versatile biocatalysts with biotechnological and environmental significance. *Appl Microbiol Biot* 71: 276–288, 2006.
143. Hong SH. Systems approaches to succinic acid-producing microorganisms. *Biotechnol Bioprocess Eng* 12: 73–79, 2007.
144. Hopper DJ. Hydroxylation of *p*-cresol and its conversion to *p*-hydroxybenzaldehyde in *Pseudomonas putida*. *Biochem Biophys Res Commun* 69: 462–468, 1976.
145. Hopper DJ. Incorporation of [$^{18}$O] water in the formation of *p*-hydroxybenzyl alcohol by the *p*-cresol methylhydroxylase from *Pseudomonas putida*. *Biochem J* 175: 345–347, 1978.
146. Hopper DJ, Jones MR, and Causer MJ. Periplasmic location of *p*-cresol methylhydroxylase in *Pseudomonas putida*. *FEBS Lett* 182: 485–488, 1985.
147. Hsu HF, Que L, and Shanklin J. XAS studies of membrane bound alkane omega-hydroxylase: Evidence for a histidine-rich ligand environment in the nonheme di-iron site. *J Inorg Biochem* 74: 168–168, 1999.
148. Hummel W. Reduction of acetophenone to R(+)-phenylethanol by a new alcohol dehydrogenase from *Lactobacillus kefir*. *Appl Microbiol Biotechnol* 34: 15–19, 1990.
149. Hummel W. New alcohol dehydrogenases for the synthesis of chiral compounds. Berlin Springer, 1997, 147–184.
150. Hurh B, Yamane T, and Nagasawa T. Purification and characterization of nicotinic acid dehydrogenase from *Pseudomonas fluorescens* Tn5. *J Ferment Bioeng* 78: 19–26, 1994.
151. Idupulapati NB and Mainardi DS. Coordination and binding of ions in $Ca^{2+}$- and $Ba^{2+}$-containing methanol dehydrogenase and interactions with methanol. *J Mol Struct-Theochem* 901: 72–80, 2009.
152. Iverson TM, Luna–Chavez C, Cecchini G, and Rees DC. Structure of the *Escherichia coli* fumarate reductase respiratory complex. *Science* 284: 1961–1966, 1999.
153. Jackson JB, Peake SJ, and White SA. Structure and mechanism of proton-translocating transhydrogenase. *FEBS Lett* 464: 1–8, 1999.
154. Jamshidi N and Palsson BO. Formulating genome-scale kinetic models in the post-genome era. *Mol Syst Biol* 4: 171, 2008.
155. Janke D and Fritsche W. Nature and significance of microbial cometabolism of xenobiotics. *J Basic Microbiol* 25: 603–619, 1985.
156. Jankowski MD, Henry CS, Broadbelt LJ, and Hatzimanikatis V. Group contribution method for thermodynamic analysis of complex metabolic networks. *Biophys J* 95: 1487–1499, 2008.
157. Johnson HA, Pelletier DA, and Spormann AM. Isolation and characterization of anaerobic ethylbenzene dehydrogenase, a novel Mo-Fe-S enzyme. *J Bacteriol* 183: 4536–4542, 2001.
158. Joo H, Lin Z, and Arnold FH. Laboratory evolution of peroxide-mediated cytochrome P450 hydroxylation. *Nature* 399: 670–673, 1999.
159. Jörnvall H, Persson M, and Jeffery M. Alcohol and polyol dehydrogenases are both divided into two protein types, and structural properties cross-relate the different enzyme activities within each type. *Proc Natl Acad Sci USA* 78: 4226–4230, 1981.
160. Jouhten P, Rintala E, Huuskonen A, Tamminen A, Toivari M, Wiebe M, Ruohonen L, Penttila M, and Maaheimo H. Oxygen dependence of metabolic fluxes and energy generation of *Saccharomyces cerevisiae* CEN.PK113-1A. *BMC Systems Biol* 2: 60, 2008.
161. Julsing MK, Cornelissen S, Bühler B, and Schmid A. Heme-iron oxygenases: Powerful industrial biocatalysts? *Curr Opin Chem Biol* 12: 177–186, 2008.

162. Kabus A, Georgi T, Wendisch VF, and Bott M. Expression of the *Escherichia coli pntAB* genes encoding a membrane-bound transhydrogenase in *Corynebacterium glutamicum* improves L-lysine formation. *Appl Microbiol Biotechnol* 75: 47–53, 2007.
163. Kalnenieks U, Galinina N, Strazdina I, Kravale Z, Pickford JL, Rutkis R, and Poole RK. NADH dehydrogenase deficiency results in low respiration rate and improved aerobic growth of *Zymomonas mobilis*. *Microbiology* 154: 989–994, 2008.
164. Kamerbeek NM, Janssen DB, van Berkel WJH, and Fraaije MW. Baeyer-Villiger monooxygenases, an emerging family of flavin-dependent biocatalysts. *Adv Synth Catal* 345: 667–678, 2003.
165. Kantz A, Chin F, Nallamothu N, Nguyen T, and Gassner GT. Mechanism of flavin transfer and oxygen activation by the two-component flavoenzyme styrene monooxygenase. *Arch Biochem Biophys* 442: 102–116, 2005.
166. Kasischke KA, Vishwasrao HD, Fisher PJ, Zipfel WR, and Webb WW. Neural activity triggers neuronal oxidative metabolism followed by astrocytic glycolysis. *Science* 305: 99–103, 2004.
167. Katopodis AG, Wimalasena K, Lee J, and May S. Mechanistic studies on nonheme iron monooxygenase catalysis: Epoxidation, aldehyde formation, and demethylation by the α-hydroxylation system of *Pseudomonas oleovorans*. *J Am Chem Soc* 106: 7928–7935, 1984.
168. Katopodis AG, Smith HA, Jr., and May S. New oxyfunctionalization capabilities for ω-hydroxylases: Asymmetric aliphatic sulfoxidation and branched ether demethylation. *J Am Chem Soc* 110: 897–899, 1988.
169. Keasling JD. Synthetic biology for synthetic chemistry. *ACS Chem Biol* 3: 64–76, 2008.
170. Kennedy CJ, Boyle PM, Waks Z, and Silver PA. Systems-level engineering of non-fermentative metabolism in yeast. *Genetics* 183: 385–397, 2009.
171. Kiener A. Enzymatic oxidation of methyl-groups on aromatic heterocycles; A versatile method for the preparation of heteroaromatic carboxylic acids. *Angew Chem Int Edit* 31: 774–775, 1992.
172. Kiener A. Biosynthesis of functionalized aromatic N-heterocycles. *Chemtech* 25: 31–35, 1995.
173. Kleifeld O, Frenkel A, Martin JM, and Sagi I. Active site electronic structure and dynamics during metalloenzyme catalysis. *Nat Struct Biol* 10: 98–103, 2003.
174. Klinman JP. Mechanisms whereby mononuclear copper proteins functionalize organic substrates. *Chem Rev* 96: 2541–2561, 1996.
175. Kniemeyer O and Heider J. Ethylbenzene dehydrogenase, a novel hydrocarbon-oxidizing molybdenum/iron-sulfur/heme enzyme. *J Biol Chem* 276: 21381–21386, 2001.
176. Koebmann B, Blank LM, Solem C, Petranovic D, Nielsen LK, and Jensen PR. Increased biomass yield of *Lactococcus lactis* during energetically limited growth and respiratory conditions. *Biotechnol Appl Biochem* 50: 25–33, 2008.
177. Koebmann BJ, Nilsson D, Kuipers OP, and Jensen PR. The membrane-bound $H^+$-ATPase complex is essential for growth of *Lactococcus lactis*. *J Bacteriol* 182: 4738–4743, 2000.
178. Koehntop KD, Emerson JP, and Que L. The 2-His-1-carboxylate facial triad: A versatile platform for dioxygen activation by mononuclear nonheme iron(II) enzymes. *J Biol Inorg Chem* 10: 87–93, 2005.
179. Kopp DA and Lippard SJ. Soluble methane monooxygenase: Activation of dioxygen and methane. *Curr Opin Chem Biol* 6: 568–576, 2002.
180. Kosjek B, Stampfer W, Pogorevc M, Goessler W, Faber K, and Kroutil W. Purification and characterization of a chemotolerant alcohol dehydrogenase applicable to coupled redox reactions. *Biotechnol Bioeng* 86: 55–62, 2004.
181. Kovaleva EG and Lipscomb JD. Crystal structures of $Fe^{2+}$ dioxygenase superoxo, alkylperoxo, and bound product intermediates. *Science* 316: 453–457, 2007.
182. Kovaleva EG, Neibergall MB, Chakrabarty S, and Lipscomb JD. Finding intermediates in the $O_2$ activation pathways of nonheme iron oxygenases. *Acc Chem Res* 40: 475–483, 2007.
183. Kovaleva EG and Lipscomb JD. Versatility of biological nonheme Fe(II) centers in oxygen activation reactions. *Nature Chem Biol* 4: 186–193, 2008.
184. Kovaleva EG and Lipscomb JD. Intermediate in the O-O bond cleavage reaction of an extradiol dioxygenase. *Biochemistry* 47: 11168–11170, 2008.
185. Kragl U, VasicRacki D, and Wandrey C. Continuous production of L-*tert*-leucine in series of two enzyme membrane reactors. Modeling and computer simulation. *Bioprocess Engineering* 14: 291–297, 1996.
186. Krebs C, Fujimori DG, Walsh CT, and Bollinger JM. Non-heme Fe(IV)-oxo intermediates. *Acc Chem Res* 40: 484–492, 2007.
187. Kula MR, Wichmann R, Oden U, and Wandrey C. Influence of substrate or product inhibition on the performance of enzyme reactors. *Biochimie* 62: 523–536, 1980.
188. Kulkarni AP. Lipoxygenase. A versatile biocatalyst for biotransformation of endobiotics and xenobiotics. *Cell Mol Life Sci* 58: 1805–1825, 2001.
189. Kummel A, Panke S, and Heinemann M. Systematic assignment of thermodynamic constraints in metabolic network models. *BMC Bioinformatics* 7: 512, 2006.
190. Kweon O, Kim SJ, Baek S, Chae JC, Adjei MD, Baek DH, Kim YC, and Cerniglia CE. A new classification system for bacterial Rieske nonheme iron aromatic ring-hydroxylating oxygenases. *BMC Biochem* 9: 11, 2008.
191. Laden BP, Tang YZ, and Porter TD. Cloning, heterologous expression, and enzymological characterization of human squalene monooxygenase. *Arch Biochem Biophys* 374: 381–388, 2000.
192. Leak DJ, Sheldon RA, Woodley JM, and Adlercreutz P. Biocatalysts for selective introduction of oxygen. *Biocatal Biotransform* 27: 1–26, 2009.
193. Lee S-K, Nesheim JC, and Lipscomb JD. Transient intermediates of the methane monooxygenase catalytic cycle. *J Biol Chem* 268: 21569–21577, 1993.
194. Lee S, Phalakornkule C, Domach MM, and Grossmann IE. Recursive MILP model for finding all the alternate optima in LP models for metabolic networks. *Comput Chem Eng* 24: 711–716, 2000.
195. Lee SK and Lipscomb JD. Oxygen activation catalyzed by methane monooxygenase hydroxylase component: proton delivery during the O-O bond cleavage steps. *Biochemistry* 38: 4423–4432, 1999.
196. Lee SY, Hong SH, and Moon SY. In silico metabolic pathway analysis and design: Succinic acid production by metabolically engineered *Escherichia coli* as an example. *Genome Inform* 13: 214–223, 2002.
197. Leferink NGH, Heuts DPHM, Fraaije MW, and van Berkel WJH. The growing VAO flavoprotein family. *Arch Biochem Biophys* 474: 292–301, 2008.
198. Leferink NGH, Fraaije MW, Joosten HJ, Schaap PJ, Mattevi A, and van Berkel WJH. Identification of a gatekeeper

residue that prevents dehydrogenases from acting as oxidases. *J Biol Chem* 284: 4392–4397, 2009.
199. Lenich A and Goodman S. The purification and characterization of glutaryl-coenzyme A dehydrogenase from porcine and human liver. *J Biol Chem* 261: 4090–4096, 1986.
200. Lerondel G, Doan T, Zamboni N, Sauer U and Aymerich S. YtsJ has the major physiological role of the four paralogous malic enzyme isoforms in *Bacillus subtilis*. *J Bacteriol* 188: 4727–4736, 2006.
201. Liese A, Seelbach K and Wandrey C. *Industrial Biotransformations*. Weinheim, Germany: Wiley-VCH, 2006, p. 423.
202. Lilius EM, Multanen VM and Toivonen V. Quantitative extraction and estimation of intracellular nicotinamide nucleotides of *Escherichia coli*. *Anal Biochem* 99: 22–27, 1979.
203. Lilly MD and Woodley JM. A structured approach to design and operation of biotransformation processes. *J Ind Microbiol* 17: 24–29, 1996.
204. Lowry OH, Passonneau JV, and Rock MK. The stability of pyridine nucleotides. *J Biol Chem* 236: 2756–2759, 1961.
205. Lowry OH, Passonneau JV, Schulz DW, and Rock MK. The measurement of pyridine nucleotides by enzymatic cycling. *J Biol Chem* 236: 2746–2755, 1961.
206. Luo B, Groenke K, Takors R, Wandrey C, and Oldiges M. Simultaneous determination of multiple intracellular metabolites in glycolysis, pentose phosphate pathway and tricarboxylic acid cycle by liquid chromatography-mass spectrometry. *J Chromatogr A* 1147: 153–164, 2007.
207. Mahadevan R and Schilling CH. The effects of alternate optimal solutions in constraint-based genome-scale metabolic models. *Metab Eng* 5: 264–276, 2003.
208. Mailinger W, Baumeister A, Reuss M, and Rizzi M. Rapid and highly automated determination of adenine and pyridine nucleotides in extracts of *Saccharomyces cerevisiae* using a micro robotic sample preparation-HPLC system. *J Biotechnol* 63: 155–166, 1998.
209. Massey V. Activation of molecular oxygen by flavins and flavoproteins. *J Biol Chem* 269: 22459–22462, 1994.
210. Massey V. The chemical and biological versatility of riboflavin. *Biochem Soc Trans* 28: 283–296, 2000.
211. Mathys RG, Schmid A, and Witholt B. Integrated two-liquid phase bioconversion and product-recovery processes for the oxidation of alkanes: Process design and economic evaluation. *Biotechnol Bioeng* 64: 459–477, 1999.
212. Matin A and Gottschal JC. Influence of dilution rate on NAD(P) and NAD(P)H concentrations and ratios in a *Pseudomonas* sp. grown in continuous culture. *J Gen Microbiol* 94: 333–341, 1976.
213. Matsushita K, Toyama H, Yamada M, and Adachi O. Quinoproteins: Structure, function, and biotechnological applications. *Appl Microbiol Biotechnol* 58: 13–22, 2002.
214. Mattevi A, Fraaije MW, Mozzarelli A, Olivi L, Coda A, and van Berkel WJH. Crystal structures and inhibitor binding in the octameric flavoenzyme vanillyl-alcohol oxidase: The shape of the active-site cavity controls substrate specificity. *Structure* 5: 907–920, 1997.
215. May S and Katopodis AG. Oxygenation of alcohol and sulphide substrates by a prototypical non-haem iron monooxygenase: Catalysis and biotechnological potential. *Enzyme Microb Technol* 8: 17–21, 1986.
216. McGuirl MA and Dooley DM. Copper-containing oxidases. *Curr Opin Chem Biol* 3: 138–144, 1999.
217. Merkx M, Kopp DA, Sazinsky MH, Blazyk JL, Müller J, and Lippard SJ. Dioxygen activation and methane hydroxylation by soluble methane monooxygenase: A tale of two irons and three proteins. *Angew Chem Int Ed* 40: 2782–2807, 2001.
218. Meuller J and Rydstrom J. The membrane topology of proton-pumping *Escherichia coli* transhydrogenase determined by cysteine labeling. *J Biol Chem* 274: 19072–19080, 1999.
219. Meunier B, de Visser SP, and Shaik S. Mechanism of oxidation reactions catalyzed by cytochrome P450 enzymes. *Chem Rev* 104: 3947–3980, 2004.
220. Mihovilovic MD. Enzyme mediated Baeyer–Villiger oxidations. *Curr Org Chem* 10: 1265–1287, 2006.
221. Mirica LM and Klinman JP. The nature of $O_2$ activation by the ethylene-forming enzyme 1-aminocyclopropane-1-carboxylic acid oxidase. *Proc Natl Acad Sci USA* 105: 1814–1819, 2008.
222. Mitchell KH, Rogge CE, Gierahn T, and Fox BG. Insight into the mechanism of aromatic hydroxylation by toluene 4-monooxygenase by use of specifically deuterated toluene and *p*-xylene. *Proc Natl Acad Sci USA* 100: 3784–3789, 2003.
223. Moonen MJH, Fraaije MW, Rietjens IMCM, Laane C, and van Berkel WJH. Flavoenzyme-catalyzed oxygenations and oxidations of phenolic compounds. *Adv Synth Catal* 344: 1023–1035, 2002.
224. Munro AW, Leys DG, McLean KJ, Marshall KR, Ost TWB, Daff S, Miles CS, Chapman SK, Lysek DA, Moser CC, Page CC, and Dutton PL. P450 BM3: The very model of a modern flavocytochrome. *Trends Biochem Sci* 27: 250–257, 2002.
225. Munro AW, Girvan HM, and McLean KJ. Variations on a (t)heme. Novel mechanisms, redox partners and catalytic functions in the cytochrome P450 superfamily. *Nat Prod Rep* 24: 585–609, 2007.
226. Nagel M and Andreesen JR. Purification and characterization of the molybdoenzymes nicotinate dehydrogenase and 6-hydroxynicotinate dehydrogenase from *Bacillus niacini*. *Arch Microbiol* 154: 605–613, 1990.
227. This reference has been deleted.
228. Neves AR, Ramos A, Costa H, van S, II, Hugenholtz J, Kleerebezem M, de Vos W, and Santos H. Effect of different NADH oxidase levels on glucose metabolism by *Lactococcus lactis*: Kinetics of intracellular metabolite pools determined by *in vivo* nuclear magnetic resonance. *Appl Environ Microbiol* 68: 6332–6342, 2002.
229. Neves AR, Pool WA, Kok J, Kuipers OP, and Santos H. Overview on sugar metabolism and its control in *Lactococcus lactis*. The input from *in vivo* NMR. *FEMS Microbiol Rev* 29: 531–554, 2005.
230. Newcomb M, Hollenberg PF, and Coon MJ. Multiple mechanisms and multiple oxidants in P450-catalyzed hydroxylations. *Arch Biochem Biophys* 409: 72–79, 2003.
231. Newcomb M, Halgrimson JA, Horner JH, Wasinger EC, Chen LX, and Sligar SG. X-ray absorption spectroscopic characterization of a cytochrome P450 compound II derivative. *Proc Natl Acad Sci USA* 105: 8179–8184, 2008.
232. Nielsen JH and Villadsen J. *Bioreaction Engineering Principles*. New York; London Plenum Press, 1994, p. 456.
233. Nisselbaum JS and Green S. A simple ultramicro method for determination of pyridine nucleotides in tissues. *Anal Biochem* 27: 212–217, 1969.

234. Nizam SA, Zhu JF, Ho PY, and Shimizu K. Effects of *arcA* and *arcB* genes knockout on the metabolism in *Escherichia coli* under aerobic condition. *Biochem Eng J* 44: 240–250, 2009.
235. Noguchi Y, Nakai Y, Shimba N, Toyosaki H, Kawahara Y, Sugimoto S, and Suzuki E. The energetic conversion competence of *Escherichia coli* during aerobic respiration studied by $^{31}$P NMR using a circulating fermentation system. *J Biochem* 136: 509–515, 2004.
236. Oh IJ, Kim DH, Oh EK, Lee SY, and Lee J. Optimization and scale-up of succinic acid production by *Mannheimia succiniciproducens* LPK7. *J Microbiol Biotechnol* 19: 167–171, 2009.
237. Ohnishi T, Sled VD, Rudnitzky NI, Jacobson BW, Fukumori Y, Meinhardt SW, Calhoun MW, Gennis RB, Leif H, Friedrich T, and Weiss H. Biophysical and biochemical studies of bacterial NADH quinone oxidoreductase (Ndh-1). *Biochem Soc Trans* 22: S70–S70, 1994.
238. Okamoto K, Matsumoto K, Hille R, Eger BT, Pai EF, and Nishino T. The crystal structure of xanthine oxidoreductase during catalysis: Implications for reaction mechanism and enzyme inhibition. *Proc Natl Acad Sci USA* 101: 7931–7936, 2004.
239. Ortiz de Montellano PR, Nishida C, Rodriguez–Crespo I, and Gerber N. Nitric oxide synthase structure and electron transfer. *Drug Metab Dispos* 26: 1185–1189, 1998.
240. Orville AM and Lipscomb JD. Cyanide and nitric oxide binding to reduced protocatechuate 3,4-dioxygenase: Insight into the basis for order-dependent ligand binding by intradiol catecholic dioxygenases. *Biochemistry* 36: 14044–14055, 1997.
241. Otto K, Hofstetter K, Rothlisberger M, Witholt B, and Schmid A. Biochemical characterization of StyAB from *Pseudomonas* sp. strain VLB120 as a two-component flavin-diffusible monooxygenase. *J Bacteriol* 186: 5292–5302, 2004.
242. Overkamp KM, Bakker BM, Steensma HY, van Dijken JP, and Pronk JT. Two mechanisms for oxidation of cytosolic NADPH by *Kluyveromyces lactis* mitochondria. *Yeast* 19: 813–824, 2002.
243. Panke S, Witholt B, Schmid A, and Wubbolts MG. Towards a biocatalyst for (S)-styrene oxide production: characterization of the styrene degradation pathway of *Pseudomonas* sp. strain VLB120. *Appl Environ Microbiol* 64: 2032–2043, 1998.
244. Panke S, Wubbolts MG, Schmid A, and Witholt B. Production of enantiopure styrene oxide by recombinant *Escherichia coli* synthesizing a two-component styrene monooxygenase. *Biotechnol Bioeng* 69: 91–100, 2000.
245. Panke S, Held M, Wubbolts MG, Witholt B, and Schmid A. Pilot-scale production of (*S*)-styrene oxide from styrene by recombinant *Escherichia coli* synthesizing styrene monooxygenase. *Biotechnol Bioeng* 80: 33–41, 2002.
246. Park JB, Bühler B, Habicher T, Hauer B, Panke S, Witholt B, and Schmid A. The efficiency of recombinant *Escherichia coli* as biocatalyst for stereospecific epoxidation. *Biotechnol Bioeng* 95: 501–512, 2006.
247. Park JB and Clark DS. Deactivation mechanisms of chloroperoxidase during biotransformations. *Biotechnol Bioeng* 93: 1190–1195, 2006.
248. Patel RN. Synthesis of chiral pharmaceutical intermediates by biocatalysis. *Chem Rev* 252: 659–701, 2008.
249. Pavon JA and Fitzpatrick PF. Intrinsic isotope effects on benzylic hydroxylation by the aromatic amino acid hydroxylases: Evidence for hydrogen tunneling, coupled motion, and similar reactivities. *J Am Chem Soc* 127: 16414–16415, 2005.
250. Pavon JA and Fitzpatrick PF. Insights into the catalytic mechanisms of phenylalanine and tryptophan hydroxylase from kinetic isotope effects on aromatic hydroxylation. *Biochemistry* 45: 11030–11037, 2006.
251. Perrenoud A and Sauer U. Impact of global transcriptional regulation by ArcA, ArcB, Cra, Crp, Cya, Fnr, and Mlc on glucose catabolism in *Escherichia coli*. *J Bacteriol* 187: 3171–3179, 2005.
252. Peters FT, Dragan CA, Wilde DR, Meyer MR, Zapp J, Bureik M, and Maurer HH. Biotechnological synthesis of drug metabolites using human cytochrome P450 2D6 heterologously expressed in fission yeast exemplified for the designer drug metabolite 4′-hydroxymethyl-α-pyrrolidinobutyrophenone. *Biochem Pharmacol* 74: 511–520, 2007.
253. Peters FT, Dragan CA, Kauffels A, Schwaninger AE, Zapp J, Bureik M, and Maurer HH. Biotechnological synthesis of the designer drug metabolite 4′-hydroxymethyl-α-pyrrolidinohexanophenone in fission yeast heterologously expressing human cytochrome P450 2D6—A versatile alternative to multistep chemical synthesis. *J Anal Toxicol* 33: 190–197, 2009.
254. Peters FT, Dragan CA, Schwaninger AE, Sauer C, Zapp J, Bureik M, and Maurer HH. Use of fission yeast heterologously expressing human cytochrome P450 2B6 in biotechnological synthesis of the designer drug metabolite N-(1-phenylcyclohexyl)-2-hydroxyethanamine. *Forensic Sci Int* 184: 69–73, 2009.
255. Petersen S, de Graaf AA, Eggeling L, Mollney M, Wiechert W, and Sahm H. *In vivo* quantification of parallel and bidirectional fluxes in the anaplerosis of *Corynebacterium glutamicum*. *J Biol Chem* 275: 35932–35941, 2000.
256. Peterson JA, Basu D, and Coon MJ. Enzymatic omega-oxidation. I. Electron carriers in fatty acid and hydrocarbon hydroxylation. *J Biol Chem* 241: 5162–5164, 1966.
257. Poole RK and Cook GM. Redundancy of aerobic respiratory chains in bacteria? Routes, reasons and regulation. *Adv Microb Physiol* 43: 165–224, 2000.
258. Popov VO and Lamzin VS. $NAD^+$-dependent formate dehydrogenase. *Biochem J* 301: 625–643, 1994.
259. Prescott AG and Lloyd MD. The iron(II) and 2-oxoacid-dependent dioxygenases and their role in metabolism. *Nat Prod Rep* 17: 367–383, 2000.
260. Price ND, Reed JL, and Palsson BO. Genome-scale models of microbial cells: Evaluating the consequences of constraints. *Nature Rev Microb* 2: 886–897, 2004.
261. Purpero V and Moran GR. The diverse and pervasive chemistries of the α-keto acid dependent enzymes. *J Biol Inorg Chem* 12: 587–601, 2007.
262. Que L. One motif—Many different reactions. *Nat Struct Biol* 7: 182–184, 2000.
263. Raber DJ and Rodriguez W. Conformational properties of oxidation reduction cofactors. *J Am Chem Soc* 107: 4146–4147, 1985.
264. Rao K, Albro M, Zirrolli J, van der Velde D, Jones DN and Frerman F. Protonation of crotonyl-CoA dienolate by human glutaryl-CoA dehydrogenase occurs by solvent-derived protons. *Biochemistry* 44: 13932–13940, 2005.
265. Rao KS, Albro M, Dwyer TM and Frerman FE. Kinetic mechanism of glutaryl-CoA dehydrogenase. *Biochemistry* 45: 15853–15861, 2006.

266. Resnick SM, Lee K, and Gibson DT. Diverse reactions catalyzed by naphthalene dioxygenase from *Pseudomonas sp strain* NCIB 9816. *J Ind Microbiol Biot* 17: 438–457, 1996.
267. Richardson DJ. Bacterial respiration: A flexible process for a changing environment. *Microbiology* 146: 551–571, 2000.
268. Roach PL, Clifton IJ, Hensgens CMH, Shibata N, Schofield CJ, Hajdu J, and Baldwin JE. Structure of isopenicillin *N* synthase complexed with substrate and the mechanism of penicillin formation. *Nature* 387: 827–830, 1997.
269. Roels JA. Application of macroscopic principles to microbial metabolism. *Biotechnol Bioeng* 22: 2457–2514, 1980.
270. Romano AH and Conway T. Evolution of carbohydrate metabolic pathways. *Res Microbiol* 147: 448–455, 1996.
271. Rosenzweig AC, Frederick CA, Lippard SJ, and Nordlund P. Crystal structure of a bacterial non-haem iron hydroxylase that catalyses the biological oxidation of methane. *Nature* 366: 537–543, 1993.
272. Rosenzweig AC. The metal centres of particulate methane mono-oxygenase. *Biochem Soc Trans* 36: 1134–1137, 2008.
273. Rover Junior L, Fernandes JC, de Oliveira Neto G, Kubota LT, Katekawa E, and Serrano SH. Study of NADH stability using ultraviolet-visible spectrophotometric analysis and factorial design. *Anal Biochem* 260: 50–55, 1998.
274. Ruddat VC, Whitman S, Holman TR, and Bernasconi CF. Stopped-flow kinetic investigations of the activation of soybean lipoxygenase-1 and the influence of inhibitors on the allosteric site. *Biochemistry* 42: 4172–4178, 2003.
275. Rydstrom J. Mitochondrial transhydrogenase—A key enzyme in insulin secretion and, potentially, diabetes. *Trends Biochem Sci* 31: 355–358, 2006.
276. Ryle MJ and Hausinger RP. Nonheme iron oxygenases. *Curr Opin Chem Biol* 6: 193–201, 2002.
277. Sanchez AM, Andrews J, Hussein I, Bennett GN, and San KY. Effect of overexpression of a soluble pyridine nucleotide transhydrogenase (UdhA) on the production of poly (3-hydroxybutyrate) in *Escherichia coli*. *Biotechnol Prog* 22: 420–425, 2006.
278. Sauer U, Hatzimanikatis V, Hohmann HP, Manneberg M, van Loon AP, and Bailey JE. Physiology and metabolic fluxes of wild-type and riboflavin-producing *Bacillus subtilis*. *Appl Environ Microbiol* 62: 3687–3696, 1996.
279. Sauer U and Bailey JE. Estimation of P-to-O ratio in *Bacillus subtilis* and its influence on maximum riboflavin yield. *Biotechnol Bioeng* 64: 750–754, 1999.
280. Sauer U, Lasko DR, Fiaux J, Hochuli M, Glaser R, Szyperski T, Wuthrich K, and Bailey JE. Metabolic flux ratio analysis of genetic and environmental modulations of *Escherichia coli* central carbon metabolism. *J Bacteriol* 181: 6679–6688, 1999.
281. Sauer U, Canonaco F, Heri S, Perrenoud A, and Fischer E. The soluble and membrane-bound transhydrogenases *UdhA* and *PntAB* have divergent functions in NADPH metabolism of *Escherichia coli*. *J Biol Chem* 279: 6613–6619, 2004.
282. Sauer U. Metabolic networks in motion: $^{13}$C-based flux analysis. *Mol Syst Biol* 2: 62, 2006.
283. Savinell JM and Palsson BO. Network analysis of intermediary metabolism using linear optimization. I. Development of mathematical formalism. *J Theor Biol* 154: 421–454, 1992.
284. Savinell JM and Palsson BO. Optimal selection of metabolic fluxes for *in vivo* measurement. II. Application to *Escherichia coli* and hybridoma cell metabolism. *J Theor Biol* 155: 215–242, 1992.
285. Schadel F and Franco–Lara E. Rapid sampling devices for metabolic engineering applications. *Appl Microbiol Biotechnol* 83: 199–208, 2009.
286. Schlichting I, Berendzen J, Chu K, Stock AM, Maves SA, Benson DE, Sweet RM, Ringe D, Petsko GA, and Sligar SG. The catalytic pathway of cytochrome P450cam at atomic resolution. *Science* 287: 1615–1622, 2000.
287. Schmid A, Dordick JS, Hauer B, Kiener A, Wubbolts M, and Witholt B. Industrial biocatalysis today and tomorrow. *Nature* 409: 258–268, 2001.
288. Schmidt K, Carlsen M, Nielsen J, and Villadsen J. Modeling isotopomer distributions in biochemical networks using isotopomer mapping matrices. *Biotechnol Bioeng* 55: 831–840, 1997.
289. Schroer K, Mackfeld U, Tana IAW, Wandrey C, Heuser F, Bringer-Meyer S, Weckbecker A, Hummel W, Daussmann T, Pfaller R, Liese A, and Lutz S. Continuous asymmetric ketone reduction processes with recombinant *Escherichia coli*. *J Biotechnol* 132: 438–444, 2007.
290. Schroer K, Luef PK, Hartner FS, Glieder A, and Pscheidt B. Engineering the *Pichia pastoris* methanol oxidation pathway for improved NADH regeneration during whole-cell biotransformation. *Metab Eng* 12: 8–17, 2010.
291. Schroer K, Zelic B, Oldiges M, and Lutz S. Metabolomics for biotransformations: Intracellular redox cofactor analysis and enzyme kinetics offer insight into whole cell processes. *Biotechnol Bioeng* 104: 251–260, 2009.
292. Schuetz R, Kuepfer L, and Sauer U. Systematic evaluation of objective functions for predicting intracellular fluxes in *Escherichia coli*. *Mol Sys Biol* 3: 119, 2007.
293. Schüte H, Flossdorf J, Sahm H, and Kula MR. Purification and properties of formaldehyde dehydrogenase and formate dehydrogenase from *Candida boidinii*. *Eur J Biochem* 62: 151–160, 1976.
294. Schwartz JK, Wei PP, Mitchell KH, Fox BG, and Solomon EI. Geometric and electronic structure studies of the binuclear nonheme ferrous active site of toluene-4-monooxygenase: Parallels with methane monooxygenase and insight into the role of the effector proteins in $O_2$ activation. *J Am Chem Soc* 130: 7098–7109, 2008.
295. Shaw NM, Robins KT, and Kiener A. Lonza: 20 years of biotransformations. *Adv Synth Catal* 345: 425–435, 2003.
296. Sheng X, Zhang HM, Hollenberg PF, and Newcomb M. Kinetic isotope effects in hydroxylation reactions effected by cytochrome P450 compounds I implicate multiple electrophilic oxidants for P450-catalyzed oxidations. *Biochemistry* 48: 1620–1627, 2009.
297. Shibasaki T, Hashimoto S, Mori H, and Ozaki A. Construction of a novel hydroxyproline-producing recombinant *Escherichia coli* by introducing a proline 4-hydroxylase gene. *J Biosci Bioeng* 90: 522–525, 2000.
298. Shibasaki T, Mori H, and Ozaki A. Enzymatic production of *trans*-4-hydroxy-L-proline by regio- and stereospecific hydroxylation of L-proline. *Biosci Biotechnol Biochem* 64: 746–750, 2000.
299. Shu L, Nesheim JC, Kauffmann K, Münck E, Lipscomb JD, and Que L, Jr. An $Fe_2^{IV}O_2$ diamond core structure for the key intermediate Q of methane monooxygenase. *Science* 275: 515–518, 1997.
300. Slonczewski JL, Rosen BP, Alger JR, and Macnab RM. pH homeostasis in *Escherichia coli*: Measurement by $^{31}$P nuclear

magnetic resonance of methylphosphonate and phosphate. *Proc Natl Acad Sci USA* 78: 6271–6275, 1981.
301. Smith E and Morowitz HJ. Universality in intermediary metabolism. *Proc Natl Acad Sci USA* 101: 13168–13173, 2004.
302. Smits TH, Balada SB, Witholt B, and van Beilen JB. Functional analysis of alkane hydroxylases from gram-negative and gram-positive bacteria. *J Bacteriol* 184: 1733–1742, 2002.
303. Solomon EI, Sundaram UM, and Machonkin TE. Multicopper oxidases and oxygenases. *Chem Rev* 96: 2563–2605, 1996.
304. Solomon EI, Brunold TC, Davis MI, Kemsley JN, Lee SK, Lehnert N, Neese F, Skulan AJ, Yang YS, and Zhou J. Geometric and electronic structure/function correlations in nonheme iron enzymes. *Chem Rev* 100: 235–350, 2000.
305. Solomon EI, Augustine AJ, and Yoon J. $O_2$ Reduction to $H_2O$ by the multicopper oxidases. *Dalton Transac* 3921–3932, 2008.
306. Sono M, Roach MP, Coulter ED, and Dawson JH. Heme-containing oxygenases. *Chem Rev* 96: 2841–2887, 1996.
307. Stephanopoulos G, Aristidou AA, and Nielsen J. *Metabolic Engineering: Principles and Methodologies*. San Diego, CA: Academic Press, 1998, p. 725.
308. Steuer R and Junker BH. Computational models of metabolism: Stability and regulation in metabolic networks. *Adv Chem Phys* 142: 105–251, 2009.
309. Stewart JD. Cyclohexanone monooxygenase: A useful reagent for asymmetric Baeyer–Villiger reactions. *Curr Org Chem* 2: 195–216, 1998.
310. Stouthamer AH. The search for correlation between theoretical and experimental growth yields. In: *International Review of Biochemistry: Microbial Biochemistry*, edited by Quayle JR. Baltimore: University Park Press, 1979, pp. 1–47.
311. Straathof AJ, Panke S, and Schmid A. The production of fine chemicals by biotransformations. *Curr Opin Biotechnol* 13: 548–556, 2002.
312. Studley WK, Yamaguchi M, Hatefi Y, and Saier MH, Jr. Phylogenetic analyses of proton-translocating transhydrogenases. *Microb Comp Genom* 4: 173–186, 1999.
313. Suske WA, Held M, Schmid A, Fleischmann T, Wubbolts MG, and Kohler HP. Purification and characterization of 2-hydroxybiphenyl 3-monooxygenase, a novel NADH-dependent, FAD-containing aromatic hydroxylase from *Pseudomonas azelaica* HBP1. *J Biol Chem* 272: 24257–24265, 1997.
314. Suzuki M, Hayakawa T, Shaw JP, Rekik M, and Harayama S. Primary structure of xylene monooxygenase: Similarities to and differences from the alkane hydroxylation system. *J Bacteriol* 173: 1690–1695, 1991.
315. Szczebara FM, Chandelier C, Villeret C, Masurel A, Bourot S, Duport C, Blanchard S, Groisillier A, Testet E, Costaglioli P, Cauet G, Degryse E, Balbuena D, Winter J, Achstetter T, Spagnoli R, Pompon D, and Dumas B. Total biosynthesis of hydrocortisone from a simple carbon source in yeast. *Nat Biotechnol* 21: 143–149, 2003.
316. Tang YJ, Martin HG, Myers S, Rodriguez S, Baidoo EEK, and Keasling JD. Advances in analysis of microbial metabolic fluxes via C-13 isotopic labeling. *Mass Spectrom Rev* 28: 362–375, 2009.
317. Tarrio N, Becerra M, Cerdan ME, and Siso MIG. Reoxidation of cytosolic NADPH in *Kluyveromyces lactis*. *FEMS Yeast Res* 6: 371–380, 2006.
317a. Tempest DW and Neijssel OM. Growth yield and energy distribution. In: *Escherichia coli and Salmonella typhimurium cellular and molecular biology*, edited by Neidhardt FC and Ingraham JL. Washington, DC: American Society for Microbiology, 1987, pp. 797–805.
318. Tishkov VI and Popov VO. Catalytic mechanism and application of formate dehydrogenase. *Biochemistry* 69: 1252–1268, 2004.
319. Tran QH, Bongaerts J, Vlad D, and Unden G. Requirement for the proton-pumping NADH dehydrogenase I of *Escherichia coli* in respiration of NADH to fumarate and its bioenergetic implications. *Eur J Biochem* 244: 155–160, 1997.
320. Ullrich R and Hofrichter M. Enzymatic hydroxylation of aromatic compounds. *Cell Mol Life Sci* 64: 271–293, 2007.
321. Urlacher VB, Lutz–Wahl S, and Schmid RD. Microbial P450 enzymes in biotechnology. *Appl Microbiol Biotechnol* 64: 317–325, 2004.
322. Urlacher VB and Eiben S. Cytochrome P450 monooxygenases: Perspectives for synthetic application. *Trends Biotechnol* 24: 324–330, 2006.
323. Urlacher VB and Schmid RD. Recent advances in oxygenase-catalyzed biotransformations. *Curr Opin Chem Biol* 10: 156–161, 2006.
324. Vaillancourt FH, Bolin JT, and Eltis LD. The ins and outs of ring-cleaving dioxygenases. *Crit Rev Biochem Mol* 41: 241–267, 2006.
325. Valderrama B, Ayala M, and Vazquez–Duhalt R. Suicide inactivation of peroxidases and the challenge of engineering more robust enzymes. *Chem Biol* 9: 555–565, 2002.
326. Valentine AM, Stahl SS, and Lippard SJ. Mechanistic studies of the reaction of reduced methane monooxygenase hydroxylase with dioxygen and substrates. *J Am Chem Soc* 121: 3876–3887, 1999.
327. van Beilen JB, Kingma J, and Witholt B. Substrate specificity of the alkane hydroxylase system of *Pseudomonas oleovorans* GPo1. *Enzyme Microb Tech* 16: 904–911, 1994.
328. van Beilen JB and Funhoff EG. Expanding the alkane oxygenase toolbox: new enzymes and applications. *Curr Opin Biotech* 16: 308–314, 2005.
329. van Beilen JB, Smits THM, Roos FF, Brunner T, Balada SB, Rothlisberger M, and Witholt B. Identification of an amino acid position that determines the substrate range of integral membrane alkane hydroxylases. *J Bacteriol* 187: 85–91, 2005.
330. van Berkel WJ, Kamerbeek NM, and Fraaije MW. Flavoprotein monooxygenases: A diverse class of oxidative biocatalysts. *J Biotechnol* 124: 670–689, 2006.
331. van de Velde F, van Rantwijk F, and Sheldon RA. Improving the catalytic performance of peroxidases in organic synthesis. *Trends Biotechnol* 19: 73–80, 2001.
332. van den Heuvel RHH, Fraaije MW, Mattevi A, Laane C, and van Berkel WJH. Vanillyl-alcohol oxidase, a tasteful biocatalyst. *J Mol Catal B-Enzym* 11: 185–188, 2001.
333. van den Heuvel RHH, Laane C, and van Berkel WJH. Exploring the biocatalytic potential of vanillyl-alcohol oxidase by site-directed mutagenesis. *Adv Synth Catal* 343: 515–520, 2001.
334. van Deurzen MPJ, van Rantwijk F, and Sheldon RA. Selective oxidations catalyzed by peroxidases. *Tetrahedron* 53: 13183–13220, 1997.
335. van Gulik WM and Heijnen JJ. A metabolic network stoichiometry analysis of microbial growth and product formation. *Biotechnol Bioeng* 48: 681–698, 1995.
336. van Maris AJ, Winkler AA, Porro D, van Dijken JP, and Pronk JT. Homofermentative lactate production cannot sustain anaerobic growth of engineered *Saccharomyces cerevisiae*: Possible consequence of energy-dependent lactate export. *Appl Environ Microbiol* 70: 2898–2905, 2004.

337. van Rantwijk F and Sheldon RA. Selective oxygen transfer catalysed by heme peroxidases: Synthetic and mechanistic aspects. *Curr Opin Biotech* 11: 554–564, 2000.
338. Vanderheijden RTJM, Romein B, Heijnen JJ, Hellinga C, and Luyben KCAM. Linear constraint relations in biochemical reaction systems. 2. Diagnosis and estimation of gross errors. *Biotechnol Bioeng* 43: 11–20, 1994.
339. Varma A, Boesch BW, and Palsson BO. Biochemical production capabilities of *Escherichia coli*. *Biotechnol Bioeng* 42: 59–73, 1993.
340. Veit A, Polen T and Wendisch VF. Global gene expression analysis of glucose overflow metabolism in *Escherichia coli* and reduction of aerobic acetate formation. *Appl Microbiol Biotechnol* 74: 406–421, 2007.
341. Vemuri GN, Eiteman MA, and Altman E. Effects of growth mode and pyruvate carboxylase on succinic acid production by metabolically engineered strains of *Escherichia coli*. *Appl Environ Microbiol* 68: 1715–1727, 2002.
342. Verho R, Richard P, Jonson PH, Sundqvist L, Londesborough J, and Penttila M. Identification of the first fungal NADP-GAPDH from *Kluyveromyces lactis*. *Biochemistry* 41: 13833–13838, 2002.
343. Vetting MW, Wackett LP, Que L, Lipscomb JD, and Ohlendorf DH. Crystallographic comparison of manganese- and iron-dependent homoprotocatechuate 2,3-dioxygenases. *J Bacteriol* 186: 1945–1958, 2004.
344. Vital–Lopez FG, Armaou A, Nikolaev EV, and Maranas CD. A computational procedure for optimal engineering interventions using kinetic models of metabolism. *Biotech Progress* 22: 1507–1517, 2006.
345. Wackett LP. Mechanism and applications of Rieske nonheme iron dioxygenases. *Enzyme Microb Tech* 31: 577–587, 2002.
346. Wallar BJ and Lipscomb JD. Dioxygen activation by enzymes containing binuclear nonheme iron clusters. *Chem Rev* 96: 2625–2658, 1996.
347. Wallar BJ and Lipscomb JD. Methane monooxygenase component B mutants alter the kinetics of steps throughout the catalytic cycle. *Biochemistry* 40: 2220–2233, 2001.
348. Wang HY, Cooney CL, and Wang DIC. On-line gas analysis for material balances and control. *Biotechnol Bioeng Symp* 9: 13–23, 1979.
348a. *Webster's Encyclopedic Unabridged Dictionary of the English Language*. New York: Gramercy Books, 1996, p. 2230.
349. Weckbecker A and Hummel W. Improved synthesis of chiral alcohols with *Escherichia coli* cells co-expressing pyridine nucleotide transhydrogenase, $NADP^+$-dependent alcohol dehydrogenase and $NAD^+$-dependent formate dehydrogenase. *Biotechnol Lett* 26: 1739–1744, 2004.
350. Wermuth B and Kaplan NO. Pyridine-nucleotide transhydrogenase from *Pseudomonas aeruginosa*. Purification by affinity chromatography and physicochemical properties. *Arch Biochem Biophys* 176: 136–143, 1976.
351. Wery J, Mendes da Silva DI, and de Bont JA. A genetically modified solvent-tolerant bacterium for optimized production of a toxic fine chemical. *Appl Microbiol Biotechnol* 54: 180–185, 2000.
352. Wichmann R, Wandrey C, Buckmann AF, and Kula MR. Continuous enzymatic transformation in an enzyme membrane reactor with simultaneous NAD(H) regeneration. *Biotechnol Bioeng* 23: 2789–2802, 1981.
353. Wichmann R and Vasic–Racki D. Cofactor regeneration at the lab scale. *Adv Biochem Eng Biotechnol* 92: 225–260, 2005.
354. Widmer F and Kaplan NO. *Pseudomonas aeruginosa* transhydrogenase: Affinity of substrates for the regulatory site and possible hysteretic behavior. *Biochem Biophys Res Commun* 76: 1287–1292, 1977.
355. Wiechert W. $^{13}C$ metabolic flux analysis. *Metab Eng* 3: 195–206, 2001.
356. Wilmot CM. Oxygen activation in a copper-containing amine oxidase. *Biochem Soc Trans* 31: 493–496, 2003.
357. Wimpenny JW and Firth A. Levels of nicotinamide adenine dinucleotide and reduced nicotinamide adenine dinucleotide in facultative bacteria and effect of oxygen. *J Bacteriol* 11: 24, 1972.
358. Witayakran S and Ragauskas AJ. Synthetic applications of laccase in green chemistry. *Adv Synth Catal* 351: 1187–1209, 2009.
359. Wittmann C and Heinzle E. Genealogy profiling through strain improvement by using metabolic network analysis: Metabolic flux genealogy of several generations of lysine-producing corynebacteria. *Appl Environ Microbiol* 68: 5843–5859, 2002.
360. Woodley JM. Microbial biocatalytic processes and their development. *Adv Appl Microbiol* 60: 1–15, 2006.
361. Woodley JM. Choice of biocatalyst form for scalable processes. *Biochem Soc Trans* 34: 301–303, 2006.
362. Wu JT, Wu LH, and Knight JA. Stability of NADPH: Effect of various factors on the kinetics of degradation. *Clin Chem* 32: 314–319, 1986.
363. Wubbolts MG, Terpstra P, van Beilen JB, Kingma J, Meesters HA, and Witholt B. Variation of cofactor levels in *Escherichia coli*. Sequence analysis and expression of the *pncB* gene encoding nicotinic acid phosphoribosyltransferase. *J Biol Chem* 265: 17665–17672, 1990.
364. Wubbolts MG, Reuvekamp P, and Witholt B. Tol plasmid-specified xylene oxygenase is a wide substrate range monooxygenase capable of olefin epoxidation. *Enzyme Microb Tech* 16: 608–615, 1994.
365. Xie W, Xu A, and Yeung ES. Determination of NAD(+) and NADH in a single cell under hydrogen peroxide stress by capillary electrophoresis. *Anal Chem* 81: 1280–1284, 2009.
366. Xu M, Bhat S, Smith R, Stephens G, and Sadhukhan J. Multi-objective optimisation of metabolic productivity and thermodynamic performance. *Comput Chem Eng* 33: 1438–1450, 2009.
367. Yamada K, Hara N, Shibata T, Osago H, and Tsuchiya M. The simultaneous measurement of nicotinamide adenine dinucleotide and related compounds by liquid chromatography/electrospray ionization tandem mass spectrometry. *Anal Biochem* 352: 282–285, 2006.
368. Yamaguchi M and Hatefi Y. Energy-transducing nicotinamide nucleotide transhydrogenase. Nucleotide-sequences of the genes and predicted amino-acid-sequences of the subunits of the enzyme from *Rhodospirillum rubrum*. *J Bioenerg Biomembr* 26: 435–445, 1994.
369. Yan F, Moon SJ, Liu P, Zhao Z, Lipscomb JD, Liu A, and Liu HW. Determination of the substrate binding mode to the active site iron of (*S*)-2-hydroxypropylphosphonic acid epoxidase using $^{17}O$-Enriched substrates and substrate analogues. *Biochemistry* 46: 12628–12638, 2007.
370. Yu Q and Heikal AA. Two-photon autofluorescence dynamics imaging reveals sensitivity of intracellular NADH concentration and conformation to cell physiology at the single-cell level. *J Photochem Photobiol B* 95: 46–57, 2009.
371. Yun CH, Yim SK, Kim DH, and Ahn T. Functional expression of human cytochrome P450 enzymes in *Escherichia coli*. *Curr Drug Metabol* 7: 411–429, 2006.
372. Zamboni N, Mouncey N, Hohmann HP, and Sauer U. Reducing maintenance metabolism by metabolic engineering

of respiration improves riboflavin production by *Bacillus subtilis*. *Metab Eng* 5: 49–55, 2003.
373. Zamboni N, Fischer E, Laudert D, Aymerich S, Hohmann HP, and Sauer U. The *Bacillus subtilis yqjI* gene encodes the $NADP^+$-dependent 6-P-gluconate dehydrogenase in the pentose phosphate pathway. *J Bacteriol* 186: 4528–4534, 2004.
374. Zhao HM and van der Donk WA. Regeneration of cofactors for use in biocatalysis. *Curr Opin Biotech* 14: 583–589, 2003.
375. Zheng Y–J, Xia Z–X, Chen Z–W, Mathews F, and Bruice T. Catalytic mechanism of quinoprotein methanol dehydrogenase: A theoretical and x-ray crystallographic investigation. *Proc Natl Acad Sci USA* 98: 432–434, 2001.
376. Ziegler DM. An overview of the mechanism, substrate specificities, and structure of FMOs. *Drug Metab Rev* 34: 503–511, 2002.
377. Zilberstein D, Agmon V, Schuldiner S, and Padan E. *Escherichia coli* intracellular pH, membrane potential, and cell growth. *J Bacteriol* 158: 246–252, 1984.

Address correspondence to:
*Lars M. Blank*
*Laboratory of Chemical Biotechnology*
*Faculty of Biochemical and Chemical Engineering*
*TU Dortmund*
*Emil-Figge-Str. 66*
*D-44221 Dortmund*
*Germany*

*E-mail:* lars.blank@bci.tu-dortmund.de

Date of first submission to ARS Central, October 10, 2009; date of final revised submission, January 8, 2010; date of acceptance, January 10, 2010.

**Abbreviations Used**

ACCO = 1-aminocyclopropane-1-carboxylate oxidase
ADH = alcohol dehydrogenase
AMO = alkane monooxygenase
AO = amine oxidase
CoA = coenzyme A
CPO = chloroperoxidase
ED = Entner-Doudoroff
EMP = Embden–Meyerhof–Parnas
ETC = electron transport chain
$FAD/FADH_2$ = oxidized/reduced flavin adenine dinucleotide
FBA = flux balance analysis
FDH = formate dehydrogenase
$FMN/FMNH_2$ = oxidized/reduced flavin mononucleotide
FOS = fosfomycin synthase
GC = gas chromatography
GCD = glutaryl-CoA dehydrogenase
HLADH = horse liver alcohol dehydrogenase
HPLC = high-pressure liquid chromatography
IPNS = isopenicillin N-synthase
LBADH = dehydrogenase of *Lactobacillus brevis*
LC = liquid chromatography
L-DOPA = 3,4-dihydroxyphenylalanine
MDH = methanol dehydrogenase
MFA = metabolic flux analysis
mGDH = membrane bound glucose dehydrogenase
MILP = mixed integer linear programming
MMO = methane monooxygenase
MO = monooxygenase
MQ = menaquinone
MQH2 = menaquinol
MS = mass spectrometry
MTT = thiazolyl blue tetrazolium bromide
NDH = NADH-dehydrogenases
NMR = nuclear magnetic resonance
PEP = phosphoenolpyruvate
PP = pentose phosphate
PQQ = pyrroloquinoline quinone
T2MO = toluene-2-monooxygenase
T4MO = toluene-4-monooxygenase
TCA = tricarboxylic acid
TPQ = 2,4,5-trihydroxylphenylalanine quinone
UQ = ubiquinone
UQH2 = ubiquinol
VAO = vanillyl-alcohol oxidase
XMO = xylene monooxygenase

**This article has been cited by:**


1. Enzymes Involved in Redox Reactions: Natural Sources and Mechanistic Overview 1-85. [CrossRef]
2. Reactions Involving Oxidases and Peroxidases 303-432. [CrossRef]
3. Daniel Kuhn, Bruno Bühler, Andreas Schmid. 2012. Production host selection for asymmetric styrene epoxidation: Escherichia coli vs. solvent-tolerant Pseudomonas. *Journal of Industrial Microbiology & Biotechnology* **39**:8, 1125-1133. [CrossRef]
4. Daniel Kuhn, Frederik S.O. Fritzsch, Xiumei Zhang, Volker F. Wendisch, Lars M. Blank, Bruno Bühler, Andreas Schmid. 2012. Subtoxic product levels limit the epoxidation capacity of recombinant E. coli by increasing microbial energy demands. *Journal of Biotechnology* . [CrossRef]
5. Stuart G. Jarrett, Michael E. Boulton. 2012. Consequences of oxidative stress in age-related macular degeneration. *Molecular Aspects of Medicine* . [CrossRef]
6. Rama Krishna Gudiminchi, Charlene Randall, Diederik J. Opperman, Oluwafemi A. Olaofe, Susan T. L. Harrison, Jacobus Albertyn, Martha S. Smit. 2012. Whole-cell hydroxylation of n-octane by Escherichia coli strains expressing the CYP153A6 operon. *Applied Microbiology and Biotechnology* . [CrossRef]
7. Stuart G. Jarrett, Michael E. Boulton. 2012. Consequences of oxidative stress in age-related macular degeneration. *Molecular Aspects of Medicine* . [CrossRef]
8. Debin Ji, Lei Wang, Shuhua Hou, Wujun Liu, Jinxia Wang, Qian Wang, Zongbao K. Zhao. 2011. Creation of Bioorthogonal Redox Systems Depending on Nicotinamide Flucytosine Dinucleotide. *Journal of the American Chemical Society* 111206082027001. [CrossRef]
9. Solvej Siedler, Stephanie Bringer, Lars M. Blank, Michael Bott. 2011. Engineering yield and rate of reductive biotransformation in Escherichia coli by partial cyclization of the pentose phosphate pathway and PTS-independent glucose transport. *Applied Microbiology and Biotechnology* . [CrossRef]
10. Katja Bühler, Andreas Schmid. 2011. Neue mikrobiologische Wege in der Chemie. *BIOspektrum* **17**:5, 528-530. [CrossRef]
11. Rodrigo S. Martins, Dávila S. Zampieri, J. Augusto R. Rodrigues, Patrícia O. Carvalho, Paulo J. S. Moran. 2011. Stereoselective Oxidation of 1-Phenyl-1,2-propanediol Mediated by Microorganisms. *ChemCatChem* n/a-n/a. [CrossRef]
12. Na-Rae Lee, Jang Won Yoon, Jin-Byung Park. 2011. Effect of lipopolysaccharide mutation on oxygenation of linoleic acid by recombinant Escherichia coli expressing CYP102A2 of Bacillus subtilis. *Biotechnology and Bioprocess Engineering* **16**:1, 7-12. [CrossRef]
13. Frank Hollmann, Isabel W. C. E. Arends, Katja Buehler, Anett Schallmey, Bruno Bühler. 2011. Enzyme-mediated oxidations for the chemist. *Green Chemistry* **13**:2, 226. [CrossRef]
14. Stefano Raimondi, Diego Romano, Alberto Amaretti, Francesco Molinari, Maddalena Rossi. 2010. Enoate reductases from non conventional yeasts: Bioconversion, cloning, and functional expression in Saccharomyces cerevisiae. *Journal of Biotechnology* **156**:4, 279-285. [CrossRef]
15. F. Özde Ütkür, Sushil Gaykawad, Bruno Bühler, Andreas Schmid. 2010. Regioselective aromatic hydroxylation of quinaldine by water using quinaldine 4-oxidase in recombinant Pseudomonas putida. *Journal of Industrial Microbiology & Biotechnology* . [CrossRef]
16. Daniel Kuhn, Lars M. Blank, Andreas Schmid, Bruno Bühler. 2010. Systems biotechnology - Rational whole-cell biocatalyst and bioprocess design. *Engineering in Life Sciences* **10**:5, 384-397. [CrossRef]